<u>**Non-Proprietary Version**</u>

Materials Reliability Program Probabilistic Fracture Mechanics Analysis of PWR Reactor Pressure Vessel Top Head Nozzle Cracking (MRP-105 NP)

1007834

Final Report, April 2004

NON-PROPRIETARY INFORMATION

NOTICE: This report contains the non-proprietary information that is included in the proprietary version of this report. The proprietary version of this report contains proprietary information that is the intellectual property of MRP utility members and EPRI. Accordingly, the proprietary versions are only available under license from EPRI and may not be reproduced or disclosed, wholly or in part, by any Licensee to any other person or organization.

EPRI Project Manager
Christine King

EPRI • 3412 Hillview Avenue, Palo Alto, California 94304 • PO Box 10412, Palo Alto, California 94303 • USA
800.313.3774 • 650.855.2121 • askepri@epri.com • www.epri.com

DISCLAIMER OF WARRANTIES AND LIMITATION OF LIABILITIES

ORGANIZATION(S) THAT PREPARED THIS DOCUMENT

Structural Integrity Associates, Inc.

ORDERING INFORMATION

Requests for copies of this report should be directed to EPRI Orders and Conferences, 1355 Willow Way, Suite 278, Concord, CA 94520. Toll-free number: 800.313.3774, press 2, or internally x5379; voice: 925.609.9169; fax: 925.609.1310.

CITATIONS

This report was prepared by:

Structural Integrity Associates, Inc.
6595 S. Dayton Street, Suite 3000
Greenwood Village, Colorado 80111

Principal Investigator:
P.C. Riccardella

Structural Integrity Associates Contributors:

MRPERCRD Software	S.S. Tang,
Finite Element Analyses	G.A. Miessi, C. Fourcade, F. Ku, C.R. Limpus, K. Evon
Fracture Mechanics Analyses	H.L. Gustin, B. Templeton
Technical Typist	Kelly Teague

Other Contributors:
Glenn White, John Broussard, Dominion Engineering
Christine King, John Hickling, EPRI
Larry Mathews, Southern Nuclear Operating Co.
Craig Harrington, TXU Energy

This report describes research sponsored by EPRI.

The report is a corporate document that should be cited in the literature in the following manner:

Materials Reliability Program Probabilistic Fracture Mechanics Analysis of PWR Reactor Pressure Vessel Top Head Nozzle Cracking (MRP-105 NP), EPRI, Palo Alto, CA: 2004. 1007834.

PRODUCT DESCRIPTION

Cracking and leakage has been observed for several years in the reactor pressure vessel (RPV) top head nozzles of operating PWRs in the United States and elsewhere. The cracking is attributed to a phenomenon known as Primary Water Stress Corrosion Cracking (PWSCC) of the nozzle material and associated weldments. EPRI and the PWR Materials Reliability Program (MRP) have undertaken a major effort to define and quantify the potential impact of such cracking on safe operation of the plants. The effort includes a failure modes and effects analysis (FMEA) identifying all possible event sequences (failure modes) that could be initiated by the nozzle cracking, plus a comprehensive safety assessment of the potential impact of the most significant of these failure modes. One of the most serious failure modes identified is the possibility of a top head nozzle rupturing and ejecting from the head due to circumferentially oriented cracks developing in the nozzles and growing to a critical size. This report documents a probabilistic fracture mechanics (PFM) evaluation of the probability of circumferential cracks initiating (or forming as a consequence of branching or redirection of axial cracks), and growing to a size that could cause a nozzle ejection-type failure. It provides a detailed description of a PFM tool developed for this purpose (*MRPERCRD*). It also documents an extensive series of applications of the tool to representative U.S. PWRs, to determine the sensitivities of the analysis to various assumptions, to benchmark the tool, and ultimately to evaluate the probabilities of leakage and nozzle ejection under a set of assumed top head inspection programs.

Results & Findings

The analyses presented in this report demonstrate that, when run with a set of "benchmarked" input parameters, the *MRPERCRD* tool predicts probabilities of nozzle leakage and large circumferential cracking that agree well with a significant database developed from U.S. PWR inspections. The database consists of 2233 nozzles in 30 plants in which non-destructive examinations (NDE) were performed. 137 nozzles in 14 of the plants were found to contain cracking, 53 of which leaked, and 11 of which showed evidence of circumferential cracking, ranging from 30º to 165º of nozzle circumference.

Once benchmarked with respect to this database, the PFM tool was used to analyze a series of case studies of U.S. PWRs under three assumed inspection scenarios. The inspection scenarios include inspections in accordance with U.S. NRC Order EA-03-009 as well as two alternative inspection plans proposed by the MRP. The MRP alternative plans include different inspection options depending on whether or not weld inspections are performed in addition to nozzle inspections. These alternatives are shown to yield essentially the same probabilities of leakage and failure as are achieved by inspections in accordance with the NRC Order, and they offer an incentive, in terms of reduced inspection frequencies, for plants to perform inspections of their J-groove welds.

Challenges & Objectives

The primary objective of this report is to develop and document a methodology of assessing the potential for failure of RPV top head nozzles due to PWSCC. An intermediate objective in the assessment is to determine the probability of nozzles developing cracks or leaks. A third objective is to determine the effects of various inspection options, including inspection type, frequency and effectiveness.

Although the predicted probabilities of leakage and failure are a function of many input variables assumed in the analysis, the specific set of variables used to compare inspection programs have been benchmarked and calibrated with respect to field experience. Also, changes to these variables would affect both the analyses of inspections in accordance with the NRC Order, as well as of inspections in accordance with the two MRP inspection plans, in approximately the same manner. Thus the comparison and conclusions of this study are expected to remain the same for realistic ranges of the input variables

Applications, Values & Use

In addition to the stated applications of comparing the effectiveness of various inspection alternatives, and supporting the generic safety assessment of PWR top head nozzle cracking, the *MRPERCRD* methodology and software also provide a convenient tool for plant specific analyses. Possible plant specific applications include evaluation of limitations in inspection coverage or of inspection programs that might differ from the generic programs evaluated herein. It also establishes an overall approach and methodology for this type of probabilistic fracture mechanics assessment that could be applied to other PWSCC problems, such as RPV bottom head penetrations, pressurizer penetrations, and PWSCC susceptible butt welds in primary coolant piping.

EPRI Perspective

The methodology and software developed in this project are useful for assessing the potential for failure of RPV top head nozzles due to PWSCC. *MRPERCRD* methodology and software were used to perform probabilistic fracture mechanics (PFM) evaluations for four case study plants including low, moderate, and high susceptibility plants. The evaluations calculated the probability of a circumferential crack initiating (or forming as a consequence of branching or redirection of an axial crack), and growing to a size that could cause a nozzle ejection-type failure. The results of these evaluations are below generally accepted limits (Probability of Leakage < 5% and Probability of Failure < 1×10^{-3}) for plants that have performed initial baseline examinations. The results in this document will be combined with probabilistic assessments of the likelihood of occurrence of the various failure modes to produce an overall safety assessment of the RPV top head nozzle cracking issue. The inclusion of evaluations for alternate inspection plans will be useful for plants that are looking for ways to optimize inspection methodology and frequency.

Approach

Major elements of the PFM evaluation include:

- computation of applied stress intensity factors for circumferential cracks in various nozzle geometries as a function of crack length,
- determination of critical circumferential flaw sizes for nozzle failure,
- an empirical (Weibull) analysis of the probability of nozzle cracking or leakage as a function of operating time and temperature of the RPV head,
- statistical analysis of PWSCC crack growth rates in the PWR primary water environment as a function of applied stress intensity factor and service temperature, and
- determination of the effects of inspections (inspection type, frequency and effectiveness).

Keywords
Primary Water Stress Corrosion Cracking
PWSCC
PWSCC Leakage
Stress corrosion
Boric acid corrosion
Alloy 600
Alloy 82/182
Alloy 52/152
CRDM nozzle
CEDM nozzle
J-groove weld
Reactor vessel head
Reactor vessel closure head
Reactor vessel upper head
Safety Assessment
Circumferential cracking
Inspection
Probabilistic Fracture Mechanics

CONTENTS

LIST OF FIGURES

LIST OF TABLES

1 INTRODUCTION

Cracking and leakage has been observed for several years in the reactor pressure vessel (RPV) top head nozzles of operating PWRs in the United States and elsewhere. The cracking is attributed to a phenomenon known as Primary Water Stress Corrosion Cracking (PWSCC) of the nozzle material, Alloy-600 nickel alloy and its associated weld metals. Several plants have detected leakage and/or cracking. The leakage is generally detected in the form of small deposits of boric acid crystals that emanate from the annuli between the nozzles and the vessel head. In other cases, cracking has been detected, with or without evidence of leakage, via volumetric non-destructive examination (NDE) of the nozzles and/or weldments. A schematic of a typical RPV head CRDM nozzle configuration and the general nature of the observed cracking are shown in Figure 1-1.

Initially, leaking nozzles were thought to be exclusively the result of axial cracks in the nozzles, and thus it was believed that they did not present a safety concern (i.e. nozzle ejection which could lead to a loss of coolant accident). However, as more examinations were performed, several findings arose that called this hypothesis into question. Specifically:

- Relatively long circumferential cracks were observed in two nozzles in the Oconee Unit 2 RPV head, and several other plants also discovered shorter circumferentially oriented cracks.
- As a result of allowing leakage to exist for an extended period, and thus build up massive deposits of boric acid on the vessel head, the Davis-Besse plant experienced severe wastage corrosion of their RPV head, to the point that safety margins in the head were reduced below ASME Code allowables.
- Circumferential cracking was discovered in the North Anna Unit 2 head in nozzles that had no apparent signs of boric acid deposits indicating leakage. The circumferential cracks were not as long as those observed at Oconee-2; however, this discovery led the industry to question the effectiveness of visual examinations as a means of confirming the safety of the nozzles with respect to nozzle ejection (i.e. gross fracture due to circumferential cracks extending to a critical size). A program of destructive examination of the North Anna-2 head is underway to achieve a better understanding of the nature and root cause of this inspection finding.

As a result of these discoveries, the industry embarked on a comprehensive failure modes and effects study of RPV top heads to identify all possible failure modes that could lead to reactor safety concerns. The FMEA results will be combined with probabilistic assessments of the likelihood of occurrence of the various failure modes to produce an overall safety assessment of the RPV top head nozzle cracking issue. An overview of the safety assessment process is provided in Figure 1-2.

This report documents one aspect of the safety assessment – a probabilistic fracture mechanics (PFM) evaluation of the probability of a circumferential crack initiating (or forming as a consequence of branching or redirection of an axial crack), and growing to a size that could cause a nozzle ejection-type failure. Major elements of the PFM evaluation include:

- computation of applied stress intensity factors for circumferential cracks in various nozzle geometries as a function of crack length,
- determination of critical circumferential flaw sizes for nozzle failure,
- an empirical (Weibull) analysis of the probability of nozzle cracking or leakage as a function of operating time and temperature of the RPV head,
- statistical analysis of PWSCC crack growth rates in the PWR primary water environment as a function of applied stress intensity factor and service temperature, and
- determination of the effects of inspections (inspection type, frequency and effectiveness).

These elements of the analysis are described in detail in this report, and the resulting probabilities of nozzle leakage and ejection as a function of operating time and temperature for various RPV top head nozzle designs are presented. Sensitivity studies are also presented to evaluate the effects of various uncertainties and assumptions in the analyses.

As a by-product of this work, deterministic analyses of crack growth rates are also performed for various RPV top head designs and operating temperatures, to determine the predicted time for an initiated circumferential crack to grow to the ASME Section XI allowable flaw size. The results of both the probabilistic and deterministic studies are used as the basis for recommended inspection intervals that yield acceptable probabilities of leakage and failure.

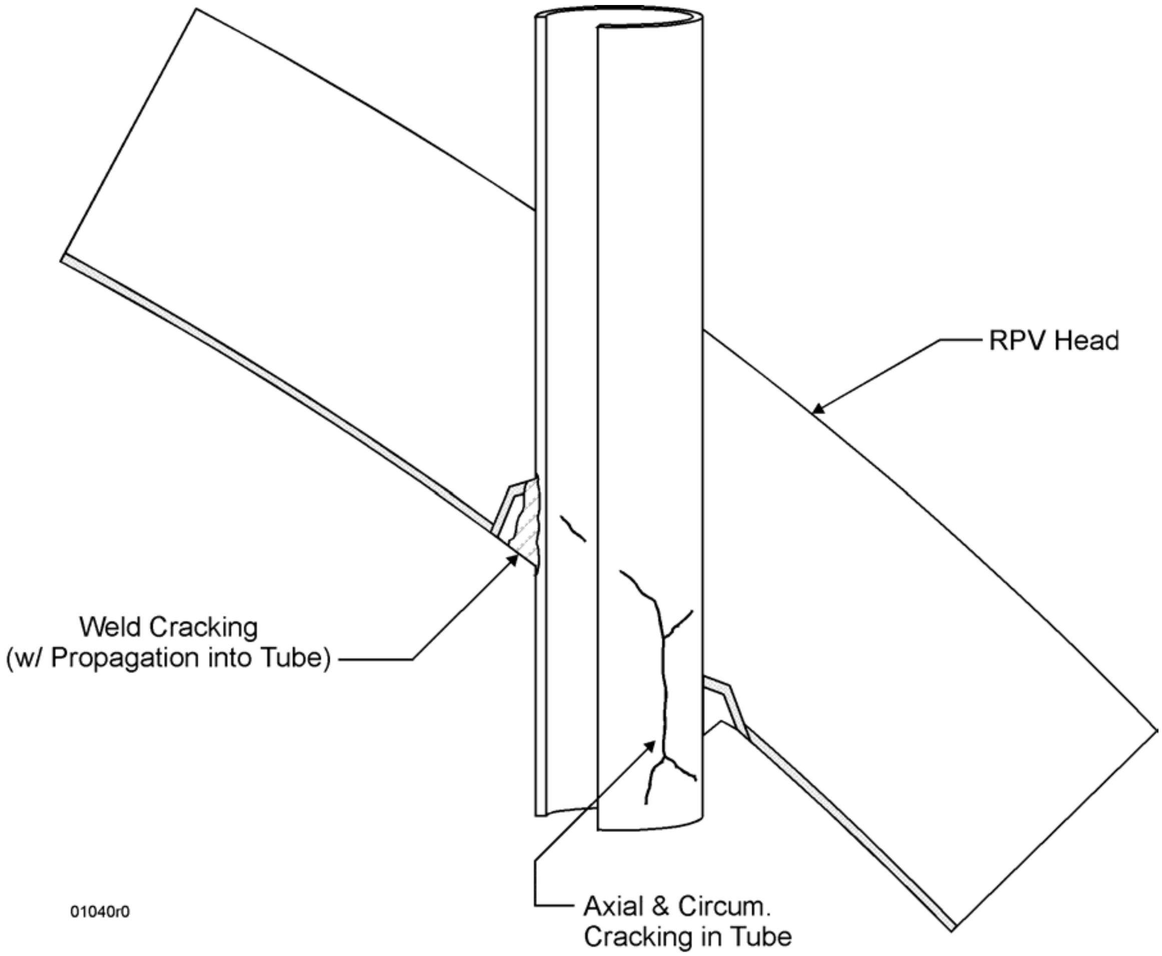

Figure 1-1
Schematic of RPV Top Head Nozzle Geometry and Nature of Observed Cracking

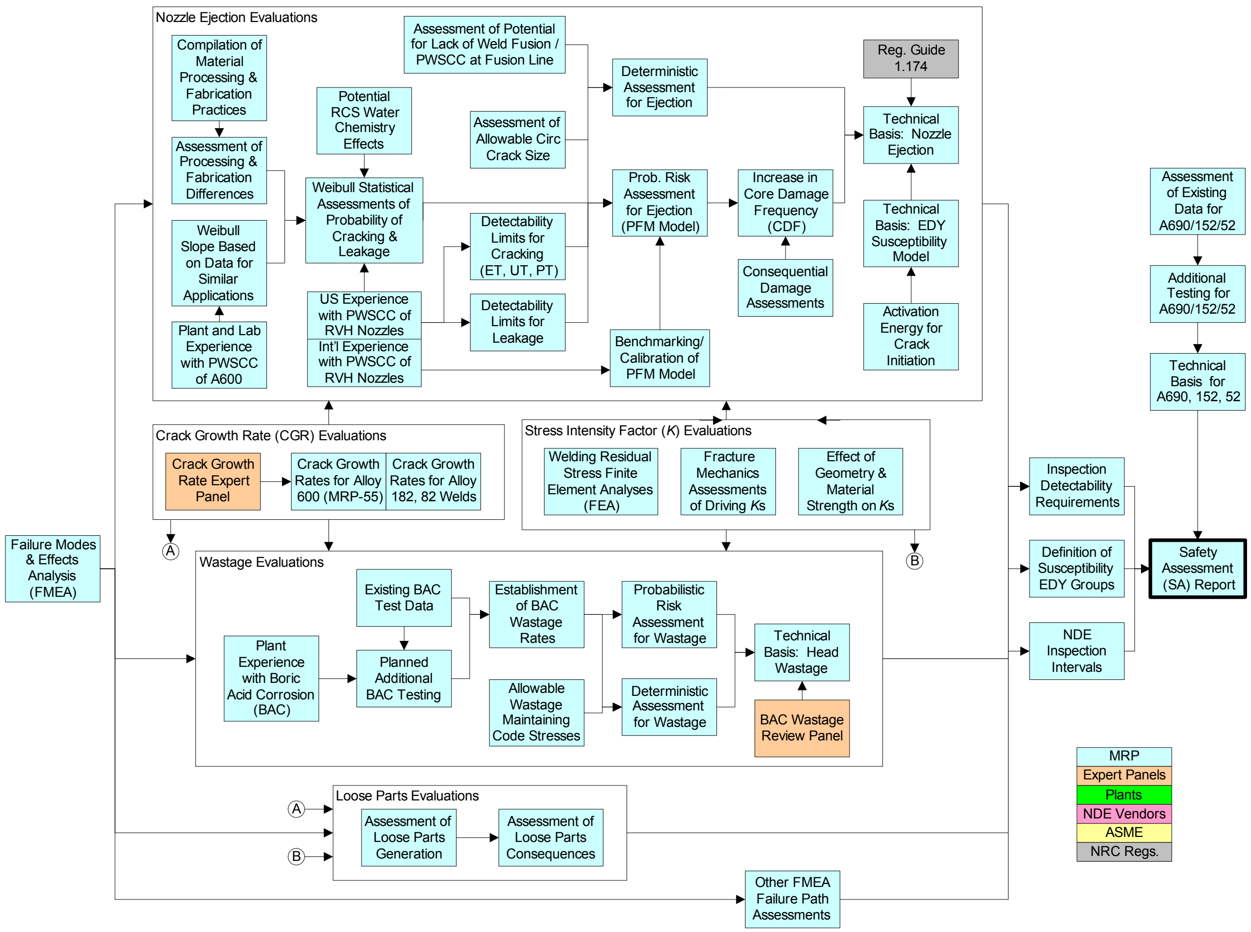

Figure 1-2
Summary of RPV Top Head FMEA Analysis /Safety Assessment Process

2
OVERVIEW OF PFM METHODOLOGY

Figure 2-1 presents a flow chart of the probabilistic fracture mechanics methodology developed for the RPV top head nozzles. The methodology has been implemented in a computer program (*MRPERCRD*, Reference [1]). The *MRPERCRD* methodology implements a time-dependent Monte Carlo analysis scheme which predicts the probability of leakage and nozzle ejection versus time for a specific set of top head parameters. Deterministic parameters specific to the top head being analyzed include number of nozzles, the angle of each nozzle with respect to the head, nozzle diameter and wall thickness, number of heats of nozzle material, and identification of which nozzles are from which heat. Another plant-specific input consists of K-matrices for each of several nozzle angles. These are matrices of stress intensity factor versus crack length for several characteristic nozzle angles (usually four) into which the nozzles are lumped based on their angle. The K-matrices are obtained from deterministic fracture mechanics analyses of the specific head geometry (see Section 3 below) and may include stress intensity factor data for ranges of nozzle yield strengths and nozzle-to-vessel interference fits, for cracks centered at both the uphill and downhill sides of the nozzles.

Statistical parameters (random variables) utilized in the Monte Carlo analysis include:

- head operating temperature
- yield strengths for each heat of nozzle material
- nozzle interferences (or gaps)
- number of assumed cracks per nozzle (for NDE detection)
- initial crack size (for NDE detection)
- distribution of crack locations (uphill or downhill)
- Weibull distribution of time to leakage or cracking (dependent on plant operating time and head temperature)
- stress corrosion crack growth law
- correlation factor between time to crack initiation and crack growth, and
- critical crack size for each characteristic nozzle angle.

The statistical parameters are input as distribution type (normal, triangular, log –normal, log-triangular, Poisson, Weibull, etc.), mean and standard deviation or range. As illustrated in Figure 2-1, the analysis algorithm consists of two nested Monte Carlo simulation loops, which step through time for each nozzle in a head, and then for the total number of head simulations specified. For each nozzle simulation, a time to leakage (or cracking) is predicted based on the

Weibull distribution. When leakage is predicted, a circumferential crack equal to 30º of nozzle circumference is assumed to exist, of a through-wall depth specified by the user (50% and 100% through wall cases have been assumed in most runs). The assumed circumferential crack is then grown based on the nozzle-specific stress intensity factor, which is interpolated based on nozzle yield strength and interference fit, and using a stress corrosion crack growth law obtained from random sampling of the crack growth law distribution. The crack growth analysis for each nozzle continues until either the end of the evaluation period, or until the crack length reaches the critical flaw size for that nozzle (established based on random sampling of the critical crack size distribution). The analysis is repeated for each nozzle in the head, and then for the total number of top head simulations specified by the user. The software records the total number of top heads predicted to experience at least one leak or failure as a function of operating time, as well as the total number of nozzles with predicted leaks or failures versus time. The probability of a nozzle leak or failure at a given time is the ratio of the number of top heads predicted to have leaks or failures divided by the total number of top heads simulated.

A correlation factor between crack initiation and crack growth is included as a user input, which allows one to simulate an inter-relationship between the time to initiation and the crack growth rate for each nozzle. A high negative correlation factor (-0.9 or -1) implies that a material heat that tends to be bad from the perspective of crack initiation (i.e. leaks early in life) would also have a high crack growth rate. A correlation factor of 0 implies no correlation.

The program also permits the user to specify inspections performed at various times within the analysis interval. Either visual inspections (for leakage) or non-destructive examinations (for cracking) or some combination thereof may be specified. The user also specifies inspection coverage (% of nozzles inspected) and reliability for each inspection (probability of detecting a leak if it exists in a visual examination or probability of detection versus crack depth for a non-destructive examination). When inspections are performed, cracks in nozzles that are predicted to be detected are removed from the simulation, and are no longer considered threats to grow to leakage or failure. One can thus perform multiple analyses, with and without various forms of inspection, at various intervals, to compare the probabilities of leakage and failure, and thus evaluate the effectiveness of different inspection regimens.

Content Deleted – MRP/EPRI Proprietary Material

Figure 2-1
Flow Chart of PFM Methodology

3 STRESS INTENSITY FACTOR AND CRITICAL FLAW SIZE COMPUTATIONS

A key element of this PFM evaluation is computation of applied stress intensity factors for circumferential cracks of various lengths ranging from relatively small cracks that might be initiated once leakage is detected, up to and including critical crack lengths that could potentially lead to gross failure of the nozzles (nozzle ejection). Figure 3-1 illustrates the general nature of the circumferential cracking assumed for this evaluation. Located in a plane above and parallel to the top of the J-groove weld, the circumferential cracking can begin and end at any azimuth around the nozzle, but for purposes of this evaluation, two flaw locations were assumed as illustrated, one centered on the uphill side of angled nozzles, and the other centered on the downhill side.

The basic approach used to determine stress intensity factors for the assumed top head nozzle cracks is the well-known superposition technique for fracture mechanics analysis of complex geometries and stresses [2] illustrated schematically in Figure 3-2. Operating and residual stress analyses are first performed using three dimensional, elastic-plastic finite element models of the nozzle, head and J-groove weld region, but with no cracks (Section 3.1). Stresses from these uncracked nozzle models are then superimposed on simplified elastic finite element models of just the nozzles, without the vessel head or J-groove welds, but with cracks of various lengths and depths built into the models, and with boundary conditions applied that represent the constraints imposed by the vessel head and J-groove welds (Section 3.3). The resulting stress intensity factors are tabulated, in the form of K-matrices, for input to the PFM model.

Since U.S. plants have varying numbers of nozzles, ranging from 37 to 101 depending on plant size and type, and with nozzles penetrating the heads at various angles with respect to the head tangent angle at the attachment point, numerous nozzle and flaw geometries need to be addressed. Different plant types also have different nozzle, head and J-groove weld geometries, and as mentioned above, the cracks are assumed to be located at either the uphill or downhill sides of the angled nozzles. To limit the analyses to a practical number of cases, a set of characteristic plants (one each from two PWR vendors and two from a third vendor) have been selected for analysis. An evaluation is presented in Section 3.2, which demonstrates that the characteristic plants selected for analysis bound the U.S. PWR fleet in terms of the parameters important to nozzle stresses in the vicinity of the RPV top head J-groove welds.

Finally, critical flaw sizes are determined for each of the characteristic plants (Section 3.5). Due to the inherent ductility of the Alloy-600 nozzle material, limit load analysis was used to determine critical circumferential crack lengths in the nozzles. With the limit load approach, the net effect of cracking is to reduce the cross sectional area of the nozzle, and failure is predicted when net section collapse (NSC) of the nozzle cross-section minus the crack cross section is predicted. For the deterministic crack growth calculations presented in Section 6, the limit load critical crack lengths are reduced by an amount necessary to provide ASME Section XI Code allowable margins for flaw evaluation.

3.1 Stress Analyses of Uncracked Nozzles

A series of stress analyses have been performed previously for various plant top head nozzles [3-6] to determine the stresses in the vicinity the J-groove welds. The analyses consisted of three-dimensional elastic-plastic finite element models of RVH nozzle designs with temperature-dependent material properties. The nozzle model (see Figure 3-3) included a sector of the low alloy steel head with stainless steel cladding on the inside surface, a single Alloy 600 nozzle, the weld buttering layer in the J-groove weld prep, and the Alloy 182 weld material divided into two "passes" of approximately equal volume. The stainless steel cladding layer was included in the model since this material has a significantly different coefficient of thermal conductivity compared to the low alloy steel vessel head, and therefore influences the weld cooling process.

Since thermal and structural analyses were both performed, thermal and structural elements were used. The thermal analysis was performed first using eight-node three-dimensional thermal solid elements, with heat transfer between the nozzle and head limited to conduction through the J groove region. This assumption was made because the head penetrations for most plants are counter-bored at the upper and often lower portions of the penetration, and because thermal communication between the surfaces that are nominally in contact was assumed to be poor.

Once the thermal analysis was completed, a three-dimensional structural analysis was performed using eight-node three-dimensional iso-parametric solid elements and two-node interface elements to simulate the contact in the penetration region. Use of the interface elements in the annular region between the nozzle OD and the RVH penetration ID ensured that nozzle displacements due to weld cooling are appropriately bounded by the RVH penetration ID.

A conical sector of the vessel shell was included in the model. Nodes on the conical boundary plane were permitted to move only in the spherical radial direction. These boundary conditions simulated the vessel head stiffness and accurately simulated pressure stresses in the shell remote from the penetrations.

The analyses simulated the key steps in the installation of the nozzles in the RPV heads as follows:

1. Welding Simulation. A substantial portion of the analytical work in the model involved the simulation of welding processes. The modeling of the butter weld deposition and the J groove welding made use of the same basic steps to simulate the thermal and mechanical effects of a weld. Each Alloy 182 weld “pass” was modeled as a complete ring of weld material elements that are heated simultaneously.

The analytical simulation of the welding process consisted of combined thermal and structural analyses. The thermal analysis was used first to generate nodal temperature distributions at several points in time during the welding process. These nodal temperatures were then used as loading inputs to the structural analysis, which calculated the thermally induced stresses. This sequence of thermal analysis followed by structural analysis was used for each simulated weld pass.

2. Thermal Stress Relief. After completion of the butter deposition, but prior to J-groove welding, the entire model was uniformly raised to 1,100°F and then uniformly lowered to room temperature to simulate the effect of the thermal stress relief (post-weld heat treatment) performed on the vessel head. In order to simulate the stress relaxation caused by a multiple-hour stress relief at 1,100°F, the elastic limit material properties of the head shell and butter materials at 1,100°F were set at values consistent with this relaxation effect. Sensitivity cases have shown little effect on nozzle stresses by the modeling steps simulating thermal stress relief.

3. Hydrostatic Testing. The components were hydrostatically tested to approximately 3,125 psia after manufacturing and again after installation. These operations were included in the analysis since the applied hydrostatic pressure further yielded the Alloy 600 nozzle material and resulted in a reduction in peak residual tensile stresses when the hydrostatic test pressure was released. In this manner, the hydrostatic testing represented a form of "mechanical stress improvement" in areas of high stress. Aside from applying pressure to all of the wetted internal surfaces, an axial tensile stress was applied to the top end of the nozzle equal to the longitudinal pressure stress in the nozzle wall due to pressure acting in the nozzle "cap."

4. Operating Condition. Operating conditions were simulated by pressurizing the inside surfaces of the model to operating pressure and heating all of the material to the uniform operating temperature. Stresses produced by differential thermal expansion arising from the small temperature gradient within the vessel head and nozzle during the heatup and cool down transients were neglected.

Several slices or planes above the J-groove welds are also illustrated in Figure 3-3. The plane of nodes right at the top of the J-groove weld (sometimes referred to as the "triple point") is the 1400 plane. The plane of nodes just above that is the 1500 plane, and above that is the 1600 plane, etc. Figure 3-4 presents through-wall-averaged stresses along these various planes for one of the nozzles analyzed (Plant A – 38.5º nozzle angle). The stresses in Figure 3-4 have been resolved into the plane perpendicular to an assumed, circumferentially-oriented crack parallel to the root of the J-groove weld. It is seen from this figure that the highest local peak stresses at the uphill side of the nozzle occur at the triple point or 1400 plane. However, on this plane the stresses drop off rapidly, and become compressive about half way around the nozzle toward the downhill side. On higher planes, the peak stress at the uphill side of the nozzle is not as great, but the stresses remain higher throughout a greater portion of the nozzle cross-section. Also shown in Figure 3-4 is a bounding stress curve, which "envelopes" the maximum stresses at all planes above the J-groove weld. While it is likely that circumferential cracks, if they occur, would initiate at the highest peak stress location (uphill side at the triple point in this case), in which plane they would propagate is less certain. Indeed, it is not unlikely that the cracks might meander so as to follow the maximum stress path in the nozzle. Therefore, the envelope curve in Figure 3-4 (and similar envelope curves for the other nozzles) was used in the stress intensity factor calculations.

Similar analyses have been performed for a number of nozzle angles in several characteristic plant types [Refs. 3-6]. The resulting through-wall averaged stresses normal to the crack plane at several sections above the J-Groove weld are illustrated in Figures 3-4 through 3-7 for the steepest angle nozzles in the four characteristic plant types. Similar stress results have been extracted for a series of nozzles at different nozzle angles, and are used as the basis of the fracture mechanics stress intensity computations discussed in Section 3.3 below. Details of these stress distributions and the associated fracture mechanics calculations are documented in references [7-10].

3.2 Evaluation of Characteristic Plant Types

A group of characteristic plants have been selected for evaluation that reasonably bound the U.S. PWR fleet in terms of parameters expected to affect top head nozzle residual and operating stresses. The specific plant types selected are:

- Plant A – A typical B&W type plant with nozzle angles ranging from 0° to 38°, and reported nozzle yield strengths ranging from 36.8 to 50 ksi. [3]
- Plant B – A Westinghouse 2-loop plant with nozzle angles ranging from 0° to 43.5°, and reported nozzle yield strength of 58 ksi. [4]
- Plant C – A Westinghouse 4-loop plant with nozzle angles ranging from 0° to 48.8°, and reported nozzle yield strength of 63 ksi. [5]
- Plant D – A large CE type plant with nozzle angles ranging from 0° to 49.7°, and reported nozzle yield strengths ranging from 52.5 to 59 ksi.. This plant also contained ICI nozzles with a 55.3º nozzle angle and a yield strength of 39.5 ksi.[6]

In addition to nozzle angle and yield strength, weld geometry is an important factor influencing residual stress. Figure 3-8 summarizes a wide range of PWR top head nozzle geometries, which have been previously analyzed. Specifics of the plant types and nozzle angles included in this Figure are listed in Table 3-1. Plotted on the horizontal axis of Figure 3-8 is the average J-groove weld cross-sectional area for each of the plants, distinguished by ranges of nozzle angle. Plotted on the vertical axis is the ratio of uphill to downhill weld cross-sectional area for the same nozzles. In general, the larger the weld size, the higher the residual stress one would expect. The ratio of uphill to downhill weld areas is also expected to affect the distribution of stress around the nozzle. Data points representing the nozzles analyzed for the four characteristic plants (A – D) are labeled and identified by the solid symbols in this chart. It is seen from Figure 3-8 that the four plants selected are reasonable bounds to the complete collection of points. Plant B represents the largest average weld size in the group, and also has relatively high yield strength. Plants A and C have about average weld sizes but span the range of uphill to downhill weld size ratios, from the highest (uphill weld area almost twice that of the downhill weld) to the lowest (downhill weld area more than twice that of the uphill weld). Plant D is somewhat central to the group, both in terms of average weld size and ratio. This group of plants also spans a wide range of nozzle yield strengths, from 36.8 ksi to 63 ksi. In addition to the highest angle nozzles for each plant, the evaluation also includes selected intermediate and low angle welds from the same plant types, as well as ICI nozzles in the CE type plant, to cover the full range of possible nozzles.

Content Deleted – MRP/EPRI Proprietary Material

Table 3-1
Plants Reflected in Weld Geometry Variables Illustrated in Figure 3-8

These analyses reflect only as-designed weld configurations, since data were not generally available for as-built welds sizes. However, some plant specific analyses have been performed for as-built weld sizes that were considerably larger than design. These analyses showed that, while the larger weld sizes tended to displace the locations of maximum stress, they did not significantly increase them. Because of this observation, and the envelop stress approach used for computing stress intensity factors (as discussed in Section 3.1 above), the stress intensity factors used in this analysis are believed to conservatively bound any that might result from as-built weld dimensions that are larger than design values.

The conclusion from this evaluation is that the characteristic plant and nozzle analyses selected for the PFM analyses bound the fleet of U.S. plants in terms of weld geometries and yield strengths, and that the PFM results are therefore applicable to all U.S. PWRs.

3.3 Through-Wall Crack Analyses

The stresses presented in Figures 3-4 through 3-7 have been utilized in fracture mechanics models of nozzles containing circumferential cracks of various lengths in the plane immediately above the J-groove welds. Figure 3-9 illustrates a typical through wall crack model used in such analyses. The model contains the nozzle only, with the crack modeled at a plane parallel to the root of the J-groove weld. Details of the fracture mechanics models and analyses are described in Refs. [7-10]. A number of cases were analyzed. The analysis cases were based on the following variable parameters:

- Nozzle Angle (several nozzle locations on the top heads ranging from top dead center to the steepest angled nozzles)
- Flaw Location (uphill or downhill)
- Flaw Length (a series of crack lengths ranging from 30º to 300º)
- Stress Location (the location of the plane for which the stresses are obtained – analyses were performed for the 1400 and 1500 planes as well as for the envelop stress distributions)
- Yield Strength of the CRDM nozzle material
- Interference Fit Values

Key physical and geometric parameters for the analyses of each of the plant types and nozzles are summarized in Table 3-2 below.

<table>
<tr><th></th><th>Plant A
(B&W)</th><th>Plant B
(W 2-Loop)</th><th>Plant C
(W 4-Loop)</th><th colspan="2">Plant D
(CE)</th></tr>
<tr><td></td><td></td><td></td><td></td><td>CEDM</td><td>ICI</td></tr>
<tr><td>Top Head:
ID (in.)
thickness (in)</td><td colspan="5" rowspan="5">Content Deleted – MRP/EPRI Proprietary Material</td></tr>
<tr><td>Nozzle:
OD (in.)
thickness (in)</td></tr>
<tr><td>Total #
Nozzles</td></tr>
<tr><td>Nozzle Angles
Analyzed (°)</td></tr>
<tr><td>Nozzle Yield
Strengths (ksi)</td></tr>
</table>

Table 3-2
Key Physical and Geometric Parameters used in the Fracture Mechanics Analyses

Stresses from the uncracked models normal to the crack plane are input to the fracture mechanics models as pressures on the crack faces. Cases were run for stresses at the triple point (1400 plane), above the triple-point (1500 plane) and for the envelope stress distributions, and in some nozzles for both high and low yield strength cases. In addition to the normal operating and residual stresses from the uncracked models, since through-wall flaws are being analyzed, the normal operating internal pressure of 2235 psi is also applied on the crack faces.

Three kinds of stress distributions were addressed in this evaluation:

1. Actual stress distributions
2. Average stress distributions
3. Envelop stress distributions.

The residual and normal operating stresses obtained from References [3-6] are provided at five radial locations through the nozzle wall thickness, including the ID, OD and three intermediate locations. In order to apply those stresses to the fracture mechanics model, the crack faces are divided into four one-quarter-thickness concentric rings. Hence, the stresses are first resolved into four curves, and then, each of the four stress distributions is curve-fit with a fourth order polynomial. Thus, the circumferential location of each element is used to determine the corresponding pressure load. Figure 3-10 illustrates a typical pattern of pressure loading applied to the crack face.

The average stress distribution method utilizes the averages of the actual stresses (described above) for a given plane (i.e., 1400s) through the thickness of the nozzle wall. The average stress is derived from the five radial locations, curve-fitted and applied uniformly through the thickness of the nozzle (i.e., the stress varies only in the circumferential direction). Analyses were performed using this averaged stress approach for the 1400 and 1500 planes in [7] and compared to the actual stress approach to demonstrate that the two approaches give the same stress intensity factor result.

The envelop stress distribution method utilizes the calculated average stresses along each plane in order to bound all the stresses at sections at and above the triple-point. The envelop stress distribution is curve-fitted and applied uniformly through the thickness of the nozzle in the same manner as described above for the average stress distribution. The average and envelope stress distributions for the steepest angled nozzles in the four plants are presented in Figures 3-4 through 3-7.

Boundary conditions are applied to the fracture mechanics models, as illustrated in Figure 3-9 to represent the physical constraints of the J-groove weld and the interference fit zone between the nozzle and the head. The J-groove weld is represented by a zero radial constraint boundary condition at the Nozzle OD nodes adjacent to the weld. The radial interference fit zones above the crack plane, which limit the bending of the nozzle within the top head wall, are simulated with point-to-point gap elements along the height of the interference fit region (I in Figure 3-11). In general, the gap elements are modeled only at the uphill (0°) and downhill (180°) circumferential azimuths of the nozzle. The nodes that represent the top head wall are fixed in all directions. The amount of gap or interference imposed on the gap elements is based on specified initial interference fit applied during construction, plus calculations for the individual heads indicating how much the interferences will open or close during plant operation. Details of the interference zone and fit assumptions are listed in Refs. [7-10].

Analyses are performed for several crack sizes (typically 30°, 90°, 160°, 180°, 220°, 260° and 300°) at the uphill and downhill locations for the four CRDM nozzles using the high yield strength stresses. Additional analyses are performed for all the nozzles, for uphill side flaws only, using the low yield strength stress distribution in order to bound the analysis with respect to nozzle yield strength. In addition, the effect of the interference fit gaps on the stress intensity factors is evaluated by analyzing the 38.5° nozzle for the case with 3 mil gap in the interference zone.

In each of the analysis cases, the stress intensity factors are computed at three locations on each of the crack fronts: outside surface, mid-radius point and inside surface. Due to the geometry and loading on the nozzle, the stress intensity factors are significant for all three modes of cracking. Thus, the stress intensity factors K_I, K_{II} and K_{III} are used to derive a single stress intensity factor for the combined mode cracking as follows:

$$K = \left[(1-\upsilon^2)(K_I^2 + K_{II}^2) + (1+\upsilon)K_{III}^2\right]^{1/2}$$

where ν is Poisson's ratio. Since the PFM is addressing growth of through-wall cracks in the circumferential direction, the stress intensity factors from the outside surface, mid-radius point and inside surface have been averaged to yield a single stress intensity factor for each crack length. The averaged stress intensity factor values for each of the plant types and nozzle angles analyzed are presented in Figures 3-12 through 3-18 for uphill and downhill flaws.

In the case of Plant A, analyses were performed for high and low yield strength and for large and small interference fit conditions. These cases are tabulated and compared in Table 3-3. Inspection of this table and PFM analyses using these values (Section 8) indicate that the differences are not significant, so only worst case conditions (high yield strength and small interference fits) were analyzed for the remaining three plant types.

Crack Angle	**Stress Intensity Factors ksi√in**
30º	Content Deleted – MRP/EPRI Proprietary Material
90º	
160º	
180º	
220º	
260º	
300º	
Yield Strength =	
Init. Gap =	

Table 3-3
Effect of Nozzle Yield Strength and Interference on Stress Intensity Factors Plant Type A, 38º Nozzle, Uphill Cracks

3.4 Circumferential Crack Initiation versus Formation

Deterministic analyses have also been performed comparing the crack growth rates for a long, circumferentially oriented part-through-wall crack with those for the through-wall 30º of circumference crack assumed in this PFM analysis. The part-through-wall crack results depend strongly on the initial crack depth assumed, since for very small initial crack depths, the stress intensity factor will be at or below the PWSCC threshold, and the calculations will predict essentially infinite times for the cracks to grow through the nozzle wall thickness. However, assuming a crack of sufficient depth that the applied K just exceeds the PWSCC threshold, the crack growth time is seen to be comparable to that required to grow a through wall 30º of circumference crack to 180º. Therefore, it is argued that assuming a through wall 30º of circumference crack as the starting point, when leakage is predicted to occur, is conservative, and covers the case of multiple flaws initiating along the outside surface of a nozzle and propagating through wall.

3.5 Critical Flaw Size Computations

In order to compute the number of cases in the PFM analyses in which nozzle failures are predicted, it is necessary to determine critical flaw sizes for each nozzle type for comparison to the PWSCC crack length versus time computations. Two forms of critical flaw sizes are computed, the first being the actual critical size (safety factor of 1.0) and the second being the ASME Section XI allowable flaw size (safety factor per Section XI, depending on loading condition = 3.0 for normal/upset or 1.4 for emergency/faulted). ASME Section XI, IWB-3640 and Appendix C provide criteria for determining the end of inspection interval allowable flaw sizes based on the net section collapse criterion. This method is appropriate for the highly ductile Alloy 600 CRDM penetration material.

Equation 5.1 from Reference 12 and appropriate safety factors can be used to calculate the allowable and critical flaw sizes for circumferentially oriented through wall flaws in the CRDM penetrations for the characteristic B&W, Westinghouse, and C-E plants addressed in this report. The use of a through-wall circumferential flaw analysis is conservative with respect to part through wall circumferential flaws that may occur.

Allowable Flaw Size:

$$P = (\sigma_{flow}/SF)\ [A_{wall}\{1-(\Theta/360)\}/\{A_{bore} + A_{wall}(\Theta/360)\}$$

where:

P= maximum normal operating pressure on the nozzle bore and crack face
σ flow = flow stress = 3.0 S_m
S_m = ASME Code, Section III design stress intensity at temperature
A_{bore} = cross-sectional area of the nozzle bore

A_{wall} = cross-sectional area of the nozzle
Θ = circumferential angle of the allowable through-wall flaw
SF = factor of safety

This equation is solved iteratively for the allowable flaw size.

Typical nozzle dimensions for the four vessel designs discussed herein are presented in Table 3-2. The material is Alloy 600. From Appendices of Section III of the ASME Code, the allowable stress intensity S_m is 23.3 ksi for this material, up to a temperature of 800°F. In accordance with Appendix C of Section XI of the ASME Code, a factor of safety of 3.0 applies, since the stresses due to operating pressure (2235 psi) represent a normal/upset loading. The flow stress is 3.0 S_m = 69.9 ksi.

By solving the above equation iteratively using the specified input values, the critical (SF=1.0) and allowable (SF=3.0) through-wall flaw lengths are determined, and the results for each plant type are summarized in Table 3-4. For the purposes of the PFM analyses, the critical flaw lengths are conservatively taken as 300º of circumference.

PLANT DESIGN	CRITICAL FLAW SIZE (safety factor = 1.0), degrees of circumference	ALLOWABLE FLAW SIZE (safety factor =3.0), degrees of circumference
Plant A (B&W)	338.7	299.7
Plants B & C (W)	338.8	300.2
Plant D (C-E)	339.8	302.8

Table 3-4
Critical and Allowable Flaw Size Results

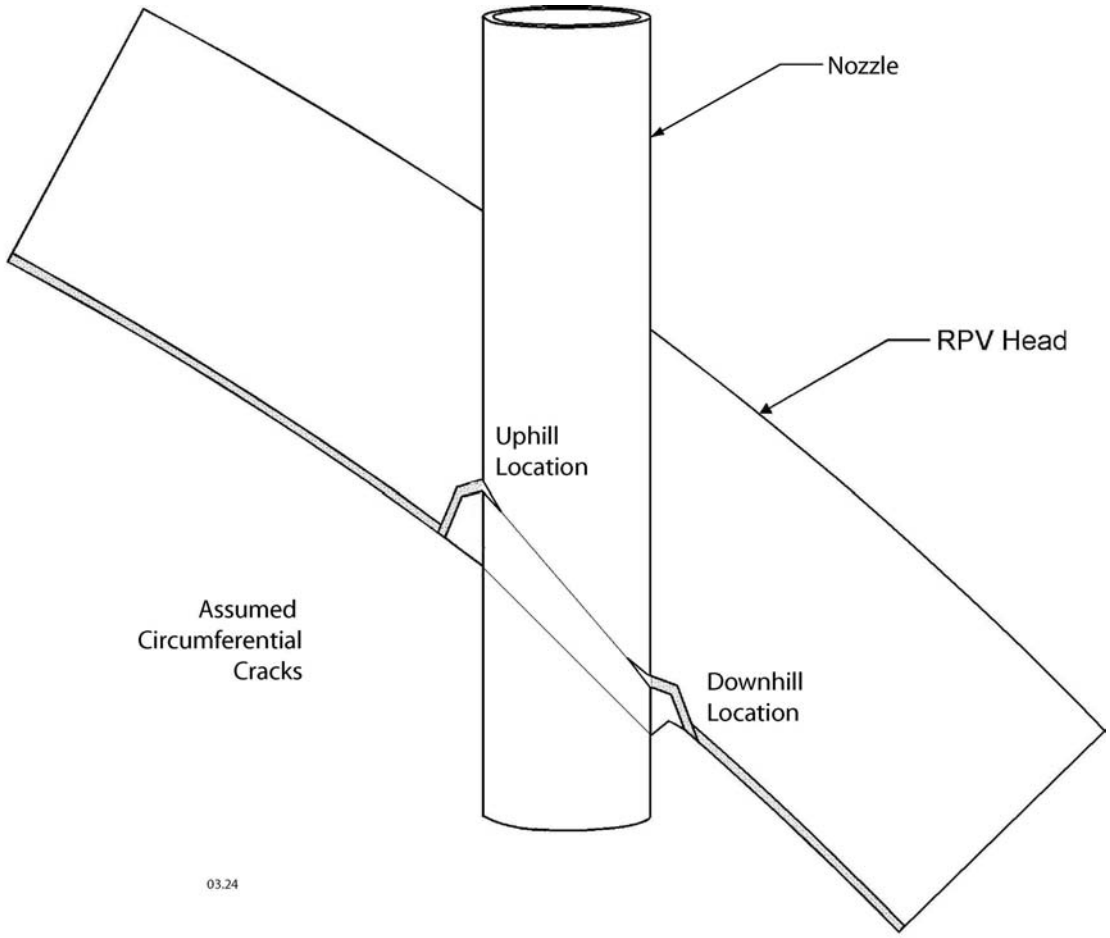

Figure 3-1
Schematic Illustration of Assumed Circumferential Flaws above J-Groove Welds

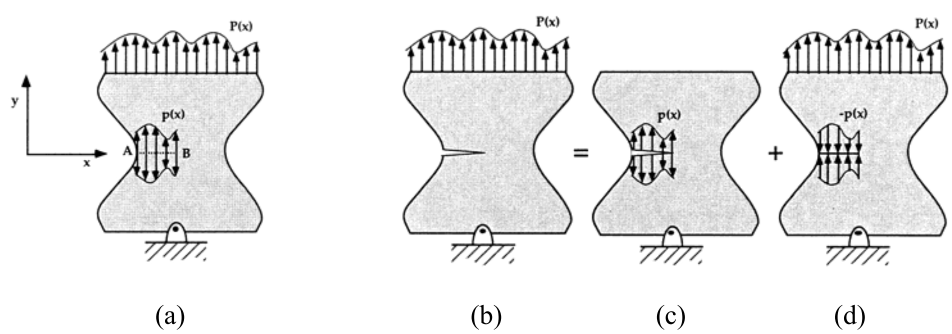

Figure 3-2
Illustration of Superposition Approach for Cracks in Complex Structures Subject to Complex Loading Patterns

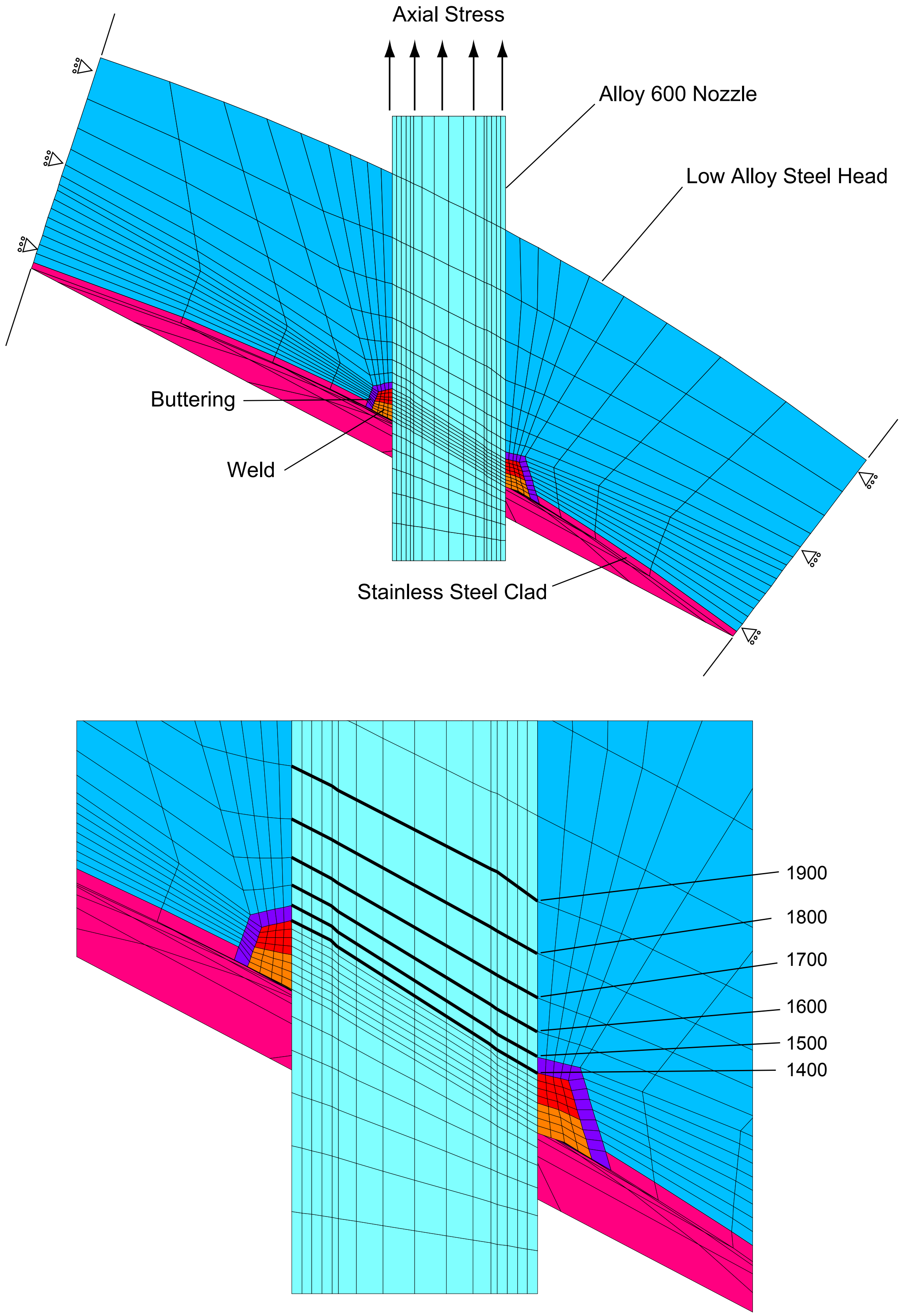

Figure 3-3
Finite Element Model for Calculating Stresses Including Welding Residual Stresses (Showing Stress Planes above the J-Groove Weld)

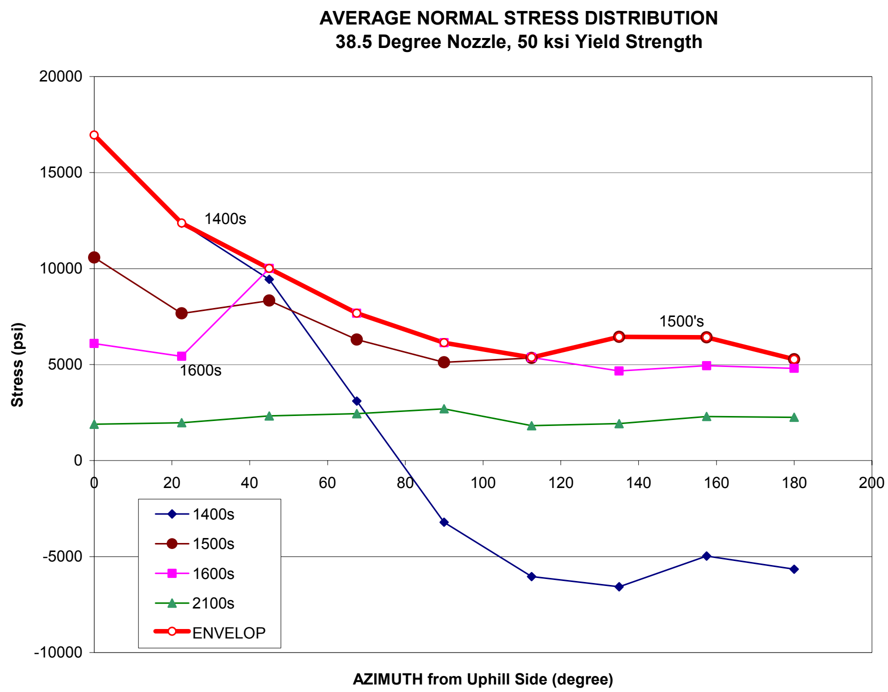

Figure 3-4
Through-Wall Averaged Stress Normal to Crack Surface vs. Distance from the Uphill Side of the Nozzle – Steepest Angle Nozzle – Plant A.

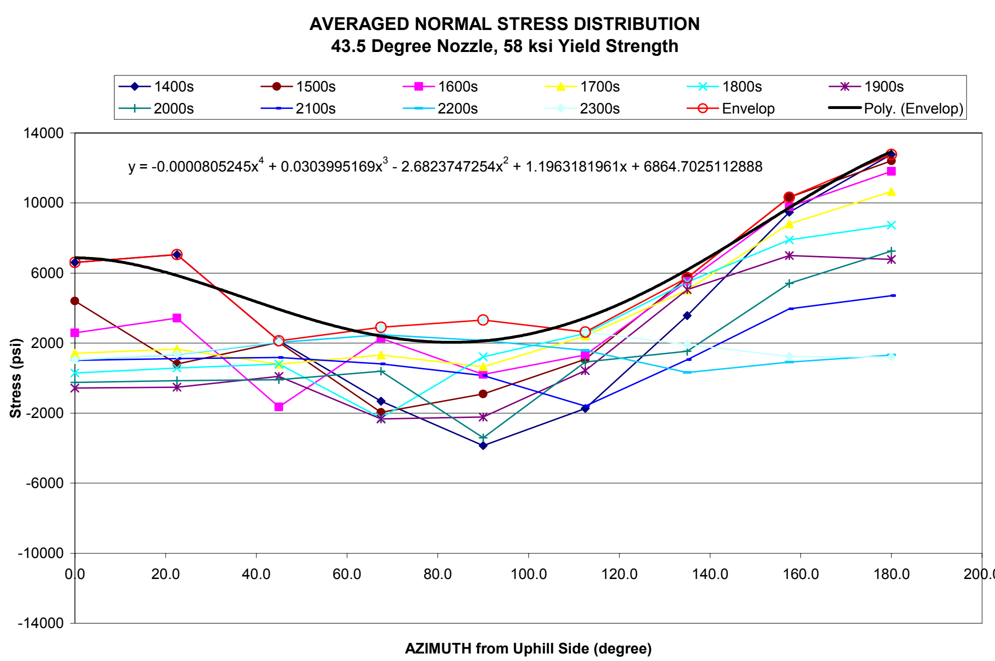

Figure 3-5
Through-Wall Averaged Stress Normal to Crack Surface vs. Distance from the Uphill Side of the Nozzle – Steepest Angle Nozzle – Plant B.

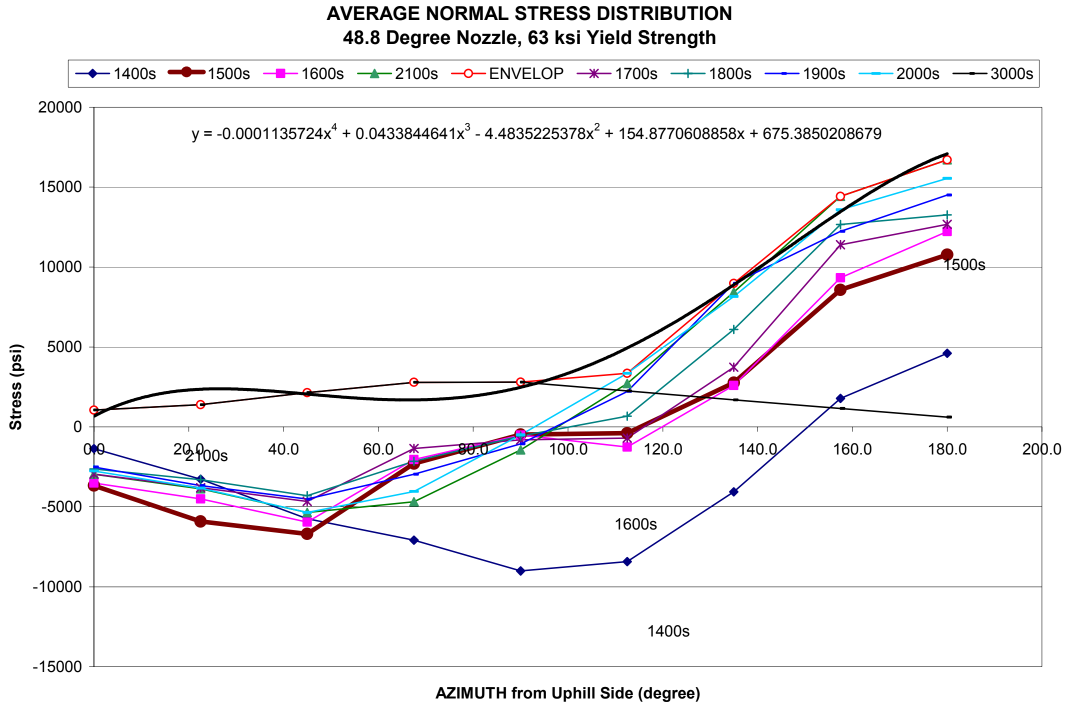

Figure 3-6
Through-Wall Averaged Stress Normal to Crack Surface vs. Distance from the Uphill Side of the Nozzle– Steepest Angle Nozzle – Plant C.

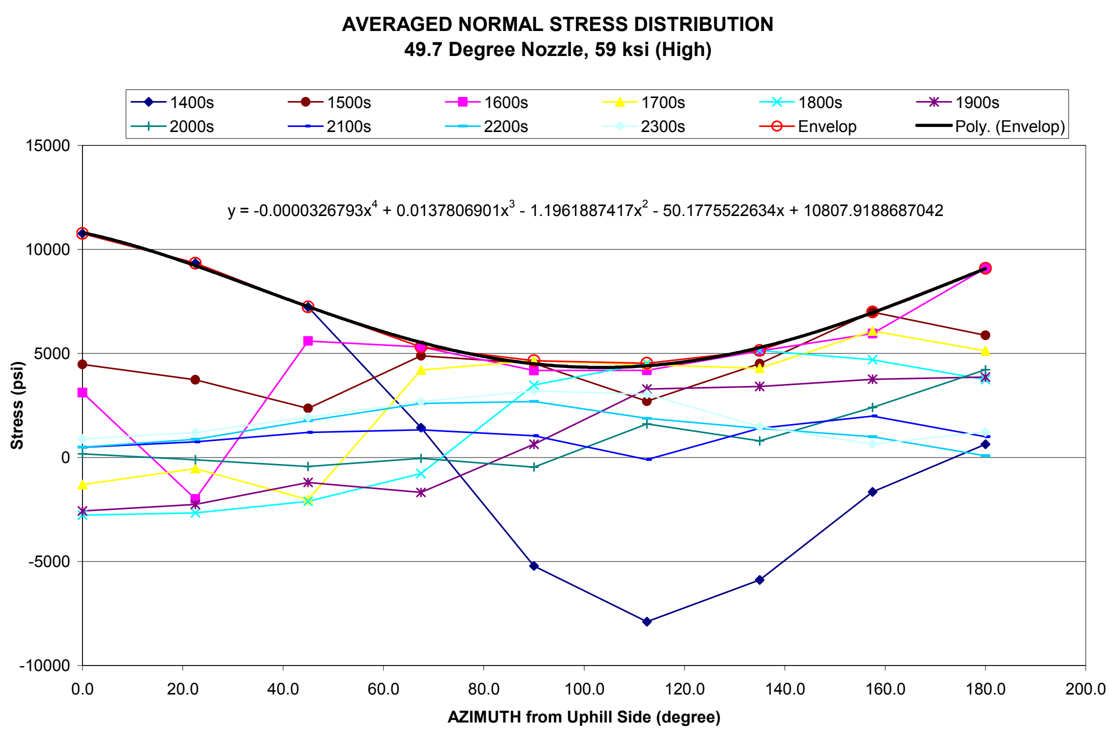

Figure 3-7
Through-Wall Averaged Stress Normal to Crack Surface vs. Distance from the Uphill Side of the Nozzle – Steepest Angle CEDM Nozzle – Plant D.

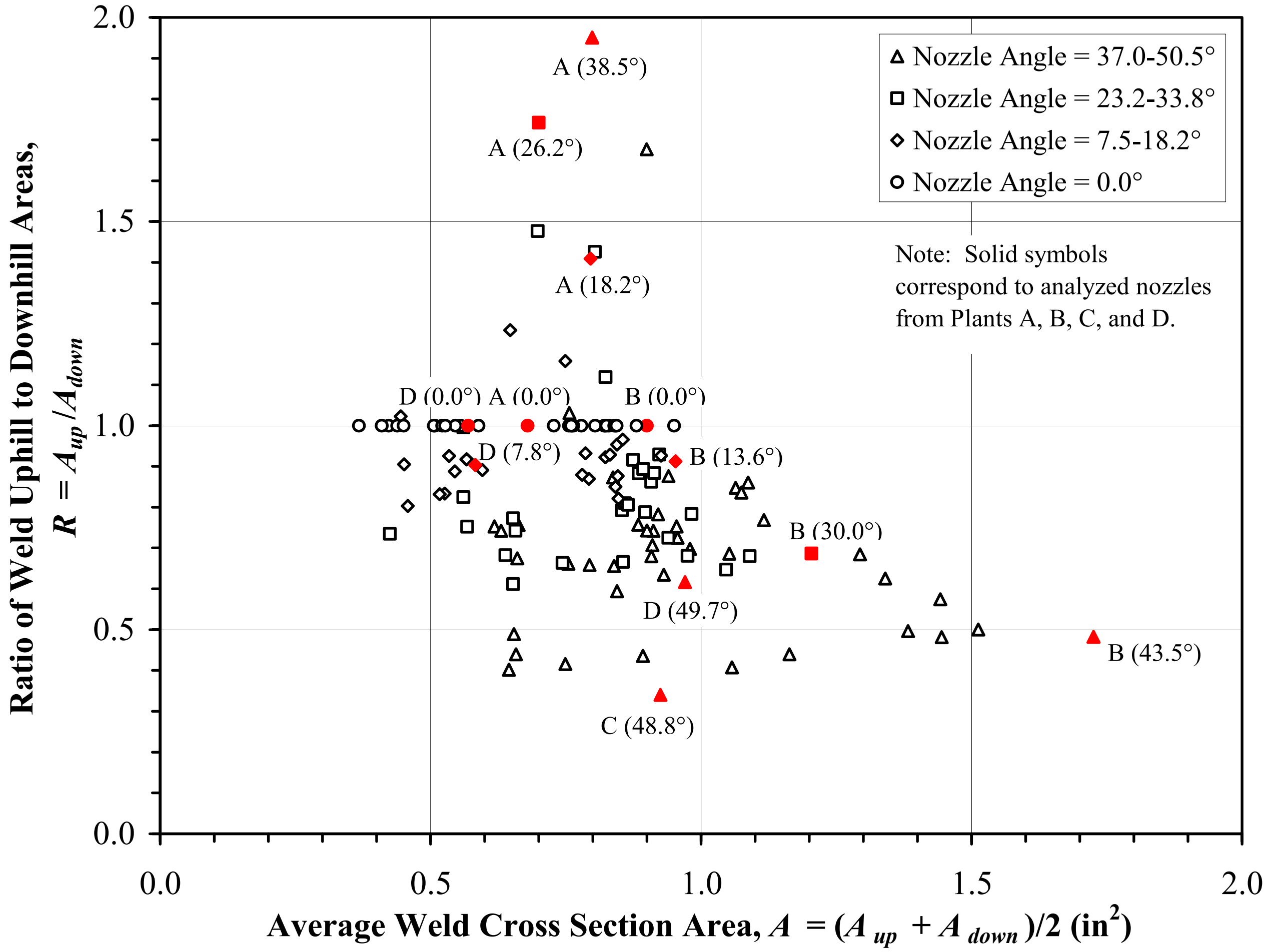

Figure 3-8
Comparison of Key Weld Geometry Variables Influencing Nozzle Residual Stresses – Characteristic Plants Evaluated in this Study are Labeled

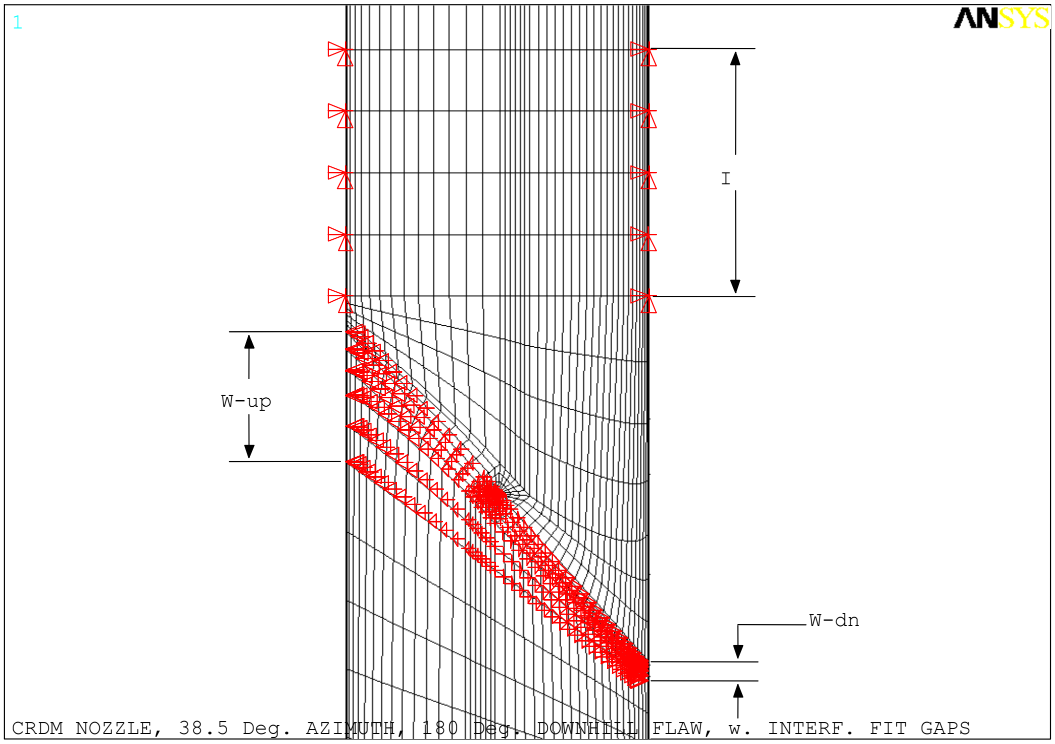

Figure 3-9
Typical Through-Wall Crack Model Showing Boundary Conditions used to Represent J-Groove Weld and Interference Fit with Head – Plant A, 38.5º Nozzle

Content Deleted – MRP/EPRI Proprietary Material

Figure 3-10
Illustration of the Application of Stresses from Uncracked Model as Pressure on the Crack Face

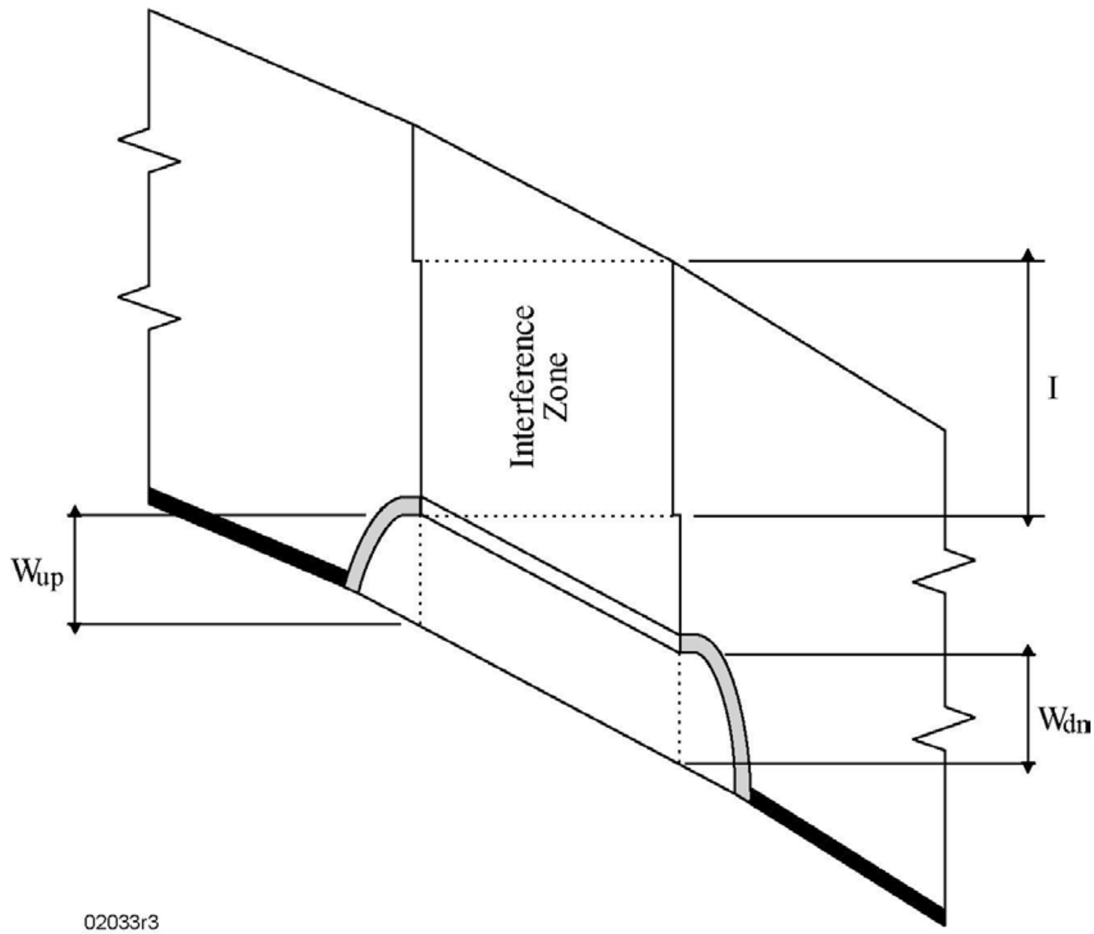

Figure 3-11
Illustration of Nozzle to Vessel Head Interference Fit Zone

Content Deleted – MRP/EPRI Proprietary Material

Figure 3-12
Stress Intensity Factors vs. Flaw Size: Plant A – Uphill Cracking

Content Deleted – MRP/EPRI Proprietary Material

Figure 3-13
Stress Intensity Factors vs. Flaw Size: Plant A – Downhill Cracking

Content Deleted – MRP/EPRI Proprietary Material

Figure 3-14
Stress Intensity Factors vs. Flaw Size: Plant B – Uphill Cracking

Content Deleted – MRP/EPRI Proprietary Material

Figure 3-15
Stress Intensity Factors vs. Flaw Size: Plant B – Downhill Cracking

Content Deleted – MRP/EPRI Proprietary Material

Figure 3-16
Stress Intensity Factors vs. Flaw Size: Plant C – Uphill and Downhill Cracking

Content Deleted – MRP/EPRI Proprietary Material

Figure 3-17
Stress Intensity Factors vs. Flaw Size: Plant D – Uphill Cracking

Content Deleted – MRP/EPRI Proprietary Material

Figure 3-18
Stress Intensity Factors vs. Flaw Size: Plant D – Downhill Cracking

4
ANALYSIS OF FIELD EXPERIENCE WITH RPV HEAD CRACKING

4.1 Field Inspection Data (through Spring 2003)

RPV top head inspections have been conducted in U.S. PWRs since the mid-1990s. Initially, only a sampling of U.S. plants was inspected, in response to overseas cracking incidents. In 2001, when cracking and leakage began to be discovered in U.S. Plants, a more complete inspection program began to evolve, which primarily consisted of bare metal visual (BMV) examinations of the top head region, looking for evidence of boric acid residue (and thus RPV coolant leakage) in the annular regions between the nozzles and vessel head. When evidence of such leakage was detected, plants would proceed to non-visual NDE (ultrasonic or eddy current examinations) to verify the source(s). Eventually, as time progressed, and more degradation was detected, plants began to perform pre-emptive NDE, even when no evidence of leakage was present. In February 2003, the U.S. NRC issued an order requiring extensive NDE examinations in many plants, and a substantial number were performed in the Spring 2003 outage season. By the end of the Spring 2003, outage season, a total of 30 of the 69 U.S. PWRs had performed some form of NDE, of which 14 plants had detected leakage or some form of cracking.

U.S. plants have been prioritized for inspection using an approximate susceptibility ranking for top head nozzle cracking, which is based on a parameter known as Effective Degradation Years (EDYs). The definition of EDYs takes into account the widely accepted temperature dependence of the PWSCC cracking phenomenon. [11-13]. EDYs are effective operational years at a reference temperature of 600ºF, and are determined from plant effective full power years (EFPYs) at various head temperatures by the following expression:

$$EDY_{600°\mathrm{F}} = \sum_{j=1}^{n}\left\{\Delta EFPY_j \exp\left[-\frac{Q_i}{R}\left(\frac{1}{T_{head,j}} - \frac{1}{T_{ref}}\right)\right]\right\}$$

where:

$EDY_{600°\mathrm{F}}$	=	total effective degradation years through February 2001, normalized to a reference temperature of 600°F
$EFPYj$	=	effective full power years at head temperature j
Q_i	=	activation energy for crack initiation (50 kcal/mole)
R	=	universal gas constant (1.103×10^{-3} kcal/mol-°R)
$T_{head,j}$	=	100% power head temp. during time period *j* (°R = °F + 459.67)
T_{ref}	=	reference temperature (600°F = 1059.67°R)

n = number of different head temperatures during plant history

Figure 4-1 presents a summary of inspection results from U.S. PWR top heads through the Spring 2003 outage season. The data are plotted in terms of head operating temperature (horizontal axis), and number of effective full power years at the current head operating temperature (vertical axis). A few plants have operated at multiple head operating temperatures, in which cases the data are plotted at equivalent EFPYs at the current temperature using the above equation, but with the reference temperature set equal to the current head temperature for that plant instead of 600ºF. Data points in Figure 4-1 are differentiated by type of inspections performed (BMV or NDE), and inspection findings (clean, leaks, or cracks but no leaks). Also shown in Figure 4-1 are lines of constant EDY, plotted in accordance with the above equation. Since EDYs correspond to effective operating years at 600ºF, not surprisingly, the constant EDY curves go through their corresponding numbers of EFPYs at that temperature (i.e. The 10 EDY curve goes through 10 EFPYs at 600ºF.) Referring to the 10 EDY curve, it is seen that, in accordance with the above-described EDY algorithm, a plant operating at a 560ºF head temperature requires more than 50 years to accumulate the same effective degradation as a plant with a 600ºF head temperature would accumulate in ten years. This example illustrates the strength of the temperature dependence inherent in the EDY model.

Figure 4-1 illustrates that the above EDY model is corroborated quite well by plant inspection data to date. All plants that have observed leaks had head operating temperatures of 598ºF or greater, and all of the leakage data points (red triangles) are on or above the 15 EDY curve. Plants which have experienced cracks but not leaks (yellow squares in Figure 4-1) are also at the high temperature end of the population, and all are above the 10 EDY curve. Numerous low temperature (and low EDY) plants have performed visual examinations with no leakage observed. Most significantly, a total of 15 plants, of ages 8 EDY or greater, have performed non-visual NDE to date, with no indications of cracking.

4.2 Weibull Analysis of Time to Cracking or First Leak (w/extrapolation back)

For purposes of the Weibull analyses presented in this and subsequent sections, the population has been limited to just those plants that have performed non-visual NDE, and were either found clean or had leaks or cracks. Plants that performed only visual examinations and were found clean (blue diamond data points in Figure 4-1) are not included. Limiting the population in this manner is conservative, since it assumes that leaking or cracking may have been present and gone undetected by those visual exams.

Data for the 30 plants included in the Weibull analysis are listed in Table 4-1. The data include plant name, date of the most recent inspections, number of nozzles, number of nozzles with cracks or leaks, and EFPYs and EDYs at the time of inspection. The data are sorted by EDYs at the time of inspection, and have been used as the basis of a failure probability analysis, using a standard two-parameter Weibull cumulative distribution function [14] as follows:

$$F(t) = 1\text{-}EXP\ (-(t/\theta)^{\beta})$$

where: $F(t)$ = fraction of vessel heads with a leak or crack
t = time to most recent inspection (in EDYs)
θ = characteristic life or scale parameter
β = slope or shape parameter

Direct fitting of the data in Table 4-1 to the above two parameter Weibull distribution would lead to a very steep slope (i.e. a high value of the Weibull shape parameter β), since the data show only one plant with cracking at less than 13.9 EDYs, and a very high percentage of leakage or cracking for plants with 16 or more EDYs. However, it is argued that the data in Table 4-1 represent an "inspection transient". Since little or no top head inspections (especially NDE) were conducted in US plants before 2000, it is highly likely that the plants in Table 4-1 which experienced multiple cracks or leaks during the inspections had cracking present earlier in their operating lives that wasn't detected because of poor or no inspections. Also, based on other PWSCC experience in Alloy 600, including laboratory data and steam generator tube failures in PWRs, a Weibull slope of 3 is considered to be a reasonable value for this phenomenon. Specifically, Ref. [15] states: "A high value for the Weibull Slope β represents the case of little scatter such that all similar parts develop PWSCC over a relatively short period of time. Conversely, a low value of the Weibull slope represents the case of greater scatter and a longer time between PWSCC of the first and last parts. . . . A reasonable approach for predicting PWSCC initiation would be to use a Weibull slope of 3 for nominal predictions and then perform parametric analyses to assess the effects of Weibull slopes ranging from about 2 to 4."

Based on the above discussion, it was decided to employ a WeiBayes approach [14] to fit the data, assuming a Weibull slope of 3 ($\beta = 3$ in the above equation) as a baseline for the Weibull analysis, and to extrapolate the failure data in Table 4-1 back to the time at which cracking or leakage is first predicted to occur using this slope. The extrapolation process is illustrated in Table 4-2. The columns labeled "$CDF_{\text{1st Leak or Crack}}$" and "$CDF_{\text{\# Leaking or Cracked}}$" are the fractions of nozzles cracked or leaking, defined as follows:

$$CDF_{\text{1st Leak or Crack}} = (1 - 0.3) / (\text{\# of Nozzles} + 0.4)$$

and

$$CDF_{\text{\# Leaking or Cracked}} = (\text{\# Leaking or Cracked} - 0.3) / (\text{\# of Nozzles} + 0.4)$$

These fractions are inserted into the above two-parameter Weibull equation, assuming a slope of 3, to compute a "Time Factor" (seventh column in the table) for each of the plants in which leakage or cracking was observed. For example, for Millstone-2, in which 3 cracked nozzles (out of 69) were observed during an inspection performed at 11.2 EDYs., the fraction of nozzles cracked, in accordance with the second of the above equations, is 0.0389. If just one nozzle were cracked, the fraction, in accordance with the first of the above equations, would be 0.0101. Applying the Weibull equation with a slope of 3, the time to crack 1.01% of the nozzles is predicted to take only 0.6345 of the time necessary to crack 3.89% of the nozzles (time factor = 0.6345). Thus, since 3 nozzles were found cracked at 11.2 EDYs, it is predicted that the first cracked nozzle in the Millstone-2 head occurred at 7.11 EDYs (11.2 x 0.6345 = 7.11). This approach was used for each of the plants that had multiple cracked nozzles to determine the predicted times to 1st cracking listed in the last column of Table 4-2. The greater the number of cracked or leaking nozzles found, the smaller the time factor, and thus the greater the difference between inspection EDYs and predicted EDYs to first cracking. Conversely, for Crystal River-3, which had only one cracked nozzle during the 2001 inspection, the time factor is unity, and the time to first leakage is set equal to the time of inspection. From Table 4-2 it is seen that, although cracking or leakage was not observed in any plant until 11.2 EDYs, several plants are predicted to have experienced their first cracks between 7 and 8 EDYs. By "extrapolating back" in this manner, the analysis attempts to remove the effect of the inspection transient from the data.

Finally, the data in Table 4-2 were sorted by increasing values of the last column (time to inspection or 1st leak or crack), and used to develop a Weibull distribution for the data. The resulting Weibull plot is shown in Figure 4-2. The "extrapolated-back" EDYs at 1st cracking were curve fit via a median rank regression algorithm in Weibull graph coordinates, assuming a slope of 3, to determine the best fit straight line shown in Figure 4-2. The plants in Table 4-2 that were inspected and found clean were treated as "suspended items" in the analysis, in accordance with the standard approach described in Reference [14]. Two sets of data are plotted in Figure 4-2. The blue data-points represent the un-extrapolated data of Table 4-1, while the red points are the extrapolated data of Table 4-2. In selected cases, dashed lines are drawn connecting the data for a specific plant, so that one can see the effect of the extrapolation. It is seen from Figure 4-2 that the extrapolated data are fit very well by the Weibull line with a slope of 3, and result in a characteristic time to failure (1st cracked or leaking nozzle) of 15.2 EDYs. In fact, a two-parameter median rank regression of the extrapolated-back data yielded β = 3.35 and θ = 14.5 EDYs, with a correlation coefficient of 0.85, indicating that the WeiBayes assumption of a slope of 3 was reasonable. Further discussion of uncertainties in the Weibull distribution is presented in Section 4.4.

Plant	Date of Inspection	Head Temp (°F)	No. of Nozzles	# Nozzles w/Leaks or Cracks	EFPYs at Inspection	Temp. Factor	EDYs at Inspection
Sequoyah 1							
Indian Point 2							
Palo Verde 2							
Cook 1							
Palo Verde 1							
Millstone 2							
ANO-2							
Cook 2							
St. Lucie 2							
Beaver Valley 1							
Point Beach 1							
San Onofre 2							
San Onofre 3							
St. Lucie 1							
Indian Point 3							
Farley 2				Content Deleted – MRP/EPRI Proprietary Material			
Calvert Cliffs 2							
Crystal River 3							
Farley 1							
TMI 1							
Turkey Point 3							
Surry 1							
Davis-Besse							
North Anna 2							
Robinson 2							
ANO 1							
North Anna 1							
Oconee 3							
Oconee 1							
Oconee 2							
# Plants							
# Nozzles							

Table 4-1
Plant Inspection Data used in Weibull Analysis

Plant	No. of Nozzles	# Nozzles w/Leaks or Cracks	EDYs at Inspection	CDF 1st leak or Crack	CDF # Leaking or Cracked	Time Factor	EDYs at 1st Leak or Inspection
Sequoyah 1	Content Deleted – MRP/EPRI Proprietary Material						
North Anna 2							
Millstone 2							
Oconee 2							
Indian Point 2							
Beaver Valley 1							
TMI 1							
Oconee 3							
Cook 2							
ANO 1							
Surry 1							
Palo Verde 2							
Cook 1							
Davis-Besse							
St. Lucie 2							
North Anna 1							
Palo Verde 1							
ANO-2							
Point Beach 1							
Oconee 1							
San Onofre 2							
San Onofre 3							
St. Lucie 1							
Indian Point 3							
Farley 2							
Calvert Cliffs 2							
Crystal River 3							
Farley 1							
Turkey Point 3							
Robinson 2							
# Plants							
# Nozzles							

Table 4-2
Plant Inspection Data Extrapolated Back to Predicted Time to First Leak (Based on Weibull β = 3)

4.3 Weibull Analysis of Fraction of Nozzles Cracked

An alternative approach to performing Weibull analysis of the plant inspection data is to treat each plant that has experienced cracking as a separate test, consisting of the number of samples (nozzles) in that plant. In this approach, the vertical axis of the Weibull plot is cumulative fraction of nozzles cracked at each plant that has experienced leakage or cracking (sixth column in Table 4-2). The resulting Weibull plot is shown in Figure 4-3. Once again the WeiBayes approach has been used, assuming a slope of 3. In this approach, however, it is not possible to include suspensions (plants which inspected and were found clean). These data are shown as the green triangles in Figure 4-3 for information, conservatively assuming one nozzle cracked at each plant (since they could not be plotted at zero) but they were not included in the Weibull regression analysis.

The resulting Weibull characteristic time to failure (θ) in Figure 4-3 is 43.2 EDYs, considerably longer than that in Figure 4-2. However, in Figure 4-3, the probabilities are on a per nozzle rather than a per head basis, and the two should be related by the Binomial distribution. If one has a probability p_1 of failure per nozzle, and there are N nozzles in a head, then the probability of at least one failure in the head at any given time is higher than p_1. It can be shown than the Weibull parameter θ for the two approaches can be related as follows, based on the Binomial distribution:

$$\theta_{\text{1st leak}} = \theta_{\text{fraction cracked}} / N^{1/\beta}$$

For a plant with 69 nozzles (such as the majority of those in the data base) $\theta_{\text{fraction cracked}}$ should be approximately 4.1 x $\theta_{\text{1st leak}}$ ($69^{1/3} = 4.1$). Thus the mean $\theta_{\text{1st leak}}$ of 15.2 from Figure 4-2 should correspond to a mean $\theta_{\text{fraction cracked}}$ of 62.3 in Figure 4-3. However, it is reasonable to expect the Weibull fit in Figure 4-3 to be more conservative, since it does not include the suspensions (green triangles). If these were included in the regression, with the conservative assumption that they all had one cracked nozzle, the Weibull line would obviously move to the right, and possibly even go through θ of ~62 at the CDF of 0.63.

Other observations regarding Figure 4-3 is that it has considerably more scatter than Figure 4-2 – the resulting curvefit had a correlation coefficient of 0.65, versus 0.85 for Figure 4-2. This is most likely due to the fact that the inspection transient has not been removed. Therefore, the time to first leak Weibull approach of Figure 4-2 has been incorporated into the PFM model.

4.4 Uncertainties in Weibull analysis

The median rank regression has also been used to establish statistical bounds on the Weibull analysis. The mean θs discussed above represent a weighted average for the collection of heads included in the database. Standard deviations of the data have also been computed and Weibull lines corresponding to plus and minus 1.65 standard deviations from the mean are shown in Figures 4-4 and 4-5. These correspond approximately to 5% and 95% confidence bounds. (I.e. in Figure 4-4 we are 95% confident that the mean value of θ is greater than 10.9 EDYs.) These bounds are used as maximum and minimum of a triangular distribution of the Weibull model for time to first leakage or cracking in the PFM analysis. The effect of Weibull θ is also studied extensively in the sensitivity and benchmarking studies described in Section 8.

Studies were also performed on the variability in the Weibull slope parameter β since it is also a key assumption in the analysis. The model was iterated using various values of β to extrapolate back to time to first leakage, and then the extrapolated data were used to perform a two-parameter Weibull fit. By iterating in this manner, one can test the model for convergence to a single value of β. It was found that two different βs result, depending on whether one treats EDYs or CDF as the independent variable (i.e. fitting Y on X or X on Y in the curvefit). Treating EDYs as the independent parameter (Y on X) results in a converged value of 4.48 for β. Treating CDF as the independent parameter (X on Y) converges to 3.46, but the process is not universally convergent. In Reference [14], regression of X on Y is recommended as best practice for in-service failure data, since the X variable (EDYs) typically is subject to much larger statistical scatter than the Y variable. Therefore, 3.46 is the best estimate and agrees reasonable well with the WeiBayes assumption of 3.0. Nonetheless, sensitivity studies are presented in Section 8 for β values of 3.46 and 4.48.

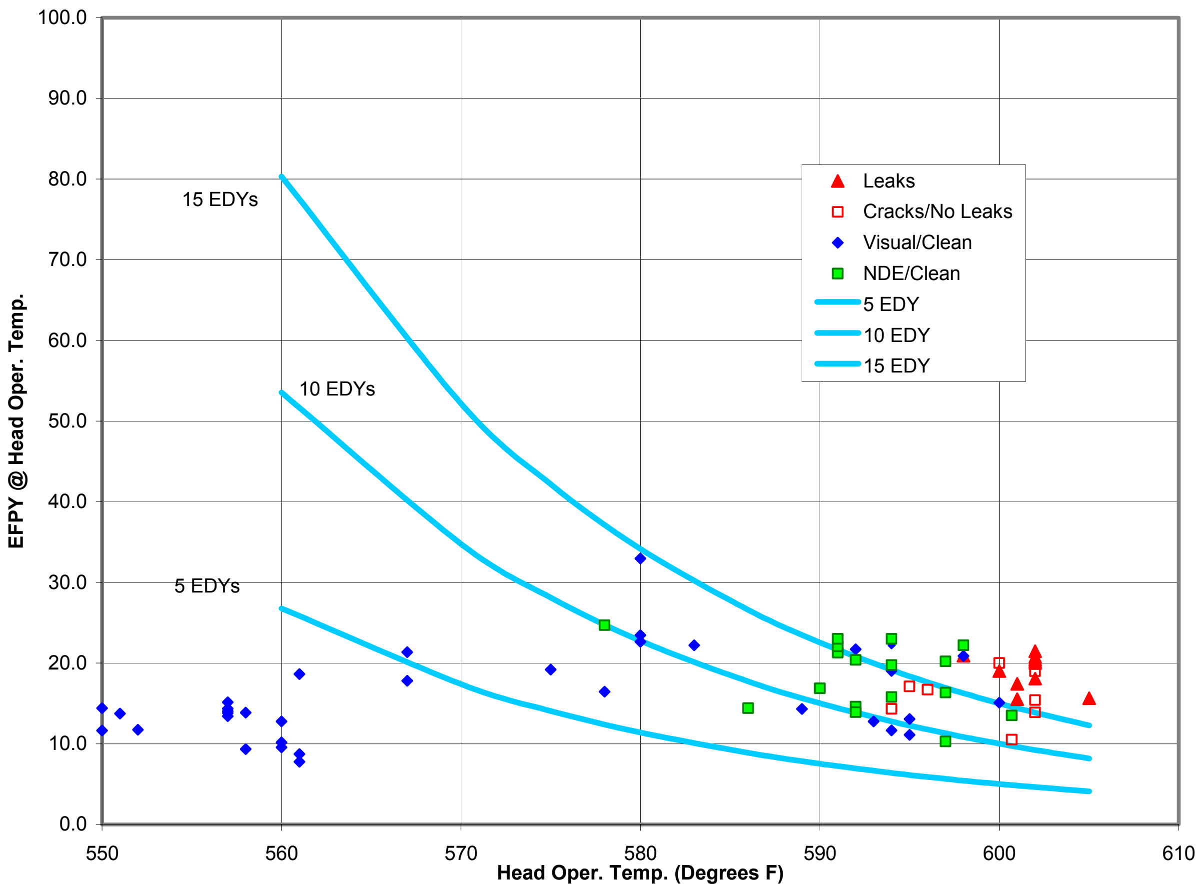

Figure 4-1
Summary of RPV Top Head Inspection Results in Terms of Years of Operation at Various Head Operating Temperatures. Constant EDY Curves Indicated

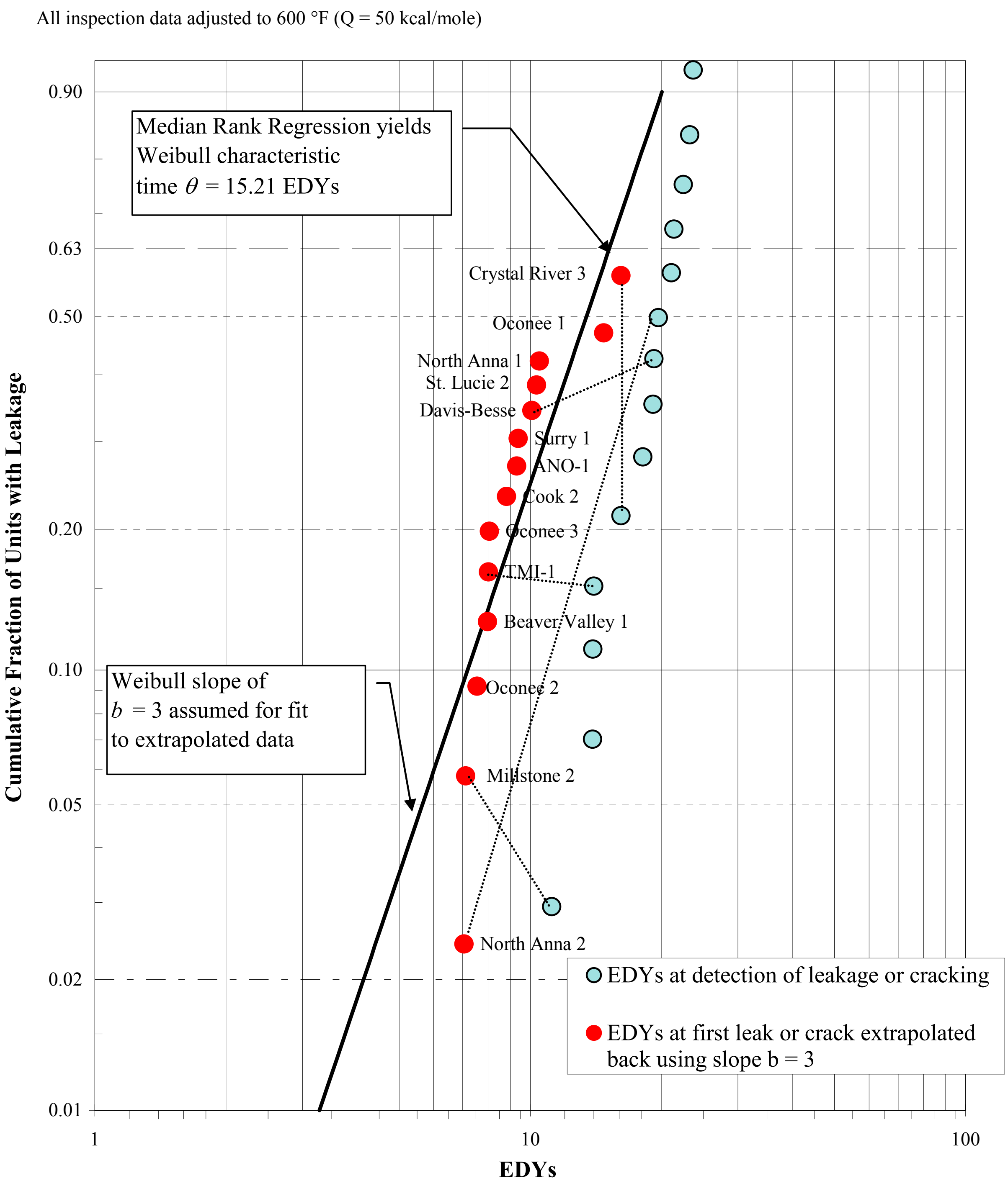

Figure 4-2
Weibull Plot of Plant Inspection Data Showing Extrapolation Back to Time of First Leakage or Cracking. Plants that Performed NDE and were found clean are treated as suspensions.

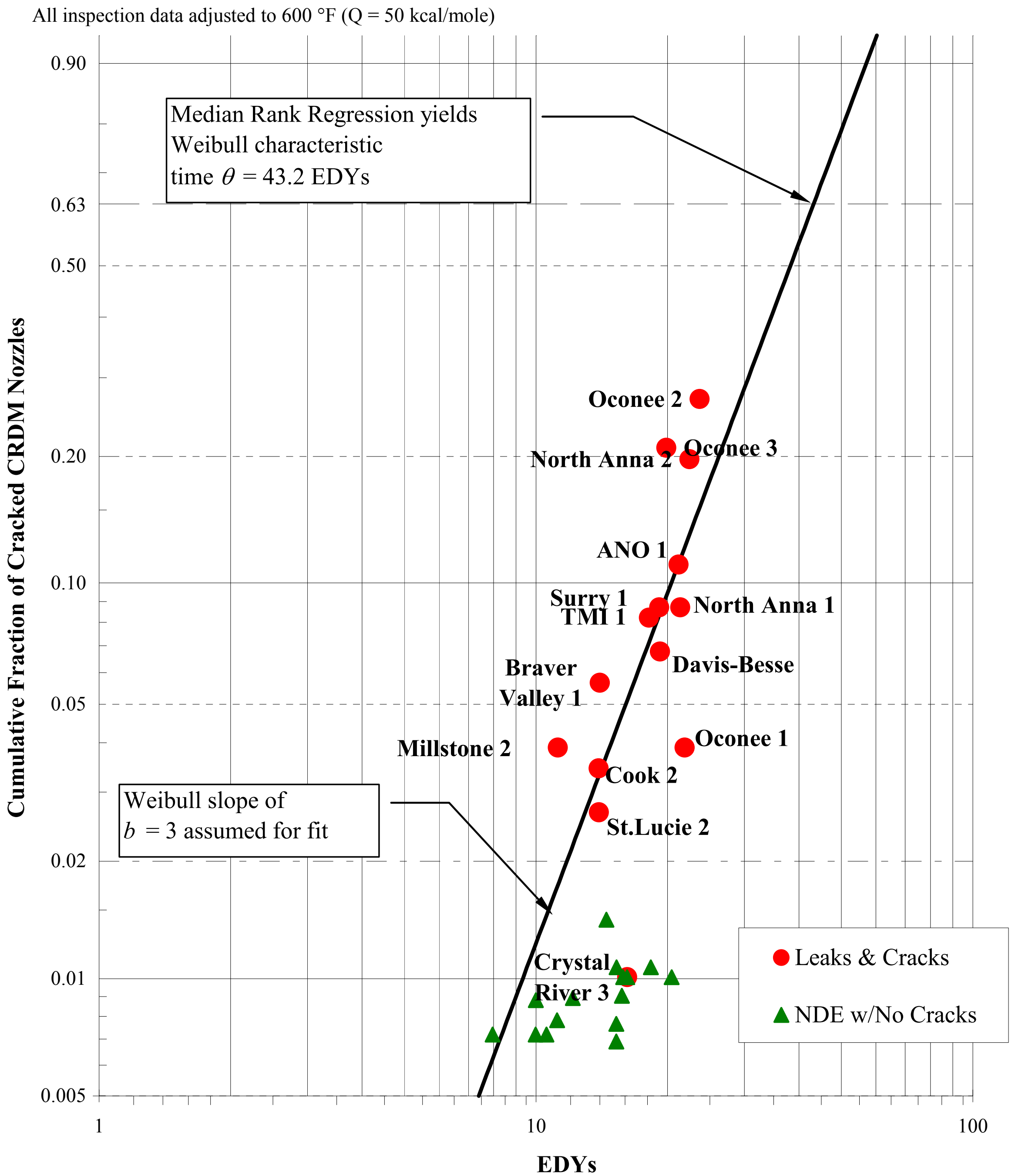

Figure 4-3
Weibull Plot of Plant Inspection Data Based on Fraction of Nozzles Cracked

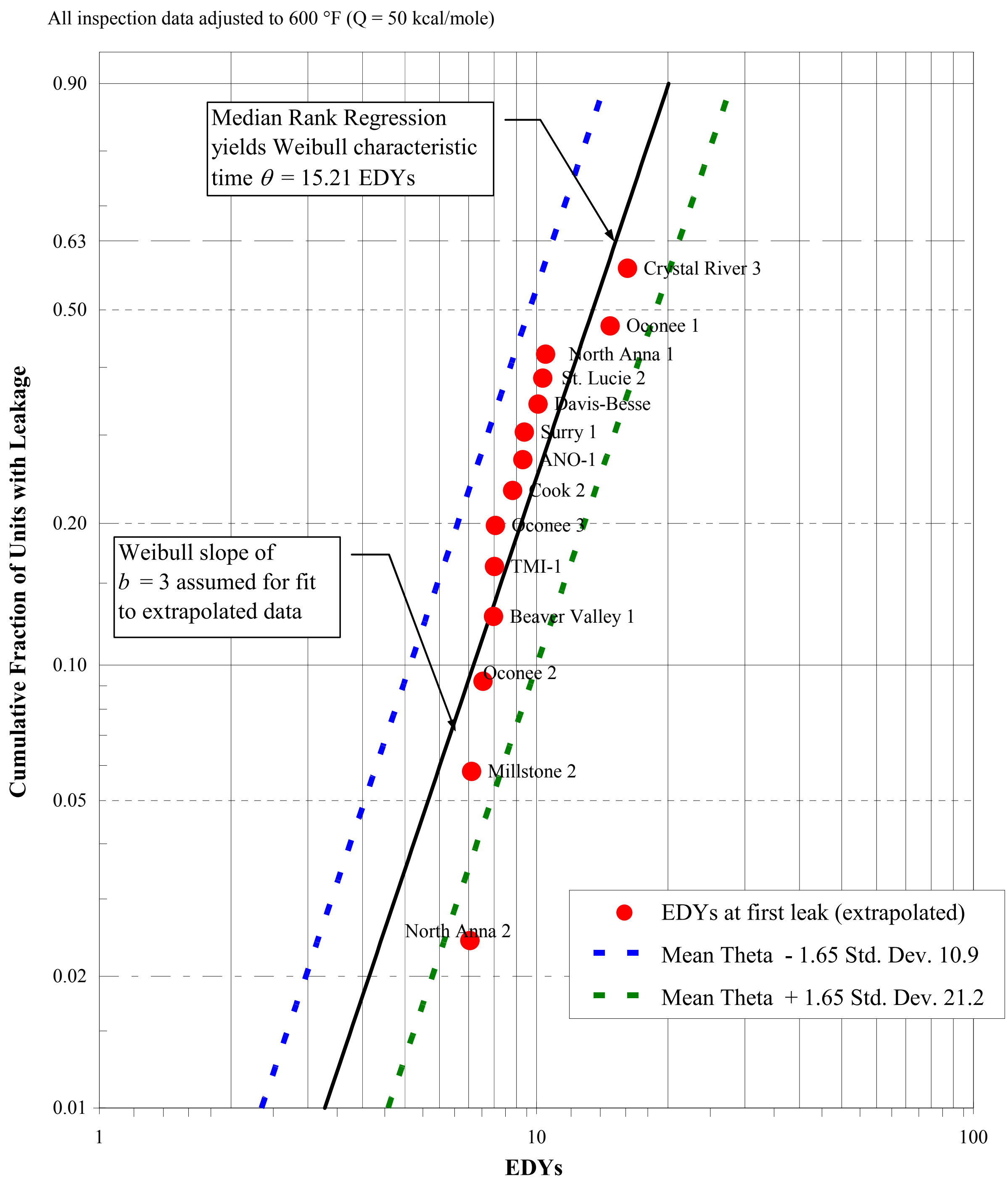

Figure 4-4
Weibull Plot of Time to 1st Leakage Data Showing Uncertainty Bounds

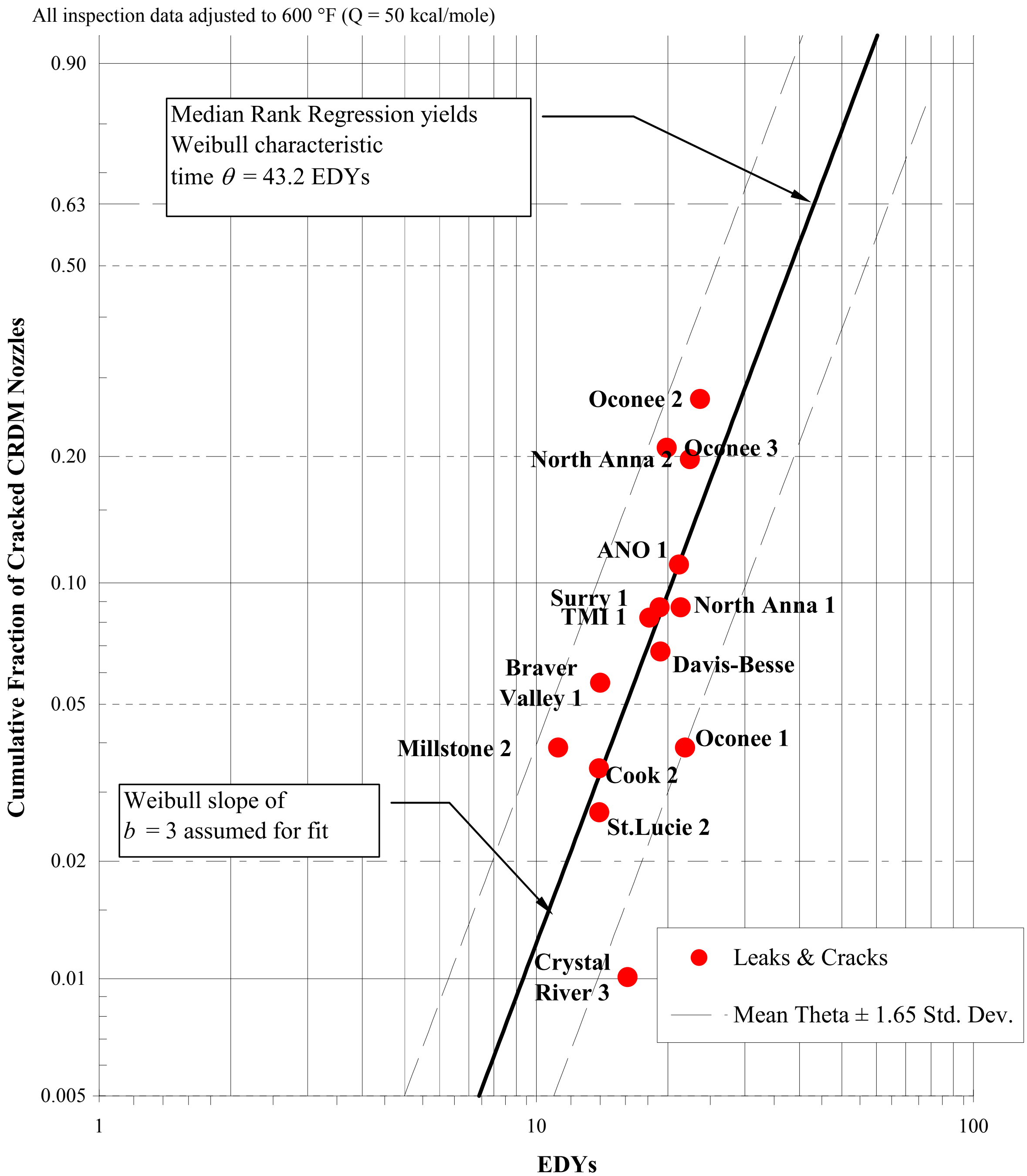

Figure 4-5
Weibull Plot of Fraction of Nozzles Cracked Data showing uncertainty bounds

5
CRACK GROWTH RATES

5.1 Crack Growth Rate Data

Reference [11] presents an extensive compilation of PWSCC crack growth rate data for Alloy 600 material in the PWR primary coolant environment. The data are from controlled testing of 156 fracture mechanics specimens fabricated from 26 heats of CRDM nozzle, thick-wall tube, rolled bar, and forged bar material and 4 heats of plate material. Data are included from tests conducted at Westinghouse in the U.S., Studsvik in Sweden, EDF and CEA in France, and CIEMAT in Spain. Only tests that incorporated careful control of applied load (stress intensity factor) and temperature as well as accurate measurement of crack growth rates (CGR) were considered. The data were reviewed by an EPRI-MRP CGR review team comprising an international panel of experts in the area of SCC crack growth. These data form the basis for a statistical analysis performed herein, to develop statistical distributions of crack growth rates for use in the PFM analyses.

5.2 Temperature and K Dependence

There is general agreement [11] that crack growth in Alloy 600 materials in the primary water environment can be modeled using a power law stress intensity factor relationship with differences in temperature accounted for by an activation energy (Arrhenius) model for thermally controlled processes:

$$\dot{a} = \exp\left[-\frac{Q_g}{R}\left(\frac{1}{T} - \frac{1}{T_{ref}}\right)\right]\alpha\left(K - K_{th}\right)^{\beta} \qquad [2]$$

where:

$\dot{a}$	=	crack growth rate at temperature T in m/s (or in/hr)
Q_g	=	thermal activation energy for crack growth
	=	130 kJ/mole (31.0 kcal/mole)
R	=	universal gas constant
	=	8.314×10^{-3} kJ/mole·K (1.103×10^{-3} kcal/mole·°R)
T	=	absolute operating temperature at location of crack, K (or °R)
T_{ref}	=	absolute reference temperature used to normalize data
	=	325ºC = 598.15ºK (617ºF = 1076.67°R)

(Note: Reference temperature for crack growth from Ref. 11 is approximate mean test temperature of the data, and differs from the reference temperature used in Section 4 to characterize plant inspection data)

α	=	crack growth amplitude
K	=	crack tip stress intensity factor, MPa $\sqrt{m}$ (or ksi $\sqrt{in}$)
Kth	=	crack tip stress intensity factor threshold
	=	9 MPa $\sqrt{m}$ (8.19 ksi $\sqrt{in}$)
β	=	exponent
	=	1.16

5.3 Statistical Distributions

The data from Reference [11] are plotted in Figures 5-1 and 5-2 in the form of distributions of the power law constant α in the above equation, plotted at the reference temperature of 617ºF (1076.67°R) in units of in/hr for CGR and ksi√in for K. The data points in Figure 5-1 are the log-mean αs for each of the 26 heats. The data set includes varying numbers of specimens per heat, ranging from 1 to 32. The data points in Figure 5-2 represent the 158 individual data points plotted as ratios to the means of their respective heats.

Two types of statistical distributions have been developed for the PFM analyses, log-normal and log-triangular. For both distribution types, separate distributions were developed for heat-to-heat variation (based on the log-means of the 26 heats in Figure 5-1), and within-heat variability (based on the ratios of the 158 data points to the log-means of their respective heats in Figure 5-2). The log-normal distribution of the heat-to-heat data was developed by computing the mean and standard deviation of the log-means of the power law constants (α) for each heat. The log-normal distribution for within heat variability was developed by computing the mean and standard deviation of the log of the ratio of each data point to the mean of its heat. The log-triangular fits were determined by curve-fitting a log-triangular function to the above log-normal distributions between fixed end-points, as illustrated in Figures 5-3 and 5-4. In the case of heat-to-heat variation (Figure 5-3), the curve-fit was performed between fixed end-points approximately 2 standard deviations above and below the mean, while in the case of within-heat variation the fixed endpoints were approximately 2.7 standard deviations above and below the mean.

The resulting log-normal and log-triangular distribution parameters are summarized in Table 5-1. They are also shown graphically in Figures 5-1 and 5-2. As indicated by the text boxes at the upper ends of the curves in the two figures, the maximum crack growth rates predicted by the log-triangular distributions are well above the maximum measured crack growth rates in any of the experiments. Specifically, the highest value of α measured in any of the 158 crack growth experiments was 3.19 x 10-6, while PFM computations using the log-triangular distributions of Figures 5-1 and 5-2 will occasionally select a value of α more than twice that value, or 7.6x10-6 (a factor of 36 greater than the median of the data). The Log-Normal distributions are of course unlimited, and PFM computations using these will occasionally select highly unrealistic (and physically unachievable) crack growth rates.

	Log-Normal Distributions for α			
	Log Mean	Log σ	Mean	Mean + nσ
Heat-to-Heat	Content Deleted – MRP/EPRI Proprietary Material			
Within-Heat Ratio				
Heat-to-Heat				
Within-Heat Ratio				
Exponent				
Ref. Temp				
Act. Energy				
K threshold				
Notes:	Content Deleted – MRP/EPRI Proprietary Material			

Table 5-1
Summary of Parameters in Crack Growth Rate Statistical Distributions

An important observation is noted in Ref. [11] concerning the distribution of CGR variability developed by the MRP. Either a French supplier or B&W Tubular Products supplied all the top 12 tested heats in terms of highest CGRs. (These are, incidentally, the materials, which have exhibited the most cracking in the field.) The tested heats from other suppliers displayed lower CGRs, with log-mean power-law constants over the range from the minimum heat value to just above the distribution mean. Therefore, it is likely that components—such as RPV head nozzles—supplied by some material vendors may tend to crack at a considerably lower growth rate than indicated by the full MRP database of CGR tests. There were insufficient data to confirm this conclusion, however, so a single CGR distribution was adopted in this work.

5.4 Environmental Factors

The EPRI-MRP CGR review team also conducted an extensive study of the potential for severe environmental conditions, which might affect cracks growing from the annulus region between a penetration and the upper head. The group concluded [11] that the most likely environments responsible for stress corrosion cracking of Alloy 600 in the annulus are either hydrogenated, superheated steam or normal PWR primary water. Based on laboratory tests, it was concluded that the CGRs in the possible hydrogenated, superheated steam environment would be similar to those in normal PWR primary water at the same temperature.

Oxygen from air cannot penetrate significantly into the crevice between the CRDM nozzle and the upper head penetration and is not relevant to the practical problem.

If the boiling interface happens to be close to the topside of the J-weld, itself a low probability occurrence, concentration of PWR primary water solutes, lithium hydroxide and boric acid, can in principle occur. However, the group concluded that the potential effect of the slightly elevated pH due to the concentrated PWR environment is small compared to the scatter observed in the database of laboratory CGR data reported in [11]. Therefore, for purposes of the PFM work reported here, the CGRs and statistics for laboratory tests performed in normal primary water are used as the basis for evaluation of the growth of SCC flaws exposed to the annular crevice environment between RVH nozzles and the reactor upper head.

However, for the deterministic crack growth studies reported in Section 6, a multiplicative factor of 2 was applied to the 75th percentile of the data, in keeping with the MRP recommendations for deterministic crack growth analysis of OD flaws.

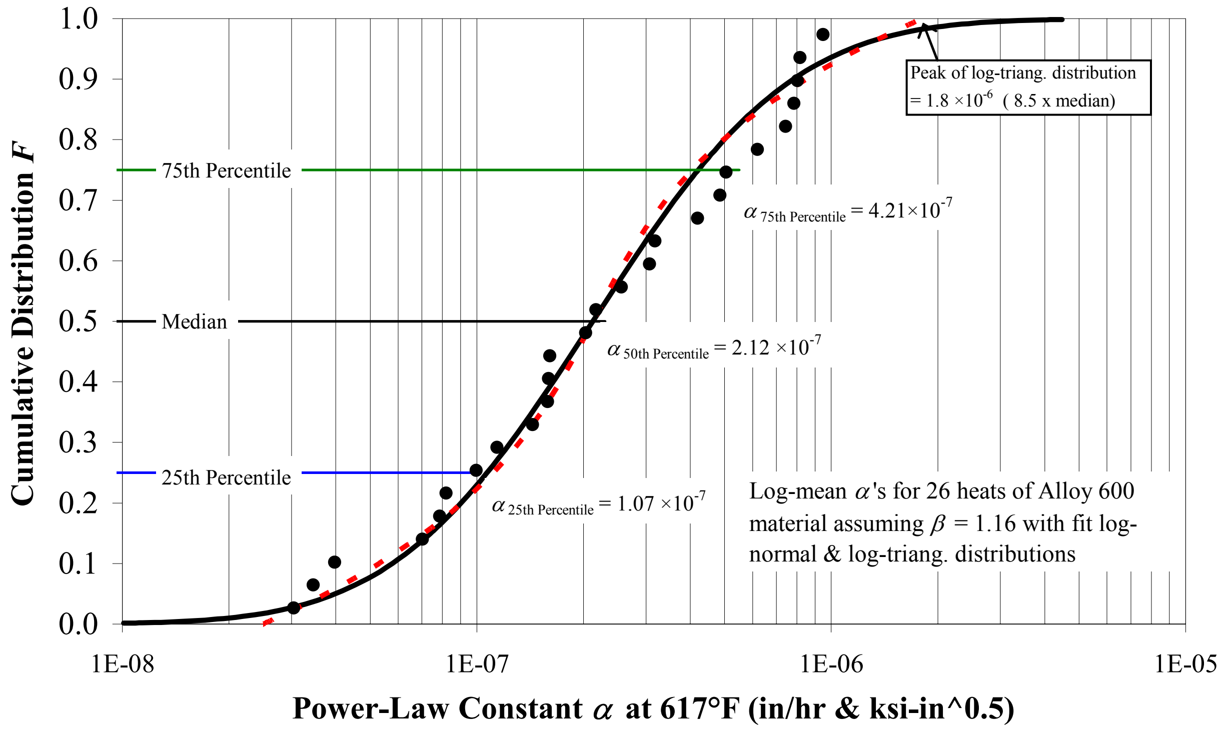

Figure 5-1
Distribution of Log-Mean CGR Power Law Constant for the 26 Heats of Material Reported in Ref. [11]. Log-Normal and Log-Triangular Fits to the Data also Shown

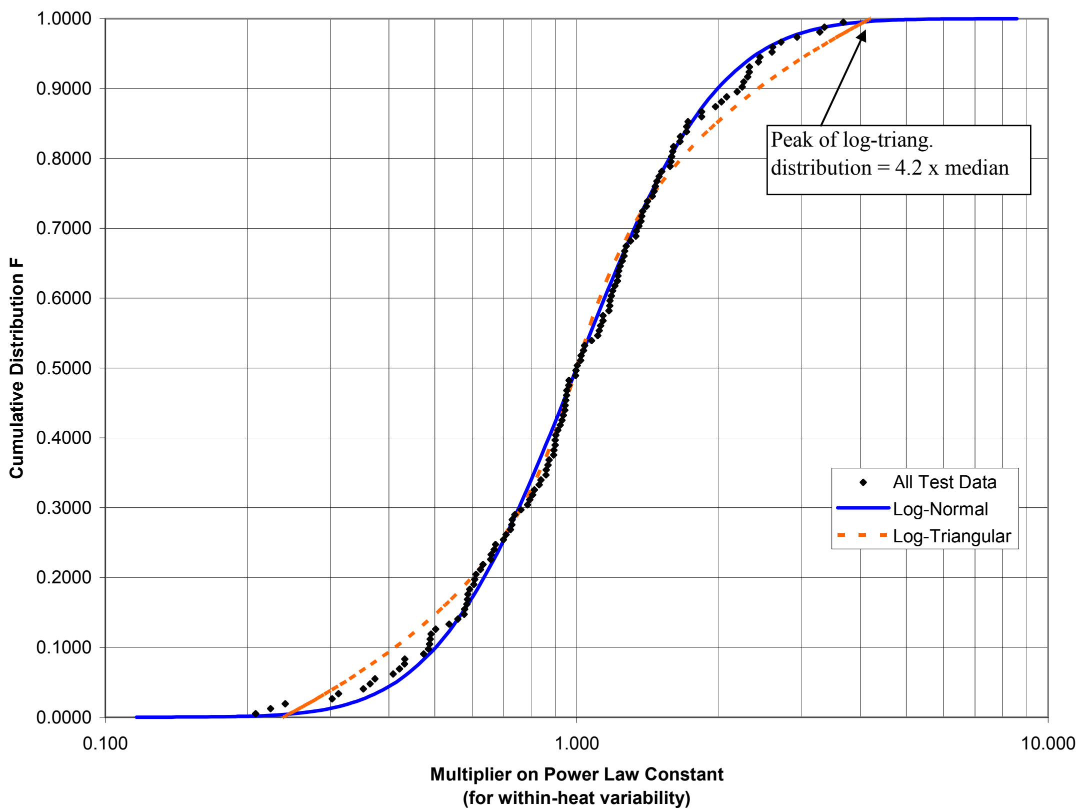

Figure 5-2
Distribution of 158 Individual Data Points from Ref. [11] Plotted Relative to the Means of their Respective Heats. Log-Normal and Log-Triangular Fits to the Data also Shown

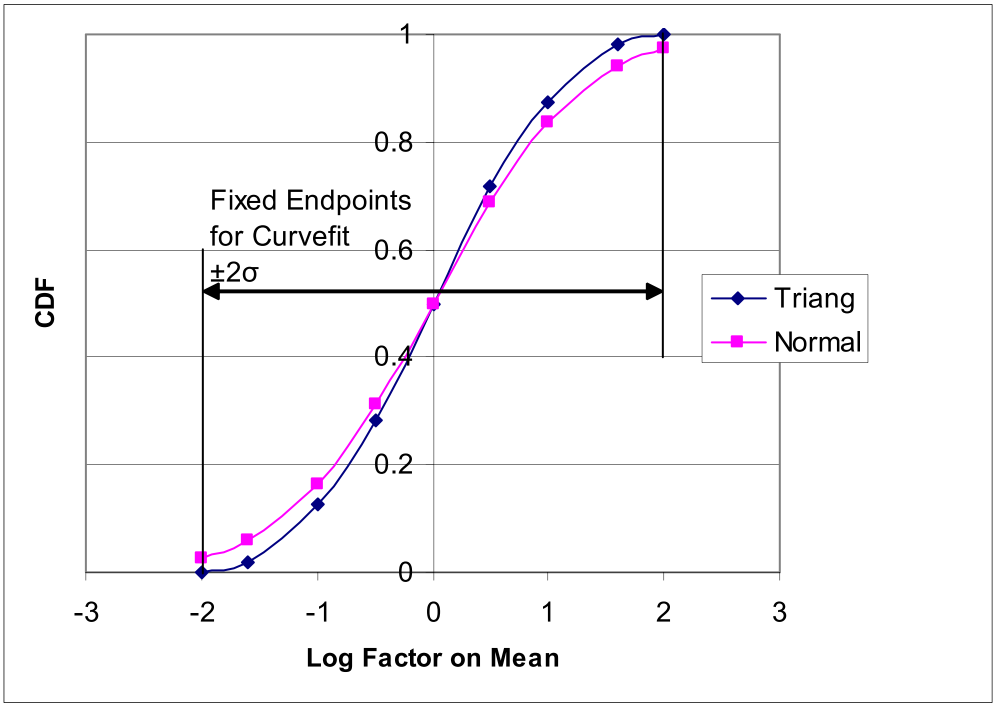

Figure 5-3
Illustration of curve-fit used to develop Triangular Distribution for Heat-to-Heat Variation

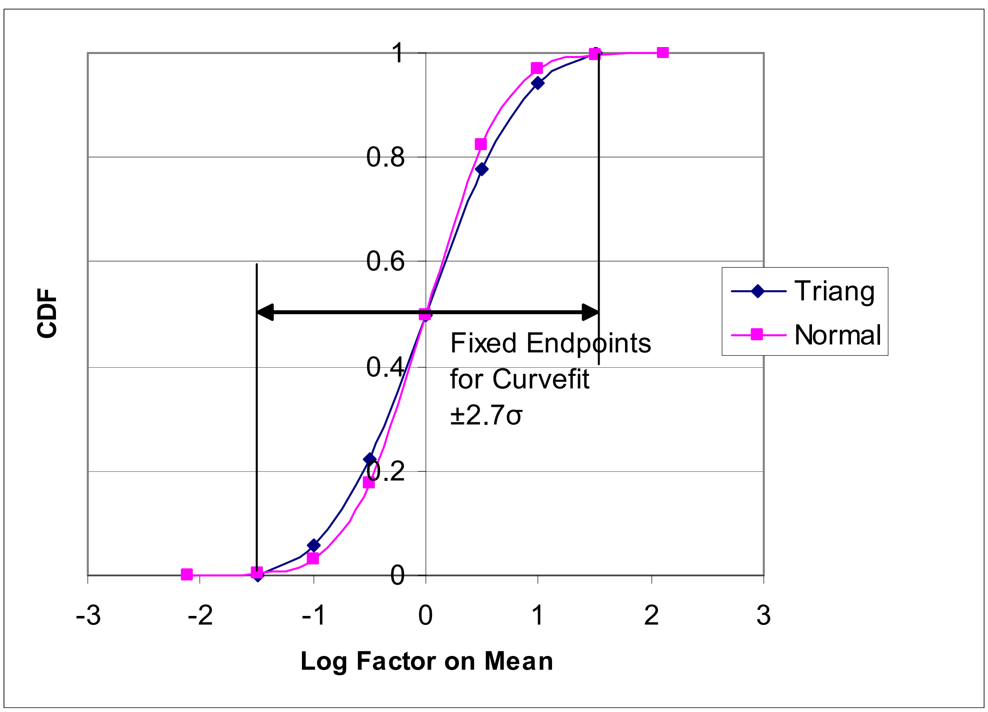

Figure 5-4
Illustration of curve-fit used to develop Triangular Distribution for Within-Heat Variation

6
DETERMINISTIC CRACK GROWTH ANALYSIS

In addition to the previously discussed statistical treatment of the crack growth data, MRP-55 [11] also contains recommended crack growth correlations for deterministic analysis of Alloy-600 RPV head nozzles. These are summarized for several assumed head operating temperatures in Table 6-1. These crack growth correlations were used in conjunction with the SI computer program **pc-CRACK** [16] to perform PWSCC crack growth calculations for initial through-wall circumferential flaws in the nozzles assumed to exist at the top edge of the J-groove welds. Initial flaw lengths corresponding to a 30° sector of the nozzle circumference, measured at an angle parallel to the root of the J-groove weld, were assumed. Crack lengths in inches corresponding to crack angles ranging from 30º to 300º for the most limiting (largest) nozzle intersection angles are listed in Table 6-2. Calculations were performed for assumed cracks centered at both the uphill and downhill azimuths.

TEMPERATURE (°F)	COEFFICIENT (ANNULUS)	EXPONENT
Content Deleted – MRP/EPRI Proprietary Material		

Table 6-1
Deterministic PWSCC Crack Growth Correlations vs. Temperature for Above Weld Annulus Region (including severe environmental factor of 2) from [11]

Crack Length (Degrees)	Crack Length, Inches							
	Plant A 38º Nozzle		Plant B 43.5˚ Nozzle		Plant C 48.8˚ Nozzle		Plant D 49.7º Nozzle	
	L	½ L	L	½ L	L	½ L	L	½ L
30	Content Deleted – MRP/EPRI Proprietary Material							
90								
160								
180								
220								
260								
300								

Table 6-2
Flaw Length Correlations, Degrees and Inches, For Limiting Nozzles

Stress intensity factor results reported in Section 3.3 above for through-wall circumferentially oriented cracks in the limiting (steepest angle) nozzles of the four characteristic plant types were used, as summarized in Figures 3-12 – 3-18. These stress intensity factor results consider envelope stress distributions of bounding residual and applied stresses above the weld, for the limiting (highest angle) nozzles, expressed in terms of K at various crack angles ranging from 30 to 300 degrees.

In accordance with Section 3.5 above, 300° corresponds generally to the greatest flaw length for which the ASME Section XI, IWB-3600 factors of safety are maintained for all nozzle types (Table 3-3). The above-weld annulus flaw growth correlations in Table 6-1 for 580, 590, 600, 602, and 605°F top head temperatures were used. Analysis details are described in Reference [17].

Calculations were performed for uphill and downhill-centered flaws, for the limiting (most outboard) nozzles, for the four characteristic plant types. Results are presented in terms of time required to grow from the assumed initial flaw size (30°) to the allowable size (300°), in Tables 6-3, 6-4, 6-5, and 6-6, in units of both effective full power hours and effective full power years. One EFPY equals 8760 EFPH.

The tabulated stress intensity factor results were input to pc-CRACK [16] in the form of user defined K vs. crack size tables, since the tables are from finite element modeling which gives an inherently more accurate representation of the complex nozzle / vessel head geometry than the crack models in pc-CRACK. The temperature specific PWSCC growth correlations as defined above were used to determine time to allowable for each temperature. A factor of two was applied as noted in Table 6-1, as recommended in MRP-55 [11] to address the potentially more aggressive environment on the CRDM annulus region.

Table 6-5 shows that further growth of an initial 30-degree crack in Plant C on the uphill side of the nozzle is not predicted at any temperature. This is because the applied stress intensity factor at the initial flaw size of 30 degrees is predicted to be lower than the threshold value for growth, (8.19 ksi-√in), as reported in the MRP-55 crack growth formulation [11].

In these analyses, because the assumed flaw is double ended, growth is assumed to occur simultaneously from both crack tips. To address this, growth is determined for a half-length flaw (see Table 6-2) to a half-allowable size, using the calculated stress intensity factors from Section 3 and the temperature dependent PWSCC crack growth correlations described above. The resulting initial and final flaw sizes and growth times are equivalent to a flaw growing at both ends.

TEMPERATURE °F	UPHILL (EFPH)	UPHILL (EFPY)	DOWNHILL (EFPH)	DOWNHILL (EFPY)
580	258177	29.47	322569	36.82
590	199476	22.77	249227	28.45
600	154874	17.68	193501	22.09
602	147314	16.82	184056	21.01
605	136709	15.61	170805	19.50

Table 6-3
Growth Time from 30° to 300° Circumferential Crack
Plant A - 38° Nozzle

TEMPERATURE °F	UPHILL (EFPH)	UPHILL (EFPY)	DOWNHILL (EFPH)	DOWNHILL (EFPY)
580	903711	103.16	158317	18.07
590	698237	79.71	122321	13.96
600	521114	61.89	94970	10.84
602	515652	58.86	90335	10.31
605	478529	54.63	83831	9.57

Table 6-4
Growth Time from 30° to 300° Circumferential Crack
Plant B 43.5° Nozzle

TEMPERATURE °F	UPHILL (EFPH)	UPHILL (EFPY)	DOWNHILL (EFPH)	DOWNHILL (EFPY)
580	no growth	no growth	135981	15.52
590	no growth	no growth	105563	11.99
600	no growth	no growth	81572	9.31
602	no growth	no growth	77590	8.86
605	no growth	no growth	72004	8.22

Table 6-5
Growth Time from 30° to 300° Circumferential Crack
Plant C – 48.8° Nozzle

TEMPERATURE °F	UPHILL (EFPH)	UPHILL (EFPY)	DOWNHILL (EFPH)	DOWNHILL (EFPY)
580	279167	31.87	273879	31.26
590	215694	24.62	211608	24.16
600	167465	19.12	164293	18.75
602	159291	18.18	156274	17.84
605	147823	16.87	145023	16.56

Table 6-6 Growth Time from 30° to 300° Circumferential Crack
Plant D – 49.7° Nozzle

In summary, deterministic crack growth calculations have been performed for various CRDM top head nozzle designs to determine the predicted times for an assumed 30º of circumference flaw to grow to the ASME Section XI allowable flaw size. The calculations were performed for various RPV head operating temperatures ranging from 580º F to 605ºF. These calculations predict crack propagation times for a crack to grow from the assumed initiation size (30º) to the critical size at which Section XI margins are exceeded (300º) ranging from 8.22 EFPY for the highest stressed, highest temperature head to more than 50 EFPY for lower temperature heads.

7 PFM COMPUTATIONAL ALGORITHM

7.1 Monte Carlo Simulation

The *MRPERCRD* computer program developed for this evaluation uses probabilistic fracture mechanics (PFM) with Monte Carlo simulation to calculate the reliability of PWR top head nozzles. The program evaluates the probability of leakage and the probability of failure due to Net Section Collapse (NSC). The random variables in the probabilistic fracture mechanics analysis are identified below. Each random variable is described by its distribution type, its mean and a measure of its variability (standard deviation or range, depending on the distribution type). Some properties, such as crack growth rates and times to leakage or cracking have two components of variability, one for heat-to-heat variation and a second for within-heat variation. For each analysis, the user specifies the number of heats of nozzle material in the vessel head, and a heat number for each nozzle. Individual nozzles from the same heat of material use the same value in each top head simulation for heat-to-heat random variables, but different values of the random variables that vary within a heat. The random parameters are determined with a random number generator for each simulation. The effect of different combinations of these variables on the leakage or failure probability of the top head can be studied through a large number of simulations, (i.e. the Monte Carlo Method). Each of these Monte Carlo simulations represents a single deterministic analysis of crack initiation and growth versus time, with a single set of random variables determined as described above. The *MRPERCRD* analysis algorithm consists of two nested Monte Carlo simulation loops, which step through time for each nozzle in a head, and then for the total number of head simulations specified.

Failure probability of the vessel top head at any given time is computed as the number of simulated top heads for which failure is predicted up to that time, divided by the total number of simulated top heads in the Monte Carlo simulations. Failure is defined as leakage, net section collapse of the nozzle or development of a large circumferential crack (size defined by the user), and the program computes and prints out results for each of these versus time. The program computes and prints these probabilities on a cumulative (CDF) basis as well as on an incremental (PDF) basis for time intervals specified by the user. Results are computed and printed out on both a “per nozzle” and a “per head” basis.

The probability of leakage for a top head is defined as:

$$PoL_{top\ head} = \frac{\begin{array}{c}Number\ of\ top\ heads\ with\ 1\ or\ more\ leaking\ nozzles\\ excluding\ top\ heads\ with\ nozzles\ failed\ by\ NSC\end{array}}{Total\ number\ of\ top\ heads}$$

The probability of leakage for nozzles is defined as:

$$PoL_{nozzle} = \frac{Number\ of\ \ leaking\ nozzles}{Total\ number\ of\ nozzles}$$

The probability of failure (NSC) for top heads is defined as

$$PoF_{top\ head} = \frac{Number\ of\ top\ heads\ with\ 1\ or\ more\ nozzles\ \ failed\ by\ NSC}{Total\ number\ of\ top\ heads}$$

The probability of failure (NSC) for nozzles is defined as

$$PoF_{nozzle} = \frac{Number\ of\ \ nozzles\ \ failed\ by\ NSC}{Total\ number\ of\ nozzles}$$

The required number of Monte Carlo simulations for any run depends on the expected failure probability of the top head. A large number of simulations is required if the failure probability is anticipated to be very small.

7.2 Key Random Variables

Probability of Leakage

The probability of leakage is established from the Weibull analysis of plant inspection data described in Section 4 above. It is assumed that nozzle leakage by a specific time is governed by the vessel top head temperature and activation energy, [1]. The leakage time is approximated by a two- parameter Weibull cumulative probability distribution,

$$F(x) = 1 - \exp((-(t/\theta) * TF)^{\beta}) \tag{1}$$

where t = leakage time in equivalent full power year (EFPY)
θ = Weibull scale parameter
β = Weibull slope or shape parameter
TF = temperature effect factor based on Arrhenius correction
$= \exp(\frac{Q}{R}(\frac{1}{T_n} - \frac{1}{T_o}))$
Q = activation energy (Kcal/mole)
R = 1.103x10-3 Kcal/mole -°R
Tn = reference vessel top head temperature (°R)
To = operating vessel top head temperature (°R)

The reference vessel top head temperature is assumed to be 600 °F (1059.67 °R).

Although the probability of leakage is formulated as time and temperature dependence only, it is implicitly implied that cracks are initiated at or near the J-groove weld. These cracks propagate, due to the PWSCC, such that leakage begins when the crack extends completely through the CRDM nozzle or J-groove weld from the bottom (top head inside surface) to the top of the J weld or from the nozzle ID to the nozzle OD. In addition, the amount of leakage is assumed to depend on the extent of shrink fit between the nozzle and the vessel top head.

Nozzles manufactured from the same heat of material are likely to have crack initiation or leakage times defined by the same distribution. Therefore, the implementation of this effect in the *MRPERCRD* code is that one random number is used to select the Weibull distribution for that heat from a triangular distribution of Weibull θ input by the user (via a mode, a maximum, and a minimum). This random number is used to determine a specific Weibull curve that all nozzles from that heat will be assumed to follow. For nozzles within that heat of material, the local variability on the leakage time is done by a different random number for each nozzle, to obtain the local variation on time to failure for that individual nozzle.

The above equation provides only the probability of leakage or cracking in a top head for a specific time in EFPY. It does not provide any information on which nozzle is leaking and at what time that nozzle starts leaking. The following provides an algorithm to determine the leaking time for an individual nozzle in a top head. The probability of leaking in an individual nozzle in a top head is assumed to follow a binominal distribution.

$$F(x) = \sum_{k=0}^{x} b(k;n,p) = \sum_{k=0}^{x} \binom{n}{k} p^k q^{n-k} \tag{2}$$

where n = number of nozzles in top head

x = number of leaking nozzles

p = probability of not leaking

q = 1-p (probability of leaking)

k = index for summation over leaking nozzles

It is also assumed that the leaking nozzles are independent. Therefore, the probability of leakage in each nozzle can be determined independently from other nozzles by setting x= 0. This reduces Equation (2) to

$$F(x) = q^n \tag{3}$$

Using a random number generator for q, the time to start of leakage in each nozzle can be determined.

Crack Growth Rate

A detailed description of material crack growth rate distributions developed for this analysis is provided in Section 5 above. The crack growth rate is defined in the *MRPERCRD* code by the following equation.

$$\dot{a} = \exp\left[-\frac{Q_g}{R}\left(\frac{1}{T} - \frac{1}{T_{ref}}\right)\right]\alpha(K - K_{th})^{\beta} \tag{4}$$

where $\dot{a}$ = crack growth rate m/s (in/hr)

Q_g = thermal activation energy for crack growth
= 130 KJ/mole (31.0Kcal/mole)

R = universal gas constant
= 8.314×10^{-3} KJ/mole-°K (1.103×10^{-3} Kcal/mole °R)

T = absolute operating temperature at location of crack (°K or °R)

T_{ref} = absolute reference temperature used in normalized data

α = crack growth amplitude (see below)

β = exponent
= 1.16

K = crack tip stress intensity factor (MPa√m or Ksi√in)

K_{th} = crack tip stress intensity factor threshold
= 9 MPa√m (8.91 Ksi√in)

The parameter α is determined by a random number selection from distributions input by the user. As described in Section 5 above, the user may choose to input either a log-normal or a log triangular representation for both heat to heat and within heat variation.

It is expected that nozzles made from the same heat of material should have crack growth rates defined by a single distribution for that heat. Therefore, a single random number is selected for each heat of material in a given Monte Carlo simulation, and that random number is used to select a mean crack growth rate for that heat from the heat to heat distribution input by the user. Local variability is then simulated with a second set of random numbers for each nozzle within that heat. The variability is simulated as the ratio of actual crack growth rate for each nozzle to the mean for the heat in accordance with the heat-to-heat distribution input by the user. The distribution can be a log-normal distribution or log-triangle distribution. For a normal distribution, the mean should be 1 with standard deviation as a fraction of the mean. For a triangular distribution, the mode is 1 with the upper bound and the lower bound value as defined as a fraction of the mode.

Correlation of CGR with Leakage

The program has the capability to correlate short leakage times (small random number) to high crack growth rates (high random number) through the input of a correlation factor between the leakage random number and the crack growth random number. Two correlation factors are input, one for correlation of heat to heat properties, and a second for correlation of within heat properties.

The correlation factor, $\rho_{x,y}$, between two parameters, x and y, is defined as

$$\rho_{x,y} = \frac{Cov(x,y)}{\sigma_x \sigma_y} \tag{5}$$

where $-1 \le \rho_{x,y} \le 1$

and $$Cov(x,y) = \frac{1}{n}\sum_{i=1}^{n}(x_i - \mu_x)(y_i - \mu_y)$$

μ_x, μ_y = mean of the two parameters, x and y.

If $\rho_{x,y} = 0$, the two parameters are unrelated to each other. If $\rho_{x,y} > 0$, positive correlation, the large values of x are associated with the large values of y. If $\rho_{x,y} < 0$, negative correlation, the large values of x are associated with the small values of y. Figure 7-1 illustrates the degree of correlation implied by typical values of the correlation factor.

7.3 Other Input Parameters

Modeling of cracking involves consideration of different aspects of the reliability evaluation of the vessel top head. These considerations include crack sizes, initiation locations, crack types, crack growth due to stress corrosion, and the path of crack growth. Modeling of crack initiation, crack types and the path of crack growth are based on field inspection data on leaked nozzles in PWRs, as described in Section 4. Consideration of crack size before nozzle leakage is also necessary in the modeling, to address the effect of periodic inspections for cracks (NDE) on the reliability of top heads.

Number of Cracks Per Nozzle

For each nozzle in the top head, the number of cracks when initiation is assumed is determined randomly. The distribution of number of cracks in the nozzle is assumed to be Poisson. Also, it is assumed that at least one crack is present in each nozzle if leakage is predicted in that nozzle from the Weibull curve. When leakage occurs, it is also assumed that all non-detected cracks coalesce into a single flaw.

Crack Types

Based on the inspection results from the leaking top head CRDM nozzles, cracks were initiated on the OD surface near the J-groove weld, at either the highest location on the uphill side or the lowest location on the downhill side.

Due to the complexity of the leaking crack configuration, the stress intensity factors are calculated for different crack lengths and crack depths, at different shrink fits and nozzle material yield strengths using finite element models. The results are put into tabular format such that, during Monte Carlo simulations, the stress intensity factor is interpolated from these tables.

Initial Crack Size

For each crack in the top head nozzles an initial crack size is randomly assigned based on user input. It is assumed that the leaking crack is initiated at some fraction of the time to leakage from the Weibull time to leakage distribution. It is also assumed that the crack grows at a constant rate from this initial crack size at time = t_{init} to the leaking crack depth at the leakage start time ($t_{Weibull}$). This input and approach is specifically used for NDE inspections performed of the top head nozzles for crack detection prior to the onset of nozzle leakage. The concept of t_{init} and initial crack size are illustrated in Figure 7-2

Stress Intensity Factors for a Leaking Crack

In *MRPERCRD*, the leaking crack is assumed to consist of a circumferential crack of a given length and depth. The general approach is for the user to input a table with stress intensity factors for various crack lengths and depths expressed as a/t ratios and crack lengths. The crack length in the table ranges from the crack length at the onset of leakage (most likely a part-through axial crack) to the critical crack length (i.e. through wall circumferential crack) leading to net section collapse. The assumed circumferential crack length at the onset of leakage, and at which the crack transitions from part-through-wall to through-wall may be specified in the user input tables.

For each entry of crack depth, (a/t) and crack length in the table, a finite element model is created to obtain the stress intensity factor. Details of such finite element models and results for four typical plant/nozzle types are described in Section 3 above. During Monte Carlo simulation, once the leakage starts in the nozzle, as determined by $t_{Weibull}$, with the crack set at the leaking crack length, the stress intensity factor is interpolated from the table. Crack growth is calculated using the interpolated stress intensity factor to obtain the updated crack depth or crack length. The stress intensity factor for the updated crack size can then be interpolated again from the same table. These steps are repeated for each time step until the crack reaches the critical crack length for that nozzle or until the end of the analysis period specified by the user (typically plant design life or extended life).

Since there are different nozzle locations in the top head, with different material properties and shrink fits, the stress intensity factor table can be formulated to represent different nozzle locations; material yield strengths and nozzle shrink fits. Based on the randomly selected value for yield strength, shrink fit, and grouping different nozzle locations into a smaller number of nozzle location categories, the stress intensity factor can be efficiently obtained for each nozzle and crack configuration without any penalty of extensive computational time.

Examples of detailed finite element fracture mechanics analyses to determine stress intensity factors for the various nozzle / crack configurations are presented in Section 3. The analyses are performed for possible combinations of maximum and minimum yield strength and shrink fit for seven nozzle categories, center, middle inner nozzle with an uphill crack, middle inner nozzle with a down hill crack, middle outer nozzle with an uphill crack, middle inner nozzle with a downhill crack, outer nozzle with an uphill crack, and outer nozzle with a downhill crack.

Nozzle Categories

Due to the large number of possible CRDM, CEDM and ICI nozzles in a top head, each with slightly different configurations in term of angle and J-groove weld geometry, each nozzle in the top head is classified into one of the four different categories as follows:

- Center
- Middle Inner
- Middle Outer
- Outer

The classification into one of the four categories is based on the nozzle angle input by the user. This classification allows the program to select the appropriate K table for interpolation of stress intensity factor.

Temperature

The top head temperature is a random variable in the *MPRERCRD* program. This temperature is used in the probability of leakage and crack growth rate.

Initial Nozzle Shrink Fit

The initial nozzle shrink fit is a random variable in the *MPRERCRD* program. This random variable is used in the interpolation of stress intensity factor and leakage inspection.

In *MRPERCRD*, a negative shrink fit means a gap between the nozzle and the top head. A positive shrink fit represents interference between the nozzle and the top head (i.e. the OD of the nozzle is larger than the ID of the opening in the top head).

Yield Strength

The nozzle material's yield strength is a random variable in the *MPERCRD* program used in the interpolation of stress intensity factor.

Critical Crack Length

The critical crack length for each nozzle category is a random variable in the *MPERCRD* program. The critical crack length is determined based on net section collapse criteria. When the crack length exceeds the critical crack length, the nozzle or top head is considered a failure.

7.4 Simulating Effect of Inspections

The user may also specify inspections of various types and inspection intervals. Probabilities of detection (PODs) for the inspections may be selected from set of a built-in curves in the program, or the user may define a custom POD curve. In either case, the program compares the crack sizes predicted to exist in each nozzle at the time the inspection is performed to the specified POD curve, and if the flaw is predicted to be detected, that nozzle is assumed to be replaced or repaired, and therefore removed from the population of potential failures.

The *MPRERCRD* program can simulate two types of inspections. They are non-destructive examination for cracks (NDE) and visual examination for leakage. The user can specify the time for inspections, the inspection coverage in percent and the method of inspection or probability of detection (POD) curve. For each type of inspection, the user can assign different inspection coverage and use a different POD curve.

The inspection coverage in percent applies to the top head nozzles. 100% inspection coverage means that all nozzles are inspected during that inspection. 50% percent inspection coverage means that only half the nozzles are inspected. The nozzles to be inspected in each inspection simulation are determined by a random number.

When a nozzle is inspected and cracks or leakage are detected, it is assumed in MPRERCRD that the nozzles are completely, properly and satisfactorily dispositioned without reintroducing any new defects. The detected cracks or nozzles are not used in the subsequent calculation of probability of leakage or failure.

Leakage Inspection (Bare Metal Visual)

The detection of leakage by visual inspection depends on when the leakage starts and the amount of initial shrink fit in each nozzle. Therefore, the POD curves for visual leakage inspection have to be defined as a function of nozzle initial shrink fit. Before the start of leakage in each nozzle, leakage inspection has no relevant effect on the reliability results even if all nozzles are inspected with a POD of one.

If leakage is not detected by the first leakage inspection after the nozzle leakage begins, it is postulated that any subsequent inspections may also have difficulty detecting the leakage in that same nozzle (i.e., the leakage is masked or for some reason very difficult to detect). A scale factor on the POD curve during the subsequent inspection is thus used to simulate a reduced probability of detection. This factor is only applied to the nozzle for which leakage was missed by the previous inspection. It is not applied to nozzles that were not included in the inspection coverage percentage in the previous inspection.

Crack Inspection (Non-Destructive Examination)

When a nozzle is determined to be within the inspection coverage percentage of a crack inspection (NDE), detection of the crack is based on the POD curve selected for that inspection. One of the built-in crack inspection POD curves in the software is illustrated in Figure 7-3. It corresponds to a FULLV ultrasonic angle beam examination defined in Reference [20]. Figure 7-3 also illustrates a comparison of that curve to performance of two NDE vendors in NDE demonstration tests on top head nozzle mockups containing fabricated defects. The bands at the bottom of the figure indicate the range of crack depths that were missed by the two vendors. The bands at the top of the chart indicate the range of crack depths that were fully detected. As expected, the POD curve transitions from very low probabilities of detection in the regime where many defects were missed, to higher PODs in the size regime where all flaws were detected. The POD curve is at about 75% at the maximum size at which flaws were missed by either vendor, and peaks at 95%, meaning that 5% of flaws are assumed to be missed no matter how large. The user also has the option to define new POD curves and input those as alternatives to the built in curves.

For crack inspections, the user also specifies an initiation time and size (a-init and t-init in Figure 7-4). For the circumferential crack growth analysis, a through-wall crack equal to 30% of the circumference is assumed at the time-to-leakage predicted for that nozzle by the Weibull distribution (t-Weibull). However, for purposes of assessing NDE detectibility, it is assumed that a part-through-wall crack of some fraction of the wall-thickness (a-init) initiates at some fraction of t-Weibull (t-init) and grows linearly in time to a/t=0.5 at t-Weibull. POD curves are then compared to the part-through-wall flaw depth predicted by this crack growth assumption at the time of inspection. Sensitivity studies of the crack initiation parameters were conducted.

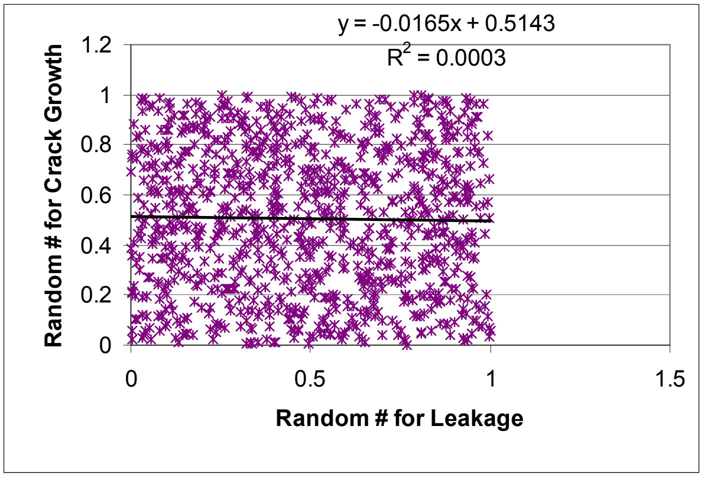

ρ = 0, uncorrelated

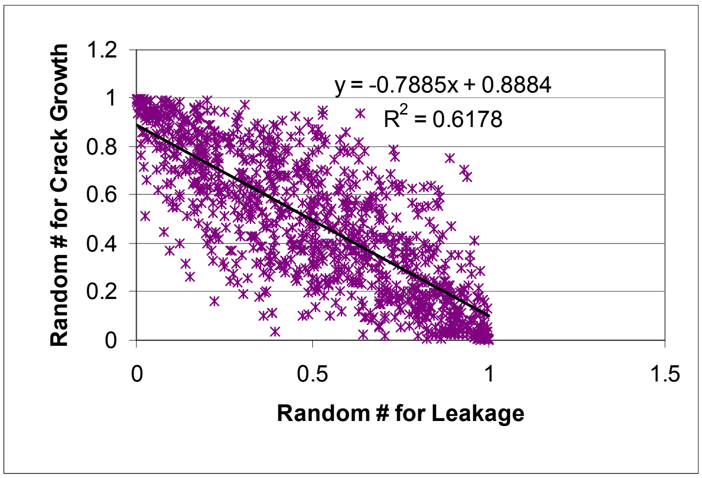

ρ = -0.8, moderate correlation

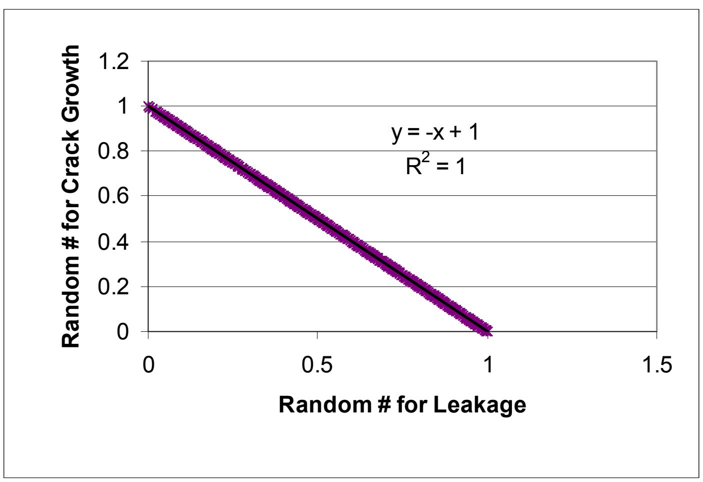

ρ = -1, totally correlated

Figure 7-1
Illustration of Correlation Factors for Crack Initiation and Growth

Content Deleted – MRP/EPRI Proprietary Material

Figure 7-2
Illustration of Crack Initiation Time Concept for Crack Detection Prior to Leakage

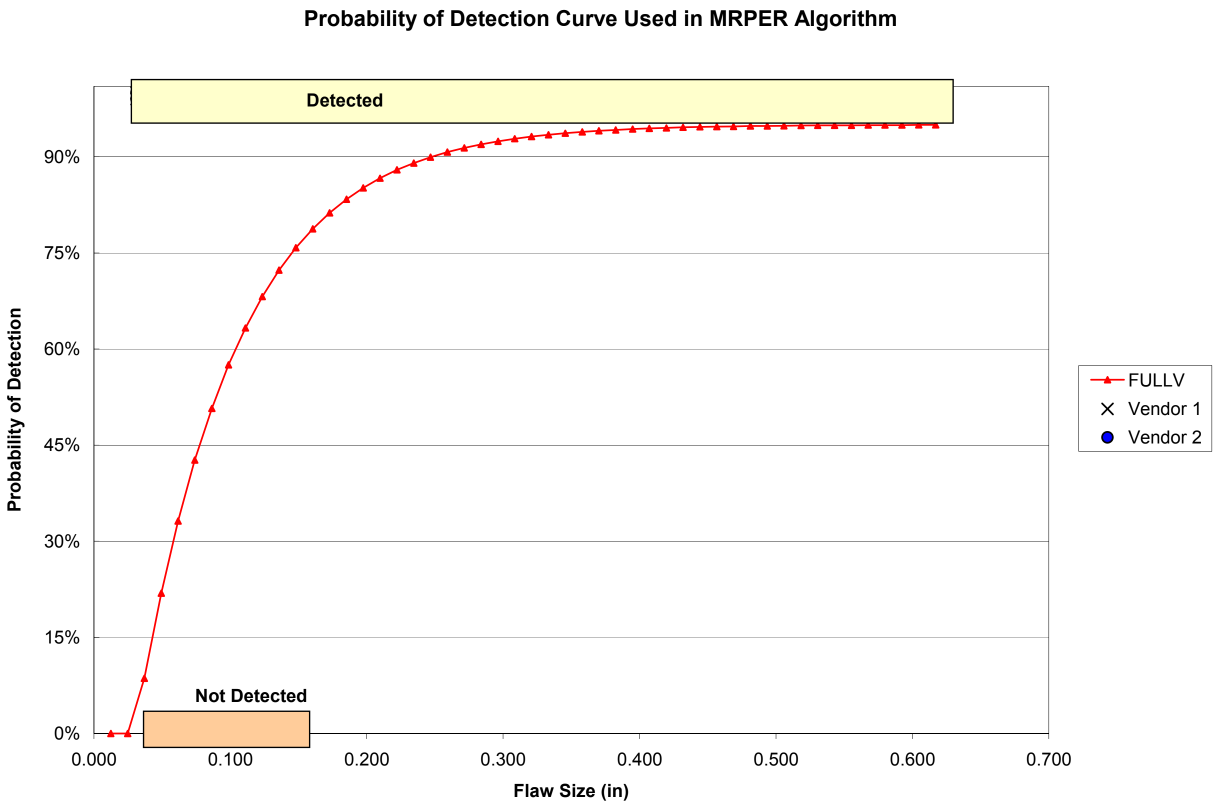

Figure 7-3
Illustration of Probability of Detection Curve for NDE and Comparison to Vendor Performances in Demonstration Program

8 PFM ANALYSES AND RESULTS

A series of PFM analyses were performed with the *MRPERCRD* program covering a wide variety of conditions and assumptions for the four characteristic plants discussed in Section 3 above. These include base cases, with and without inspections for the four plant types, and sensitivity studies to evaluate the effects of various statistical and deterministic assumptions in the analysis. The model was then benchmarked with respect to field experience with top head inspections performed, considering the observance of cracking and leakage as well as of circumferential cracks of various sizes. The benchmark cases were used to select a set of analytical parameters that characterize the probabilities of leakage and of large circumferential cracks in a reasonably conservative manner compared to field experience, and thus, to calibrate the model. Finally, the benchmarked parameters were used to analyze case studies of a sample of actual plants, to evaluate the effects of two assumed inspection programs on probability of nozzle leakage and failure:

1) inspections in accordance with the current NRC Order [19], and

2) an alternative inspection frequency proposed by the MRP.

8.1 Base Cases

The analysis matrix shown in Table 8-1 below outlines the *MRPERCRD* base case runs conducted during the current study including a summary of the significant input parameters in each. The base cases include historical runs performed using Plant A (B&W) input parameters for comparison with prior analyses , runs for the four plant types with and without inspections, runs on Plant A with various inspection intervals, and runs at various head operating temperatures. The comment column in Table 8-1 tersely describes the purpose of each run in the matrix. The subsequent paragraphs detail the individual runs and results.

Analysis Parameters								Weibull Parameters				
Run No.	Plant	Head Temp. / Ref. Temp. for Leakage [°F]	Stress Plane	Inspect. Type	Inspect. Interval	Year of 1st Inspect.	Correlation Factor	θ	Lower Bound for θ	Upper Bound for θ	β	Comments
1												
2												
3												
4												
5												
6												
7												
8												
9												
10	Content Deleted – MRP/EPRI Proprietary Material											
11												
12												
13												
14												
15												
16												
17												
18												
19												

Table 8-1:
Matrix of Base Case *MRPERCRD* Runs

Historical Runs

The first four *MRPERCRD* runs (1, 2, 3, and 4 in Table 8-1) investigate the effect of assuming crack propagation on the maximum stress plane versus the 1400 and/or 1500 stress planes as was done in prior evaluations. (For a detailed description of stress planes and associated stresses and stress intensity factors, see Section 3 of this report and Refs [7-10].) To create a meaningful comparison point, identical analysis parameters were used for run 2 as had been used for runs 3 and 4 during the prior analyses, with the only variance in data input being the K-values for the respective stress planes. Figure 8-1 graphically depicts the effect on POF of selecting the different stress planes for crack propagation.

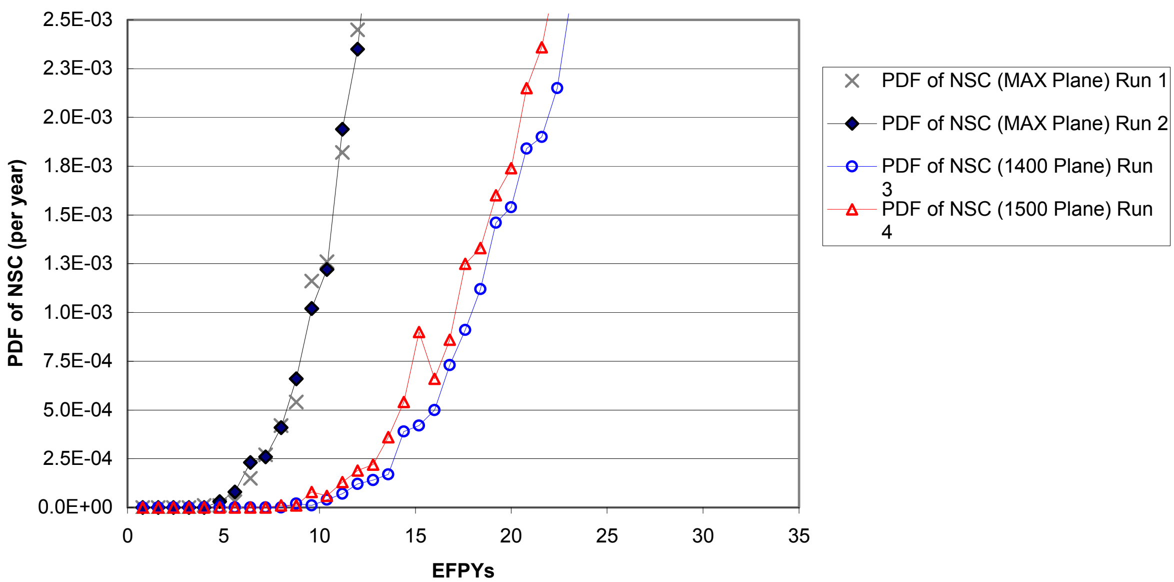

Figure 8-1
POF by Net Section Collapse at 600ºF as a Function of Stress Plane

Figure 1 demonstrates that the new maximum stress plane assumption yields more conservative POF values at every effective full power year (EFPY) than either the 1400 or the 1500 planes used in prior analyses. Detailed metallurgical investigations of cracked CRDM nozzles have not been conducted to determine on which stress planes the circumferential cracks that have been observed in service actually propagated. Furthermore, it is not implausible, and even likely, that PWSCC cracks would follow a plane of maximum stress, rather than a plane exactly parallel to the weld root. Therefore, all future runs are conducted using the maximum stress plane assumption.

As indicated in the third column of Table 8-1, runs 2 through 4, the historical *MRPERCRD* runs were performed using a 602ºF reference temperature for leakage. However, the leakage data used to develop the Weibull distributions in Section 4 were all normalized to 600^{o}F making that the appropriate reference temperature. Figure 8-1 illustrates that the difference in results between run 1 and run 2, which differ only by the input value of reference temperature for leakage (600^{o}F versus 602^{o}F), is insignificant. The remaining cases in Table 8-1 were all run at the correct, 600^{o}F reference temperature.

Effect of Inspections

MRPERCRD run 6 in Table 8-1 has thus been designated the new 'base case' for comparison of subsequent runs. The following are key variables in this new base case, some of which are significant to POF trends:

- Ks from the maximum stress plane were used.
- The head temperature and the reference temperature for leakage were set equal to 600^{o}F.
- A correlation factor of -0.8 was assumed for both heat-to-heat and within-heat correlation of time to leakage and crack growth rate. This corresponds to a moderately strong correlation; in which crack growth rates for nozzles that leak relatively early are selected from the upper portion of the distributions in Figures 5-1 and 5-2.
- The Weibull θ parameter (characteristic time to first cracking or leakage) used in these runs is described by a triangular function with a mean of 16.45 EDYs, a lower bound of 11.8 EDYs, and an upper bound of 22.95 EDYs. The beta value (Weibull slope) is consistently assumed as 3.0. Note that this was an intermediate fit used for these base case results, and is slightly different from the latest Weibull θ fit reported in Section 4. This topic is discussed in more detail in Sections 8.3 (Benchmark Evaluation).

To investigate the effects of inspection intervals on POF by net section collapse, non-destructive examinations with 80% coverage were assumed using the FULLV UT probability of detection (POD) curve described in Section 7. *MRPERCRD* runs 10, 11, and 12 in Table 4 evaluated inspection intervals of 2, 4, and 8 EFPYs, keeping all other variables constant with respect to the base case. The time of first inspection 11.8 EFPYs was selected so as to maintain a POF of less than 1 x 10^{-3} prior to the first inspection, which is an approximate safety limit for nozzle ejection. Figure 8-2 shows the results of *MRPERCRD* runs 10 through 12.

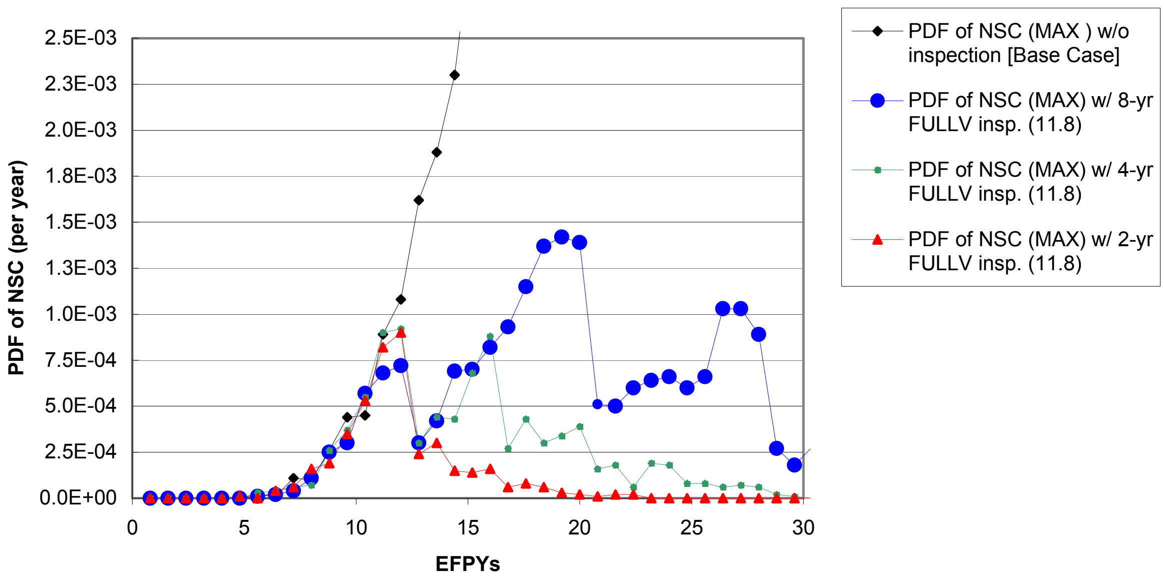

Figure 8-2
POF by Net Section Collapse at 600°F Investigating The Effect of Inspection Intervals

Figure 8-2 illustrates the following points:

The FULLV inspection protocol modeled in the *MRPERCRD* program results in a significant reduction in the POF by net section collapse immediately following the initial inspection, as flaws which are detected are assumed to be repaired or otherwise removed from the population and therefore can no longer lead to large circumferential cracks that could grow to critical size.

Following the initial drop due to the inspections, the POF trends back up again at approximately the same slope as the no-inspection curve, until a second inspection is performed.

A 4-EFPY-inspection interval appears to be the maximum interval that maintains the base case POF below 1×10^{-3}. A 2-EFPY interval further reduces the POF because subsequent inspections occur before the POF has a chance to trend back up to its pre-inspection level, while an 8-EFPY interval allows it to climb to a level higher than 1×10^{-3} before the second inspection is performed.

Comparison of PWR Plant Types

Table 3-1 summarizes the differences in top head geometric and physical parameters used to model each of the characteristic plant types. Stress intensity factors and other geometric data for each of these plant types were input to *MRPERCRD* to determine if there are significant plant-to-plant differences in probability of nozzle ejection, all other input parameters remaining the same. A total of six additional runs were performed:

- Runs 7, 8 and 9 analyzed base case conditions (no-inspection) at Plants B, C, and D, respectively, and are directly comparable to base case run 6 for Plant A.

- Runs 13, 14 and 15 examined the other plant types with a 4-EFPY-inspection interval and are directly comparable to run 11 (4-EFPY inspections, Plant A).

The results of the analyses of various plant types are summarized in Figure 8-3.

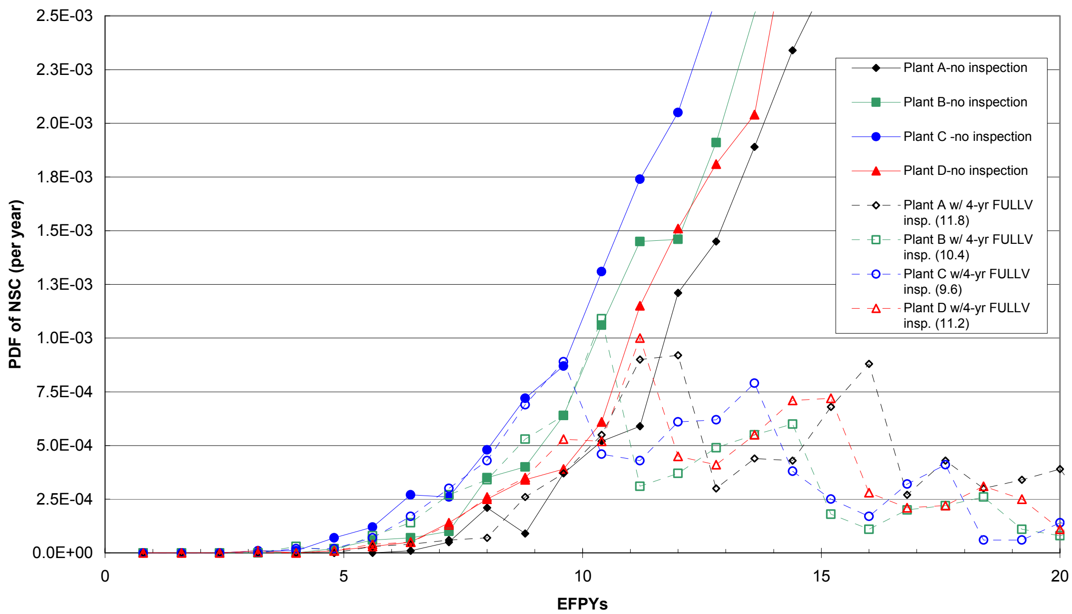

Figure 8-3
POF by Net Section Collapse at 600°F – Various Plant Types, with and without Inspections

The non-inspection curves illustrate the variation of the results for the different plant types. The two Westinghouse Plants (B and C) are furthest to the left, crossing the 1 x 10^{-3} probability of failure slightly beyond and slightly before 10 EFPYs. The CE Plant (D) is next at about 11 EFPYs, and the prior base case (B&W, Plant A) yields the longest time to 1 x 10^{-3} probability of failure, 11.8 EFPYs. The total spread on the horizontal axis is about 2 EFPYs. It is important to note that these differences are solely due to differences in crack growth rate predictions due to different stress intensity factors, and do not reflect other important differences between plants types, such as number of nozzles, head temperature, materials, and welding processes. They should not, therefore, be interpreted as a prediction of differences in PWSCC susceptibility of the different plant types. Details of the other *MRPERCRD* input parameters for these runs are summarized in Tables 8-2 through 8-5.

Review of the inspection curves in Figure 8-3 indicates that a 4 EFPY (at 600ºF) inspection interval appears to be sufficient to maintain all plants at or below a failure probability of 1 x 10^{-3}, assuming that the initial inspections are performed at the outage just before reaching 1 x 10^{-3} as indicated in the figure legend.

Item	Variable	Probability Distribution	Mean Value	Standard Deviation	Lower Bound	Upper Bound	Units
1	Content Deleted – MRP/EPRI Proprietary Material						
2							
3							
4							
5							
6							
7							
8							
9							
10							
11							
12							
13							
14							
15							
16							
17							
18							
19							
20							
21							
22							

Table 8-2
***MRPERCRD* Input Parameters for Plant A Base Case Analysis**

Item	Variable	Probability Distribution	Mean Value	Standard Deviation	Lower Bound	Upper Bound	Units
1							
2							
3							
4							
5							
6							
7							
8							
9	Content Deleted – MRP/EPRI Proprietary Material						
10							
11							
12							
13							
14							
15							
16							
17							
18							
19							
20							
21							
22							

Table 8-3
***MRPERCRD* Input Parameters for Plant B Base Case Analysis**

Item	Variable	Probability Distribution	Mean Value	Standard Deviation	Lower Bound	Upper Bound	Units
1							
2							
3							
4							
5							
6							
7							
8							
9							
10	Content Deleted – MRP/EPRI Proprietary Material						
11							
12							
13							
14							
15							
16							
17							
18							
19							
20							
21							
22							

Table 8-4
***MRPERCRD* Input Parameters for Plant C Base Case Analysis**

Item	Variable	Probability Distribution	Mean Value	Standard Deviation	Lower Bound	Upper Bound	Units
1	Content Deleted – MRP/EPRI Proprietary Material						
2							
3							
4							
5							
6							
7							
8							
9							
10							
11							
12							
13							
14							
15							
16							
17							
18							
19							
20							
21							
22							

Table 8-5
***MRPERCRD* Input Parameters for Plant D Base Case Analysis**

Operational Head Temperature Effects

MRPERCRD runs 16, 17, 18, and 19 in Table 8-1 investigate how variations in top head operational temperatures affect the POF by net section collapse, and the required inspection intervals to ensure that the POF stays below 1 x 10^{-3}. Besides the baseline operational temperature of 600°F, two other top head operational temperatures were tested: 580°F and 590°F. Since the functions incorporated into the *MRPERCRD* program for stress corrosion crack initiation and growth follow a thermodynamically based Arrhenius relationship, with exponential time-temperature terms, small variances in temperature cause relatively large changes in both the crack initiation and growth rates, and therefore changes in the POF. Using the Arrhenius functions established to normalize to EDYs, the 4-EFPY (at 600ºF) inspection interval, which successfully maintained the POF by net section collapse below 1 x 10^{-3} (with the proper inspection initiation date), was normalized to 6 years at 590°F and 9 years at 580°F for runs 17 and 19, respectively. Besides head operating temperature and inspection interval variations, all other variables were kept constant with respect to the "base case". Figure 8-4 graphically depicts the results of these 4 runs, compared to the base case at 600ºF, with and without inspections:

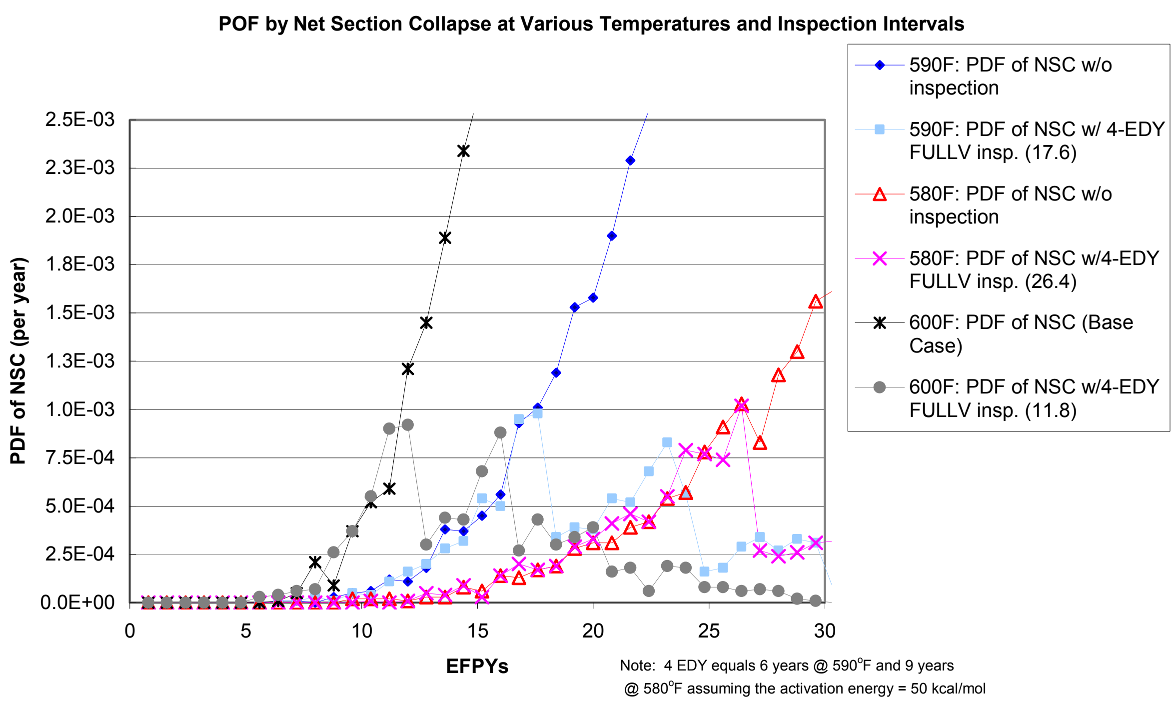

Figure 8-4
POF as a Function of Variations in Top Head Temperature and Inspection Intervals

Several important trends are demonstrated in Figure 8-4:

As expected (due to the Arrhenius functions used to describe the time-temperature behavior of crack initiation and growth), relatively small decreases (10°F) in temperature significantly decrease the predicted POF. Maintaining a 4-EDY inspection frequency regardless of operational temperature successfully prevented the POF from exceeding 1×10^{-3}, provided the inspections started before the plant initially hit the 1×10^{-3} threshold. This observation is significant because of differences in the Arrhenius equation activation energies for crack initiation versus crack growth. The generally accepted values of 50 kcal/mole for initiation (Section 4) and 31 kcal/mole for crack growth (Section 5) are used in these analyses, from which one would expect the predicted growth of circumferential cracks to be less temperature sensitive than crack initiation, which is the basis for the EDY correlation. The fact that inspection intervals at different temperatures, specified in terms of constant EDYs, produce the same degree of effectiveness in maintaining acceptable POF is indicative that the PFM calculations are more sensitive to predicted initiation of cracks (per the Weibull time to first cracking model), than to predicted growth of the 30º of circumferential cracks that are assumed to exist once crack initiation is predicted from the Weibull model.

8.2 Sensitivity Studies

In addition to the above described base case runs, several *MRPERCRD* input parameters were varied independently to determine the sensitivity of the analysis to incremental changes in these key variables. Sensitivity analyses were conducted for the following general classes of variables:

- Parameters in the Weibull time to cracking / leakage model
- Parameters related to the Crack Growth Rate (CGR) distribution
- Parameters affecting sensitivity of the analysis to inspections
- Other miscellaneous sensitivities

Table 8-6 gives a summary of the various sensitivity analyses performed. The comment column again gives a terse description of the purpose of the run, and the highlighted cells in the table indicate the major parameters studied in that run.

	Weibull Parameters				CGR Parameters		Inspection Parameters						Other Parameters		Comments
Run No.	θ	Lower Bound for θ	Upper Bound for θ	β	Distrib.	Corr. Factor	Time of Init. Fraction of $t_{Weibull}$	Init. Crack Size (for Insp.)	Inspect Type	Inspect Interval	Year of 1st Inspect	No. of Cracks/ Nozzle (Poisson μ)	Head Temp. [°F]	Head Temp.STD [°F]	
1															
2															
3															
4															
5															
6															
7															
8															
9															
10	Content Deleted – MRP/EPRI Proprietary Material														
11															
12															
13															
14															
15															
16															
17															
18															
19															

Table 8-6
Matrix of *MRPERCRD* Sensitivity Studies

Sensitivity to the Weibull θ Parameter and the Distribution of θ

Comparing *MRPERCRD* runs 1 through 4 from Table 8-6 tests the sensitivity of the POF analysis to changes in the Weibull θ parameter and its distribution. The Weibull θ parameter is the characteristic failure time of the Weibull distribution, which was used to model the empirical inspection data for time to first leak or crack. In the *MRPERCRD* algorithm, a triangular probability distribution is used to model the range of θ values shown by the empirical data. The 'base case' (run 1) has a mean θ-value of 16.45 with a lower bound of 11.8 and an upper bound of 22.95. Run 2 utilized the same mean θ-value of 16.45, but with a lower bound of 10.45 and an upper bound of 22.45. Run 3 used a mean θ-value of 15.2 with a lower bound of 10.55 and an upper bound of 21.7 (the parameters of the most recent Weibull fit reported in Section 4) and Run 4 has a θ-value of 15.0 with a lower bound of 9 and an upper bound of 21. All other critical test parameters are consistent between the four runs. Figure 8-5 below plots the four runs to illustrate trends associated with variations in θ.

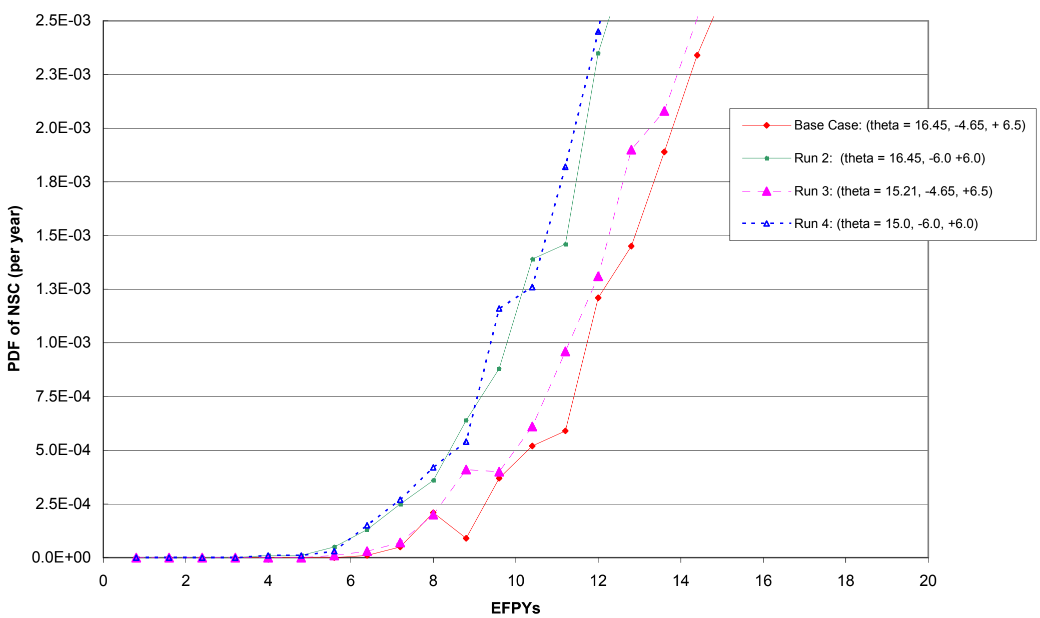

Figure 8-5
Effect of Changes in the Weibull θ Distribution on POF at 600°F

From Figure 8-5 a moderate effect of the Weibull θ distribution is observed. The times to a POF of 1 x 10^{-3} range from a low of 9.2 EFPYs to a high of 11.8 EFPYs. Another significant observation is that the POF for runs 1 and 3 and for runs 2 and 4 essentially overlap each other, indicating that changes in the mean θ-value are not as significant as changes in the range of the triangular distribution.

Sensitivity to Weibull β Term

MRPERCRD runs 5 through 8 from Table 8-6 test the sensitivity of the analysis to changes in the Weibull β term. The Weibull β term is the slope (or shape parameter) of the Weibull curve fit, which was used to model the time to first crack or leak with the available empirical inspection data. Two different β values, 3.46 and 4.48, were compared against the 'base case' value of 3, with and without inspections at four EDY intervals. All other input parameters were held constant and consistent with the 'base case' values. Figure 8-6 below depicts the results of this sensitivity analysis.

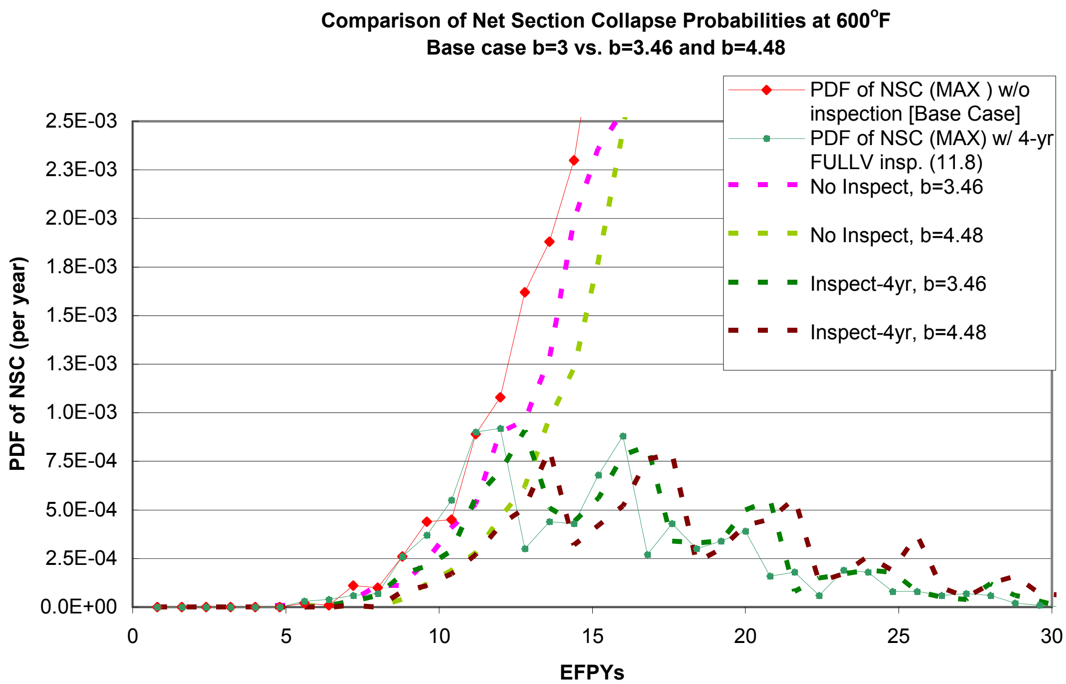

Figure 8-6
Effect of Increasing the Weibull β Parameter on POF at 600°F

The trends in Figure 8-6 clearly indicate that increasing the slope of the Weibull fit line through the empirical inspection data decreases the POF by net section collapse. The β value of 3 used in the 'base case' and other *MRPERCRD* runs produces a conservative POF estimate compared to runs with the higher β values tested in these sensitivity runs, all other variables held constant.

Sensitivity to Crack Growth Rate Distribution

MRPERCRD runs 9 and 10 from Table 8-6 investigate the sensitivity of the analysis to differences in the crack growth rate assumptions. Run 9 assumes the same, Log-Triangular distribution as the base case, but with the correlation factor between crack initiation and crack growth set equal to ±1. This assumes that the crack growth rate is perfectly correlated with time to initiation in the Weibull model, using essentially the same random number for both variables. Run 10, uses Log-Normal (versus Log-Triangular) crack growth rate distributions from Section 5, all other variables being the same as the base case. The resulting POFs are depicted in Figure 8-7.

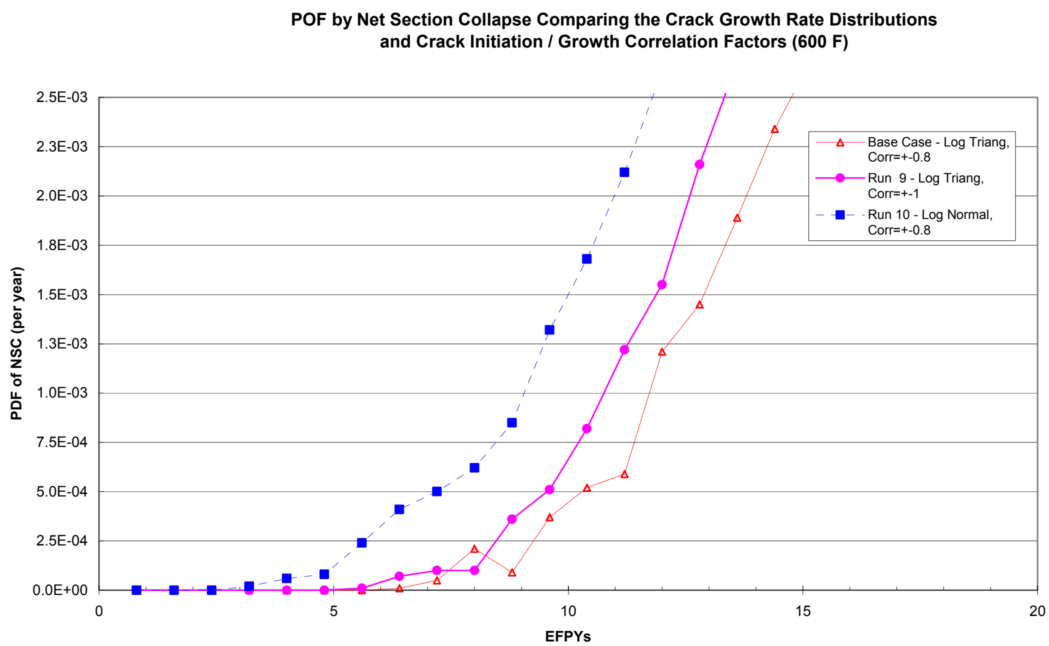

Figure 8-7
Effect of Various Crack Growth Rate Assumptions at 600°F

Figure 8-7 indicates a moderate effect of CGR assumption, with the time to POF of 1 x 10^{-3} ranging from approximately 9 EFPYs to 11.8 EFPYs. Use of the Log-Normal distribution demonstrates a stronger effect than changes in the correlation factor.

Sensitivity to Parameters Affecting Inspection

In the *MRPERCRD* algorithm, a number of assumptions are used to characterize the ability of NDE inspections to detect cracks prior to leakage or failure (see Section 7 for a complete discussion). These consist of assumptions about when and how cracks initiate and grow prior to the prediction of first leakage or cracking from the Weibull model (denoted $t_{Weibull}$ in this discussion). Sensitivity studies have been conducted to determine the effect of two of the more important parameters in this area: time of assumed PWSCC initiation (t_{init}), as a fraction of $t_{Weibull}$, and number of initiated cracks per nozzle (Poisson μ).

A Poisson distribution with a mean value μ is used to describe the assumed number of initiated cracks per nozzle. For the 'base case' analyses, and for most other runs described in this report, the μ value was assumed to be 2. *MRPERCRD* Runs 11 and 12 from Table 8-6 compare the sensitivity of the results to changes in the Poisson μ-value, with and without inspection. Figure 8-8 below compares the 'base case' runs with and without inspection (runs 6 and 11 of Table 8-1) to these runs. Note that all other input parameters were kept constant in this comparison.

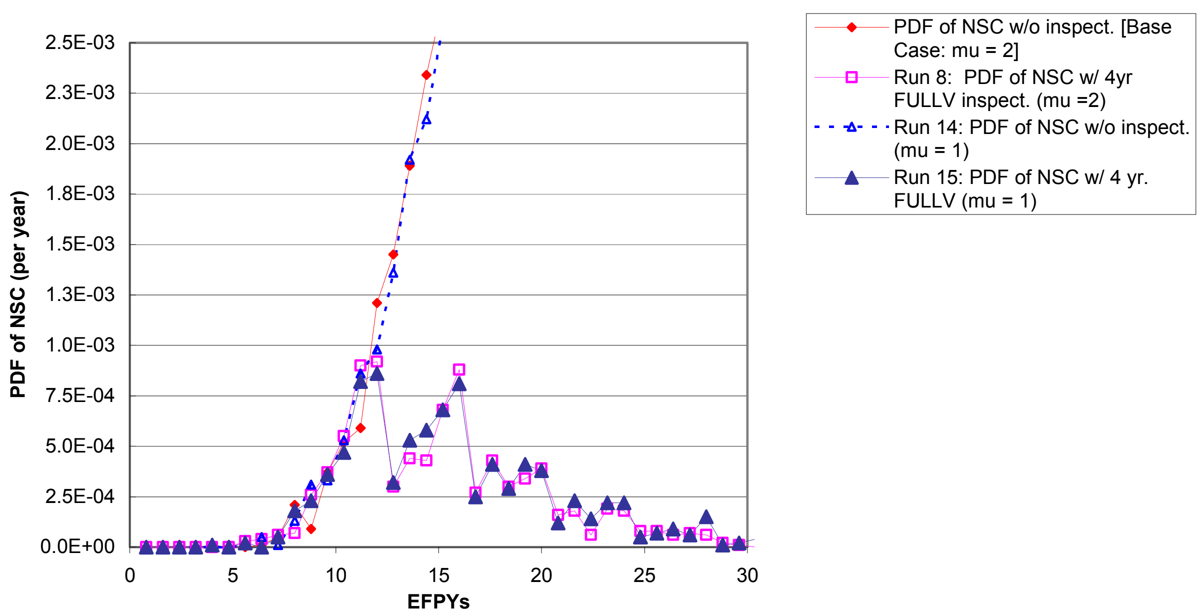

Figure 8-8
Effect of the Poisson (μ) Number of Cracks per Nozzle on POF at 600°F

In Figure 8-8 the base case values with a μ-value of 2 overlap the sensitivity analysis runs with a μ-value of 1, indicating that the *MRPERCRD* algorithm is not very sensitive to the number of assumed initial cracks per nozzle, all other parameters being held constant.

Runs 13 and 14 in Table 8-6 were used to test the sensitivity of the analysis to variations in assumed time to initiate a crack. Run 13 assumes that PWSCC cracks are initiated very early in life ($t_{init} = 0$), and grow to a size of ½ the nozzle wall thickness at $t_{Weibull}$. This assumption could be potentially non-conservative, because cracks are assumed to be present, and therefore potentially detectable by NDE, relatively early in plant life. Run 14 tests this concern by performing the base case analysis, with a four EFPY inspection interval, assuming a crack initiation time of ½ of $t_{Weibull}$. ($t_{init} = 0.5$). The results are shown, along with a non-inspection base case in Figure 8-9. Note that for more complete convergence, these runs were performed using 500,000 Monte Carlo simulations rather than the 100,000 which has been the standard in most prior analyses.

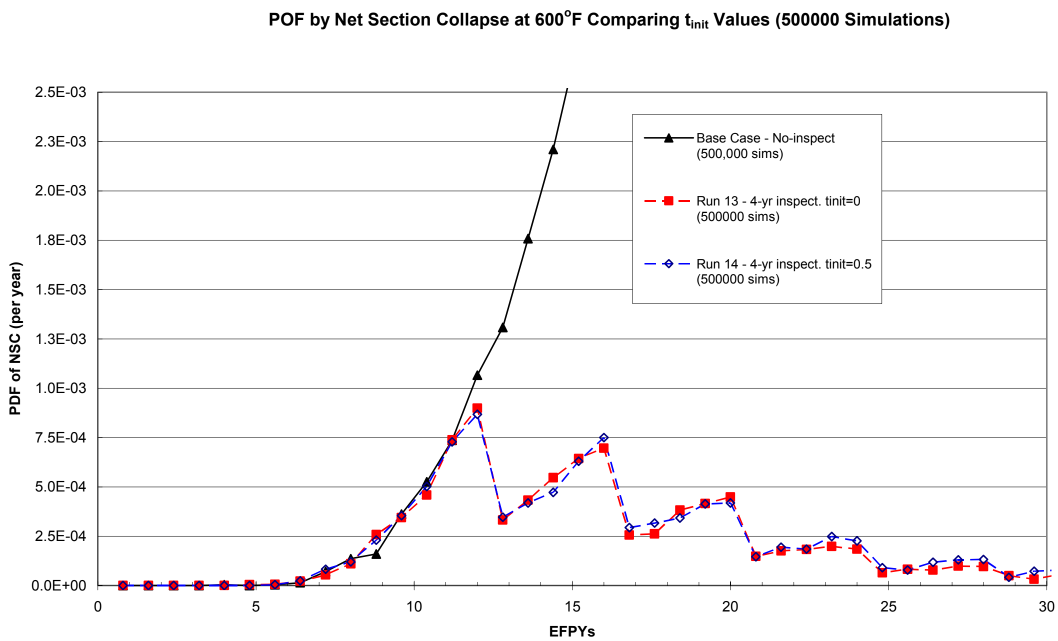

Figure 8-9
Effect of Time to Crack Initiation (and thus Availability for Detection by NDE) on POF at 600°F

The results shown in Figure 8-9 clearly demonstrate that t_{init} has a negligible effect on the analysis results for inspection protocols typical of those studied in this report. The likely reason is that, in either case, the first inspections are assumed to be conducted fairly late in life, and thus nozzles that could potentially lead to failures in a plant lifetime (i.e. those with relatively short $t_{Weibull}$s) have initiated and grown cracks approaching ½ the nozzle wall thickness under either assumption.

Top Head Temperature Variability

Since top head temperature is such an important factor in determining nozzle PWSCC sensitivity, some plants have installed temperature sensors on their top head nozzles and monitored to confirm their top head temperature. The results of at least one of these studies indicate that the vendor-supplied top head temperature estimate was an accurate mean value, but that there was significant nozzle-to-nozzle variability around that mean (as much as ±10ºF). Since 10ºF has been shown previously to produce substantial differences in POF trends (e.g. Figure 8-4), runs 15 through 17 in Table 8-6 were performed to study the effect of head temperature variability. These runs repeat prior, no-inspection base cases at 600, 590, and 580ºF, but assume that head temperature is normally distributed with a 5ºF standard deviation. The results are presented in Figure 8-10 below. The effect of head temperature variability is seen to be not that significant, assuming that the mean temperature for the plant is accurate.

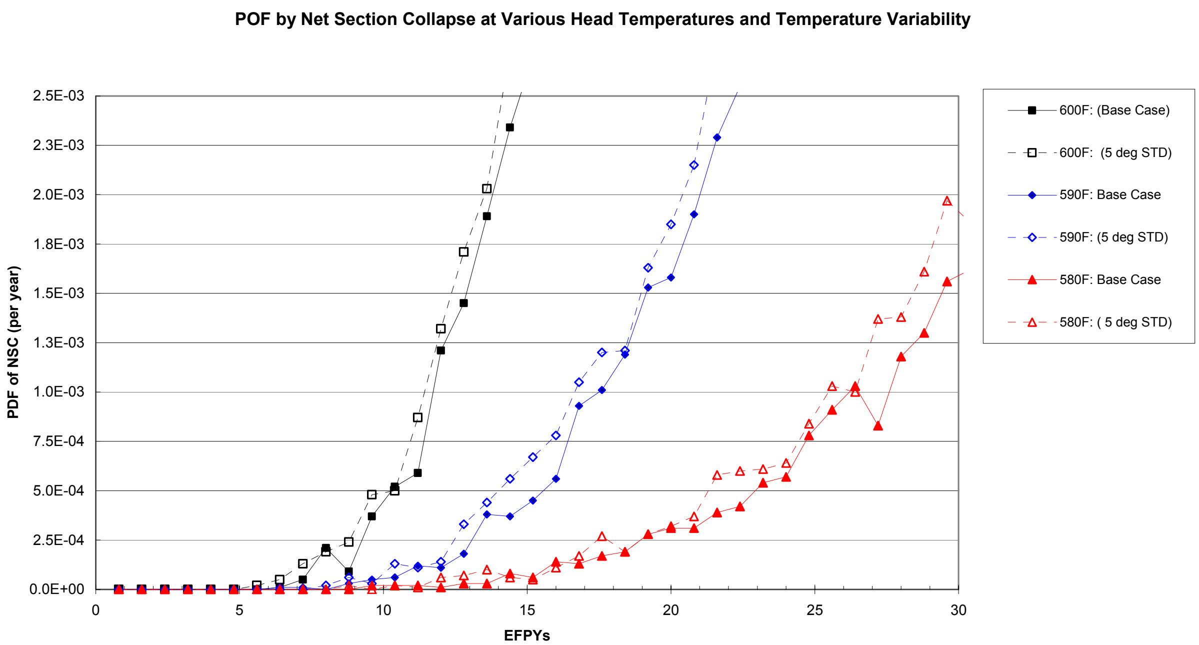

Figure 8-10
Effect of Top Head Temperature Variability

'Ultimate Sensitivity' Case

Finally, the previous sensitivity studies were reviewed to construct a worst-case scenario by combining two of the more important input parameters. POF values for the 'ultimate sensitivity case' (*MRPERCRD* runs 18 and 19 (from Table 8-6) are plotted in Figure 8-11. For the 'ultimate case' runs, the Weibull parameter θ, which describes the characteristic time to failure, was pinned at its lowest empirically determined value of 11.8 by setting the upper and lower bounds at -0.01 and +0.01, respectively. In addition the correlation coefficients relating crack initiation with crack growth were set at –1, meaning that large crack growth rates are linked to short leakage times, with essentially perfect correlation. For run 18, all other variables were kept consistent with the no-inspection ‘base case’. For run 19, inspection was assumed at a 4 EFPY interval, beginning at 11.8 EFPYs.

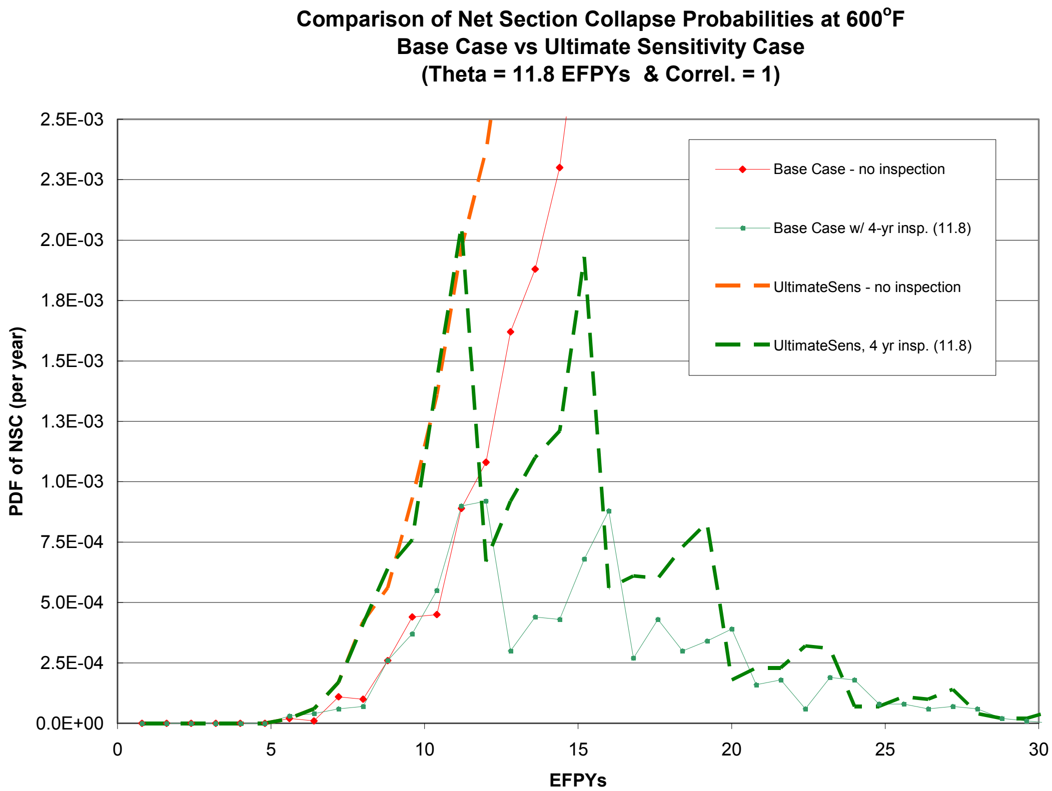

Figure 8-11
Results of “Ultimate Sensitivity” Case

Review of the Figure 8-11 results indicate that the “ultimate sensitivity” case is not significantly worse than other sensitivity cases with only one variable change. Note, however, that the initial inspection was performed at 11.8 EFPYs for both cases, resulting in the POF climbing to about 2 x 10^{-3} before the first inspection is performed. In both cases the second ‘peak’ of POF four EFPYs after the first inspection reaches essentially the same level as the POF before the first inspection. An important difference between the two cases is thus the level of POF when the first inspection was initiated. Once that level was reached, the 4 EDY inspection interval maintained the POF at or below that level, but not less than 1 x 10^{-3}.

8.3 Benchmark Analyses

Considering the broad range of base cases and sensitivity studies presented in the foregoing sections, choosing a set of analytical parameters that yield reasonably conservative POFs for real plant applications demands careful consideration. One could obviously choose a set of parameters that are grossly conservative or non-conservative with respect to observed field behavior, and the results would be of little use to the top head safety assessment. A series of "Benchmark Analyses" were thus performed to calibrate the *MRPERCRD* predictions with field behavior of top head nozzles. This approach is especially well-suited to the problem because, as described in Section 4 above, a relatively large database exists of high quality top head inspections, and these inspections have yielded a non-trivial subset of plants with cracking and leakage, including several nozzles with relatively large circumferential cracks. Indeed, as indicated in Tables 4-1 and 4-2, through the Spring 2003 refueling outages, a total of 30 US plants had conducted some form of non-visual NDE of their top head nozzles, of which 14 had discovered leaks or significant cracking. Approximately 96 nozzles (out of 2253 inspected) experienced cracking or leakage. In addition, 11 nozzles (in 4 plants) experienced circumferential cracking, ranging in length from 30º to 165º of circumference. This represents a statistically significant database with which to benchmark and calibrate the *MRPERCRD* results.

The first step in the benchmarking process is to evaluate how the analysis performs with respect to leakage predictions. This is a relatively trivial step, since it only tests the Monte Carlo simulation of the Weibull fit of time to first leakage, but it is, nonetheless, a necessary first step. Figure 8-12 presents this benchmark comparison. The data points represent the Weibull time to first leakage or cracking distribution for the fourteen plants that have experienced leaking or cracking (extrapolated back as in Table 4-2 and Figure 4-2). The solid curve represents the *MRPERCRD* Monte Carlo prediction of time to first leakage for the base case parameters. The horizontal scale on this plot is EFPYs at 600ºF, or EDYs, which is consistent with the plant data since they too are normalized to 600ºF (EDYs). As anticipated, the agreement is quite good. The dashed curve in Figure 8-12 is the leakage prediction corresponding to a set of benchmarked parameters that were developed from the circumferential crack comparison (see discussion below). It is seen that switching from base case to benchmarked parameters doesn't have a strong effect on the leakage predictions, so the dashed curve is a little more conservative, but still in reasonable agreement with the field leakage data.

A more discerning test of the PFM algorithm is, of course, its ability to predict time to grow circumferential cracks of various sizes. Table 8-7 contains data from the eleven nozzles that were found to have circumferential cracking, sorted in order of increasing crack length. Note that all of the nozzles except one (Crystal River, nozzle #32) were at essentially 20 EDYs when the cracking was discovered, with an average age at discovery of 20.3 EDYs. This allows the time dimension to be taken out of the calibration. All of the circumferential cracks will be assumed to have been discovered at 20 EFPYs, and will be compared to the *MRPERCRD* predicted probabilities of circumferential cracks of various lengths at 20 EDYs.

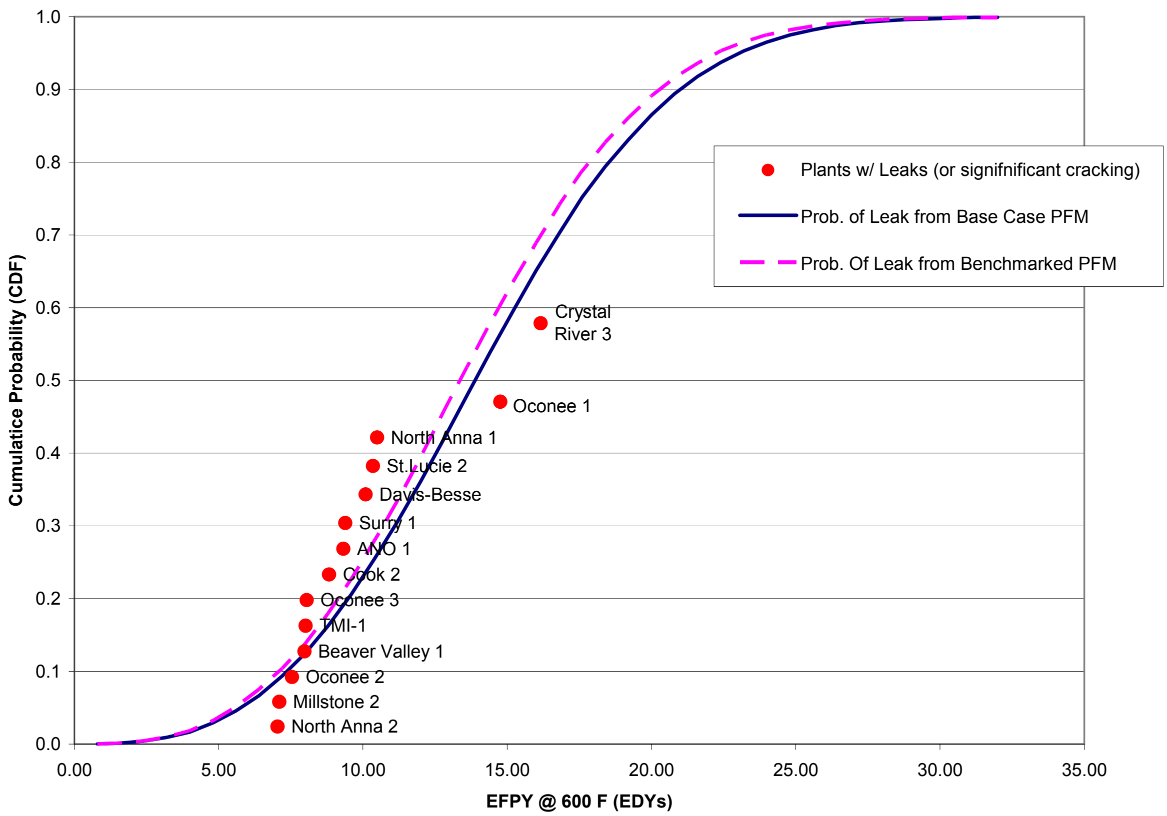

Figure 8-12
Benchmark Comparison of *MRPERCRD* Predictions of Time to First Leakage or Cracking

The data of Table 8-7 were used to produce a cumulative size distribution of crack lengths as shown in Table 8-8. The nozzles were sorted into bins of 30º crack length increments, and the bins were summed as shown in column 4 of the table. There were 11 total cracks of length greater than 30º, seven of length greater than 60º, and so on, down to two of length greater than 150º (the two 165º cracked nozzles at Oconee 3). Referring to Table 4-1, there were 13 inspected plants with operating times greater than or equal to Crystal River, constituting a total of 881 nozzles. This group of plants had an average age of 19.75 EDYs at the time of inspection (again very close to 20 EDYs). Thus 881 was used as a denominator to compute frequency of occurrence of circumferential cracks exceeding the various crack lengths in column 5 of Table 8-8. Finally, columns 6-9 of the table present *MRPERCRD* predictions of cumulative probabilities of cracking at twenty years, computed on a per nozzle (rather than a per head) basis. It is seen from these results that, except for the probability of a 30º crack (which is set to the probability of leakage, since in *MRPERCRD*, a leak or crack predicted at $t_{Weibull}$ is immediately assumed to be a 30º circumferential crack) the base case consistently under predicts the probabilities of large circumferential cracks by about a factor of 2 to 4.

Plant	Nozzle #	EDYs	Crack Lengths (Deg.)
Content Deleted – MRP/EPRI Proprietary Material			

Table 8-7
Eleven Nozzles in Four Plants Found to Contain Circumferential Cracks (Sorted by Crack Length

Plant Data				*MRPERCRD* Results			
Circ. Crack Lengths (º)	# Nozzles	Cumulative # of nozzles w/Crack Length Greater Than:	Frequency (881 Inspected)	Base Case	Correlation Factor =-1	Conservative θ and Corr. Factor = -1	Ultimate Sensitivity Case
Content Deleted – MRP/EPRI Proprietary Material							

Table 8-8
Cumulative Distribution of Circumferential Crack Lengths (Developed from Table 8-7)

The remaining columns in Table 8-8 contain *MRPERCRD* analysis results with increasingly conservative input parameters, chosen based on the sensitivity studies of Section 8.2. The first step was to change the CGR correlation factor to -1.0. This increased the circumferential crack probabilities somewhat, but they still under-predict the cumulative distribution from the plant data, especially at larger crack lengths. In the next column, a combination of correlation factor =-1 plus a more conservative Weibull θ distribution was assumed (triangular with θ-mean = 15.2, ±6.5). This gave the best general comparison of circumferential crack probabilities, over-predicting at some crack lengths, under-predicting at others, and agreeing almost exactly at the largest crack length (>150º). This case was therefore designated as the "benchmarked" parameters, and that column of Table 8-8 is highlighted. These benchmarked parameters are used for the case studies of Section 8.4 below. Finally, a *MRPERCRD* "ultimate sensitivity" run was performed, as shown in the last column (correlation factor = -1 plus a very conservative Weibull θ distribution of 10.0 ± 0.01). This case consistently over-predicted the field observations and therefore will not be used. The base and benchmarked cases are compared graphically to the cumulative circumferential crack distribution from the field data in Figure 8-13. The graph shows cumulative probability of circumferential cracks exceeding various sizes, and illustrates good agreement of the field data with the *MRPERCRD* benchmarked case.

The bottom row in Table 8-8 (predicted collapse) gives estimates of the cumulative probability of nozzle ejection prior to any inspections or repairs, projected from this group of 881 nozzles with lifetimes of ~20 EDYs. The estimated failure frequency from the plant data is based on the fact that no ejections occurred, and assumes that the number of failure occurrences is 0.5 (i.e. the mean of a uniform distribution between zero and one). For all but the base case, the *MRPERCRD* predictions conservatively over-estimate this failure frequency, over-predicting by about a factor of 1.9 in the benchmarked case.

Content Deleted – MRP/EPRI Proprietary Material

Figure 8-13
Comparison of Benchmark Analyses to Field-Observed Circumferential Cracking of Various Lengths

8.4 Case Studies

The final step in the PFM process is to use the benchmarked analysis parameters to analyze a sample of real plants and evaluate predicted nozzle leakage and failure frequencies under three inspection scenarios. The following inspection scenarios are studied:

1. Inspections exactly in accordance with the NRC Order [19].

2. Inspections under a newly proposed MRP inspection plan [21]. The proposed plan consists of baseline volumetric inspections and periodic bare metal visual examinations in accordance with the NRC Order. Subsequent volumetric (NDE) examinations of the nozzles and J-groove welds are performed in accordance with the following schedule:

    a) NDE of the nozzles at a frequency of 2EDYs or eight years, whichever is shorter, if no inspection of J-groove welds is performed (designated MRP Plan B).

    b) NDE of the nozzles plus surface examination of at least 50% of the J-groove welds at a frequency of 3 EDYs or ten years, whichever is shorter (designated MRP Plan C).

For the purpose of selecting plants for the case studies, the 69 PWRs currently operating in the US were subdivided based on head temperature, operating time and head replacement plans. These plants naturally break down into the following four groups:

- Group 1 comprises a group of 14 plants that have replaced or are in the process of replacing heads in their upcoming refueling outages. They are no longer relevant to this study.

- Group 2 comprises 15 plants with relatively high head temperatures and long operating times that have announced plans to replace heads, but have at least one additional refueling outage (RFO) before the replacements will be implemented. This group has effective ages in the range of 12 to 20 EDYs and the plants are thus in the "high" susceptibility category per the NRC Order. Therefore, they are required by the order to inspect (NDE plus BMV) every RFO until they replace.

- Group 3 consists of 17 plants predominantly in the NRC "moderate category" (although a few are high). EDYs are currently in the 8 to 12 range for this group, with a few as high as 15. These plants have not announced head replacement plans, and an optimum inspection program would be of great economic significance.

- Finally, Group 4 comprises the 23 Westinghouse cold head plants. These plants are characterized by very low head temperatures (≤ 567ºF) and correspondingly low EDYs (and risk of PWSCC in accordance with the Arrhenius model described above). They are all classified as low susceptibility per the NRC Order, and after initial inspection would require a roughly 6 to 7 year inspection interval, depending on how RFOs line up.

Plants from each of the above groups 2, 3 and 4 were selected for case studies. A brief description of each case study plant is provided in Table 8-9 below.

I - Group 2 Plant – A CE plant with a head temperature of 595.5ºF. Current EDYs are 14.6, and the plant has announced plans to replace the head in the Spring of 2006. A baseline NDE was performed in Spring 2003, and the plant is required to perform a second NDE in the Fall 2004 RFO
II - Group 3 Plant – A CE plant with a head temperature of 592ºF. Currently at 10.5 EDYs with no plans to replace the head. The plant will transition from Moderate to High susceptibility category before next RFO, and thereafter would require repeat inspections every RFO under the NRC Order.
III – Group 3 Plant – A Westinghouse plant with a head temperature of 580ºF. Currently at 11.1 EDYs and performing it's baseline inspection (NDE plus BMV in Spring 2004. The plant will transition from Moderate to High susceptibility category in 2007, and thereafter would require repeat inspections every RFO under the NRC Order.
IV - Group 4 Plant – A cold head Westinghouse plant (T = 567ºF). Current EDYs are 5.1 with no plans to replace head. BMV has been performed, and in accordance with the NRC Order, the first NDE would be required in Spring 2007. The plant will transition from low to moderate susceptibility in 2016.

Table 8-9
Summary of Case Studies

MRPERCRD runs were performed for each of these case studies, assuming inspections in accordance with the NRC Order and the two MRP inspection plan options outlined above. Detailed input parameters, including inspection schedules for these cases are listed in Tables 8-10 through 8-13, and the results are presented in Figures 8-14 through 8-17. The analyses were all performed using the "Benchmarked" input parameters derived in Section 8.3. As in the Base Case analyses of Section 8.1, NDE of the nozzles (with no weld inspection) was specified as 80% coverage, under the assumption that 20% of the chance of leakage is due to weld cracking. For cases in which 50% weld inspections are performed (MRP Plan C) the assumed inspection coverage was increased to 90% (i.e. half of the chance of leakage from J-groove welds is eliminated by the weld inspections). All inspections apply the FULLV POD described in Section 7.4 (Figure 7-3).

In Case Study I, a BMV was performed in Fall 2001, followed by a BMV plus baseline NDE of the nozzles in Spring 2003, and there is one additional RFO, Fall 2004, before the head replacement in Spring 2006. Both the NRC Order and MRP Plan B require inspection at the upcoming RFO, and therefore these two programs yield identical results. MRP Plan C would require only a BMV at that outage, but this plan is not directly applicable, since the Spring 2003 inspections did not include examinations of at least 50% of the J-groove welds. Results are reported anyway for completeness.

As seen in Figure 8-14, the probabilities of leakage and failure in Case Study I had reached relatively high levels (~20% and $7x10^{-3}$ respectively) before performing the initial BMV and baseline NDE inspections of that plant. These inspections reduced the POL to ~5% and the POF to ~$7x10^{-4}$. The *MRPERCRD* analysis indicates that a second inspection, at the next RFO (as required by the NRC Order and MRP Plan B) further reduces the POF to $3x10^{-4}$ and the POL to less than 2% at the time of head replacement in Spring 2006. Had weld inspections been performed in addition to nozzle NDE in the Spring 2003 RFO, then the NDE at the next RFO could have been deferred under MRP Plan C. This would have resulted in relatively low probabilities of leakage and failure at the time of head replacement (~5% and $7x10^{-4}$ respectively), albeit higher than the first two inspection regimens.

Case Study I:

Item	Variable	Probability Distribution	Mean Value	Standard Deviation	Lower Bound	Upper Bound	Units
1	Content Deleted – MRP/EPRI Proprietary Material						
2							
3							
4							
5							
6							
7							
8							
9							
10							
11							

Item	Variable	Probability Distribution	Mean Value	Standard Deviation	Lower Bound	Upper Bound	Units
12							
13							
14							
15							
16							
17							
18							
19							
20							
21							
22							
23							
24							
25							
26							
Inspection Schedules:							

Content Deleted – MRP/EPRI Proprietary Material

Table 8-10
Detailed *MRPERCRD* Input Parameters for Case Study I Analysis (CE Group 2 Plant)

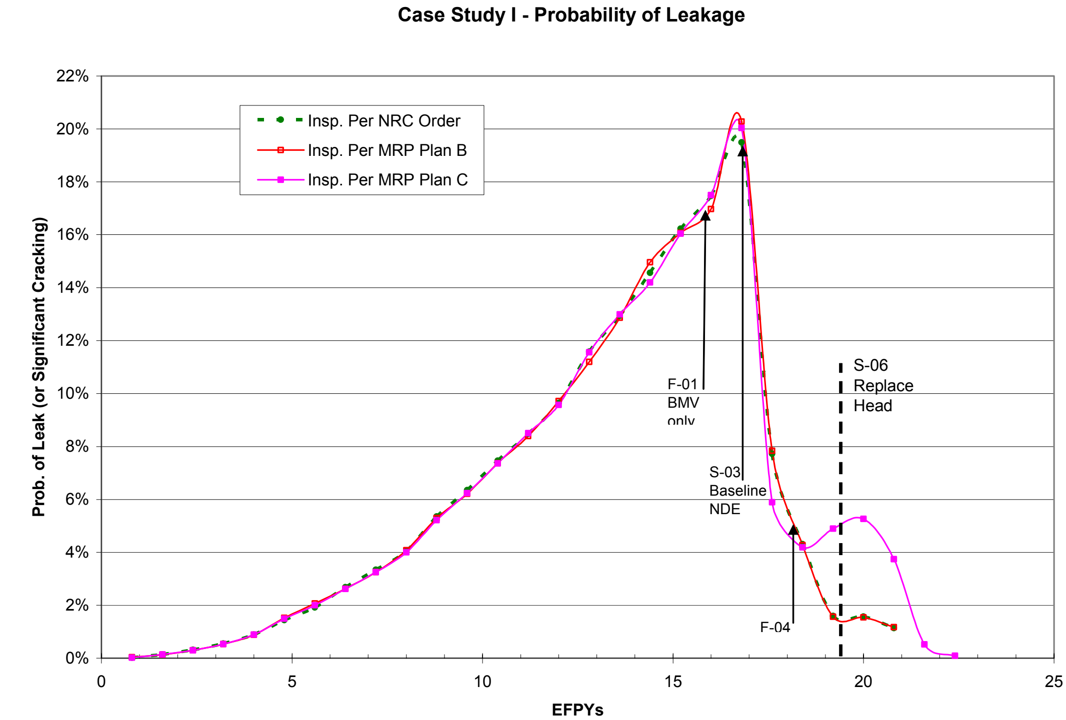

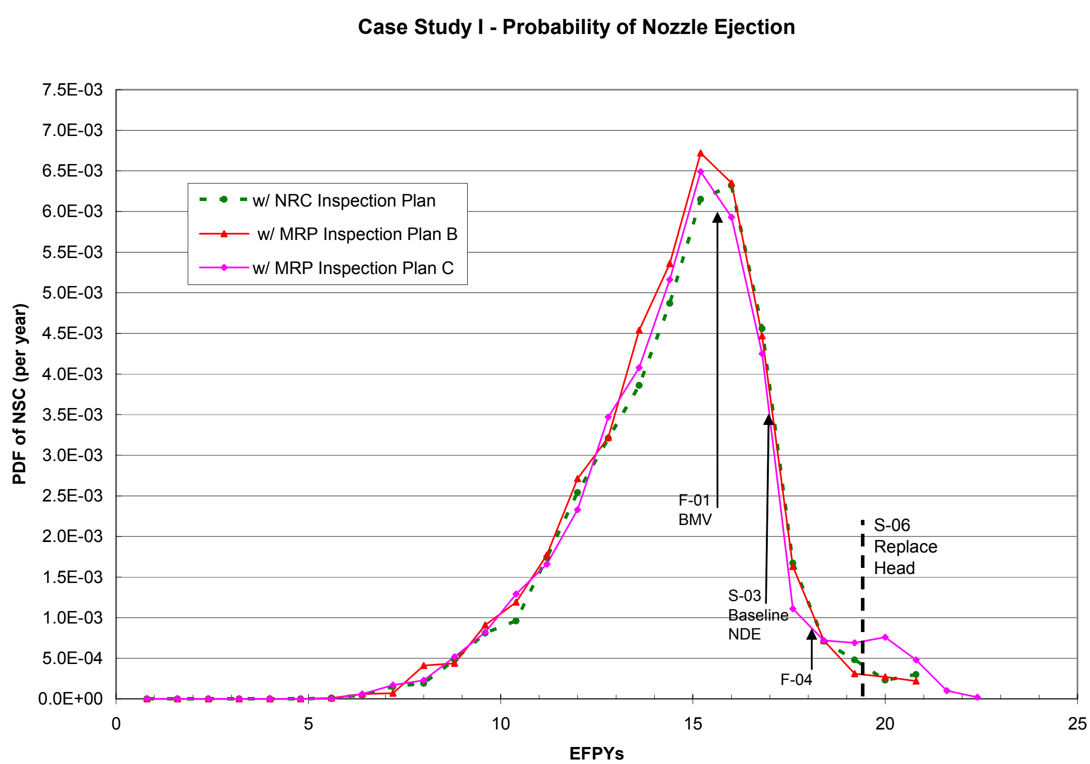

Figure 8-14
PFM Results for Case Study I (CE Group 2 Plant, Head Temperature = 595.5ºF)

MRPERCRD input and results for Case Study II are presented in Table 8-11 and Figure 8-15 below. In this Case Study, the plant performed its first top head inspections (BMV and Nozzle NDE) in Fall 2002. The plant also performed some weld inspections (~14%) during that RFO. Under the NRC Order, the plant would be required to perform its next NDE in Fall 2005 (every other RFO since it is moderate susceptibility). After that, it would switch to high susceptibility, and therefore be required to perform NDE every RFO. Under MRP Plan B, the next NDE would also be performed in Fall 2005, since it accumulates 1.7 EDYs in that time, and would be well over 2 EDYs at the subsequent RFO. However, MRP Plan B deviates from the Order in that the plant would continue performing NDE every other (as opposed to every) RFO thereafter. Under MRP Plan C, had the plant inspected at least 50% of the welds in Fall 2002, the next inspection would not be required until Spring 2007, and if weld inspections continued to be performed, subsequent inspections would be every third RFO thereafter.

From Figure 8-15, it is seen that the three inspection plans yield virtually identical POLs and POFs for this plant. In all three cases, the POL built up to ~8% prior to the first examinations, but after that was reduced to less than 4% (< 3% for MRP Plan C). The peak POL after that is ~4.5% in all three cases. Similarly, the POF built up to ~2 x 10^{-3} prior to the baseline inspections, but the peak after that is less than 4 x 10^{-4} for all three cases.

Case Study II:

Item	Variable	Probability Distribution	Mean Value	Standard Deviation	Lower Bound	Upper Bound	Units
1	Content Deleted – MRP/EPRI Proprietary Material						
2							
3							
4							
5							
6							
7							
8							
9							
10							
11							
12							
13							
14							
15							
16							
17							

Item	Variable	Probability Distribution	Mean Value	Standard Deviation	Lower Bound	Upper Bound	Units
18							
19							
20							
21							
22							
23							
24							
25							
26							

Content Deleted – MRP/EPRI Proprietary Material

Table 8-11
***MRPERCRD* Input Parameters for Case Study II Analysis (CE Group 3 Plant)**

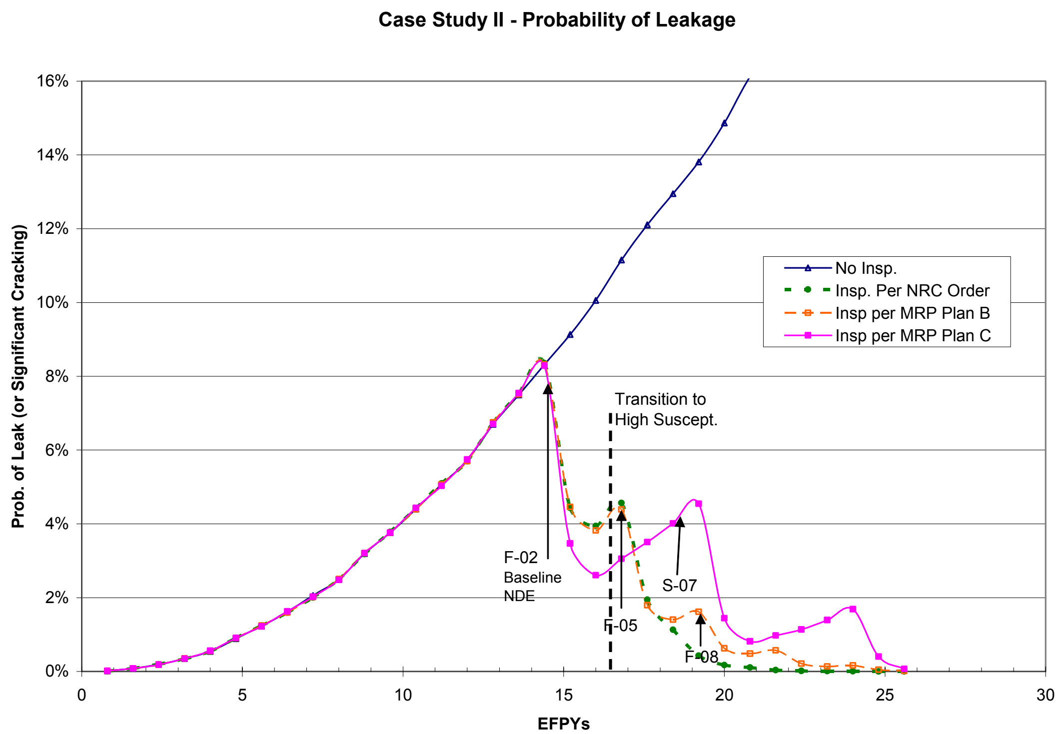

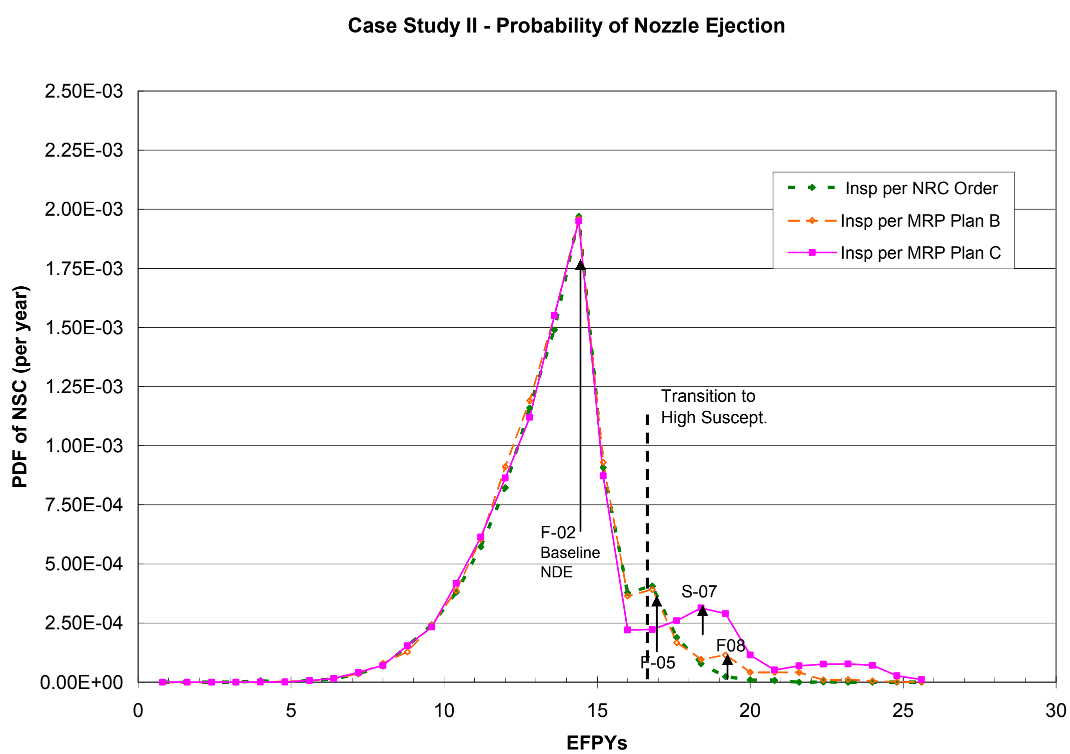

Figure 8-15
PFM Results for Case Study II (CE Group 3 Plant, Head Temperature = 592ºF)

MRPERCRD input and results for Case Study III are presented in Table 8-12 and Figure 8-16 below. In this Case Study, the plant will perform its first top head inspections (BMV and Nozzle NDE) in Spring 2004. Under the NRC Order, the plant would be required to perform its next NDE in Spring 2007 (every other RFO since it is moderate susceptibility). After that, it would switch to high susceptibility, and therefore be required to perform NDE every RFO. Under MRP Plan B, the next NDE would be performed in Fall 2008, since it accumulates 1.8 EDYs in that time, and would be well over 2 EDYs at the subsequent RFO. Under MRP Plan B, the plant would continue performing NDE every third (as opposed to every) RFO thereafter. Under MRP Plan C, if the plant inspected at least 50% of the welds in Spring 2004, the next inspection would not be required until Fall 2011, and if weld inspections continue to be performed, subsequent inspections would be every fifth RFO thereafter.

From Figure 8-16, it is seen that the three inspection plans yield virtually identical POLs and POFs for this plant. In all three cases, the POL builds up to ~3.5% prior to the first examinations, but after that the peak POL is reduced to less than 2% under all three inspection programs. Similarly, the POF builds up to ~2.5×10^{-3} prior to the baseline inspections, but the peak after that is less than 3.7×10^{-4} for all three cases.

Case Study III:

Item	Variable	Probability Distribution	Mean Value	Standard Deviation	Lower Bound	Upper Bound	Units
1	Content Deleted – MRP/EPRI Proprietary Material						
2							
3							
4							
5							
6							
7							
8							
9							
10							
11							

Item	Variable	Probability Distribution	Mean Value	Standard Deviation	Lower Bound	Upper Bound	Units
12							
13							
14							
15							
16							
17							
18							
19							
20							
21							
22							
23							
24							
25							
26							

Content Deleted – MRP/EPRI Proprietary Material

Table 8-12
***MRPERCRD* Input Parameters for Case Study III Analysis (Westinghouse Group 3 Plant)**

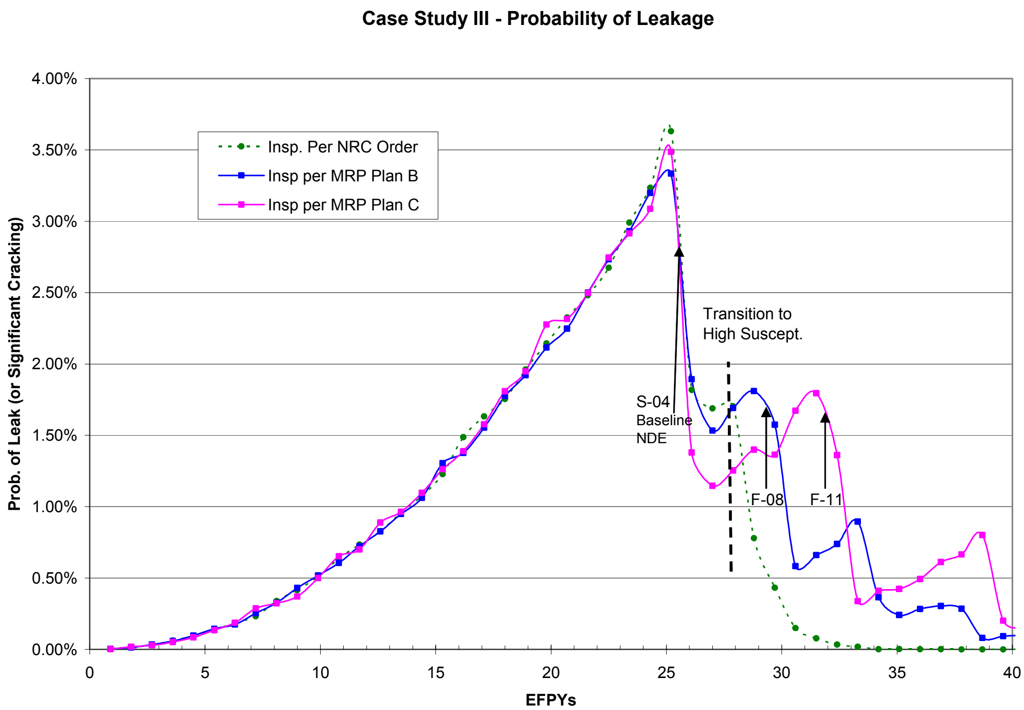

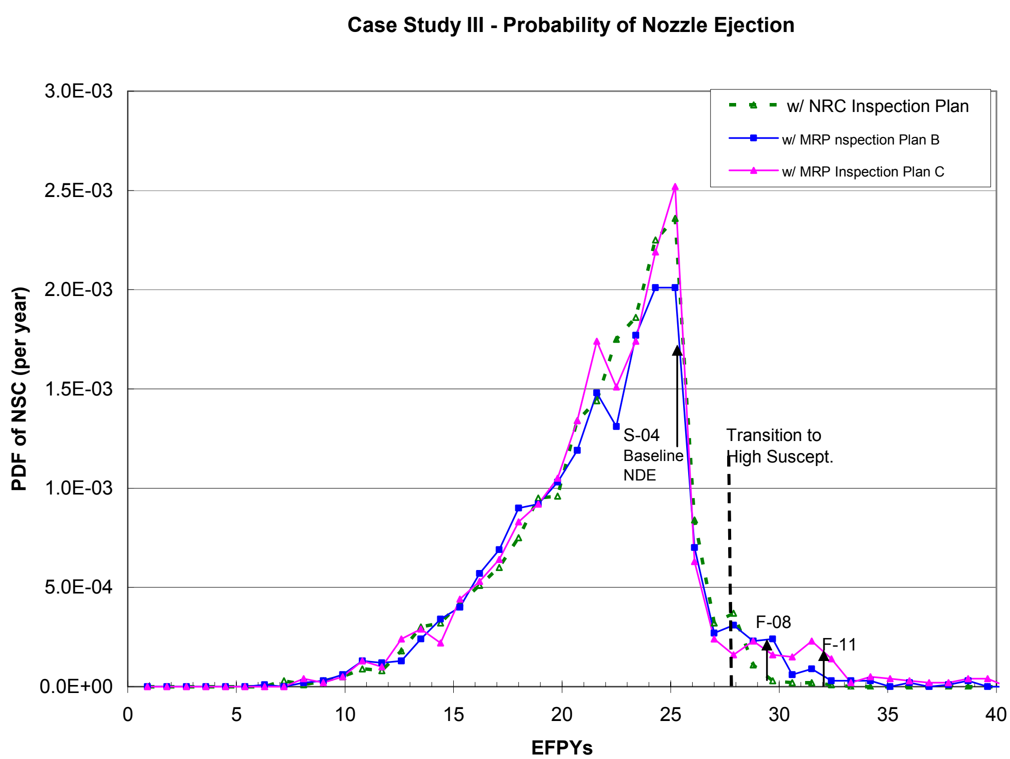

Figure 8-16
FM Results for Case Study III (Westinghouse Group 3 Plant, Head Temperature = 580ºF)

Finally, MRPERCRD input and results for Case Study IV are presented in Table 8-13 and Figure 8-17 below. In this Case Study, the Westinghouse cold head plant performed a BMV in Fall 2002, but is not required to perform its baseline NDE until Spring 2007. The subsequent NDE would be in Spring 2013 under the NRC Order, Fall 2014 under MRP Plan B, and Spring 2016 under MRP Plan C.

From Figure 8-17 it is seen that once again, the three inspection plans yield virtually identical results. The POL under all three plans peaks at approximately 0.8% prior to the baseline NDE in Spring 2007. Subsequently, the POL peaks at less than 0.5% under all three plans. The POF peaked at about 3×10^{-4} prior to the BMV in Fall 2002, but subsequent to the baseline NDE, it never exceeds 1×10^{-4} under all three NDE programs.

Case Study IV:

Item	Variable	Probability Distribution	Mean Value	Standard Deviation	Lower Bound	Upper Bound	Units
1	Content Deleted – MRP/EPRI Proprietary Material						
2							
3							
4							
5							
6							
7							
8							
9							
10							
11							
12							
13							
14							
15							
16							
17							
18							
19							

Item	Variable	Probability Distribution	Mean Value	Standard Deviation	Lower Bound	Upper Bound	Units
20							
21							
22							
23							
24							
25							
26							

Content Deleted – MRP/EPRI Proprietary Material

Table 8-13
***MRPERCRD* Input Parameters for Case Study IV (Westinghouse Group 4 Plant)**

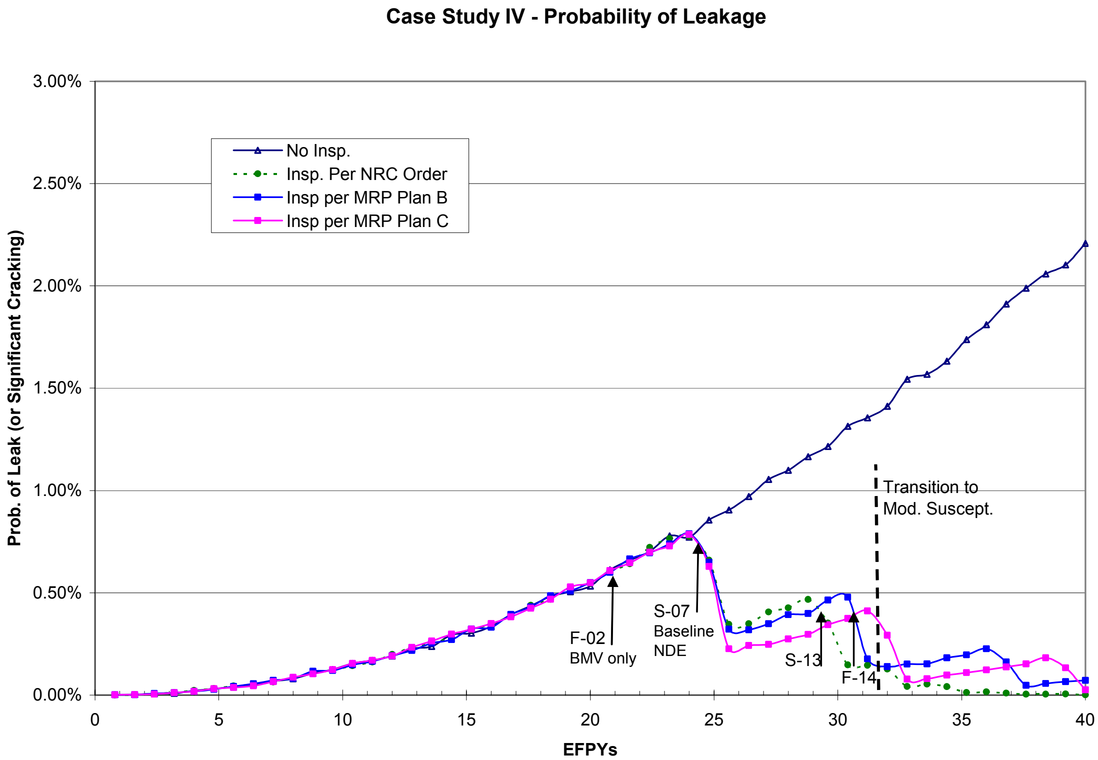

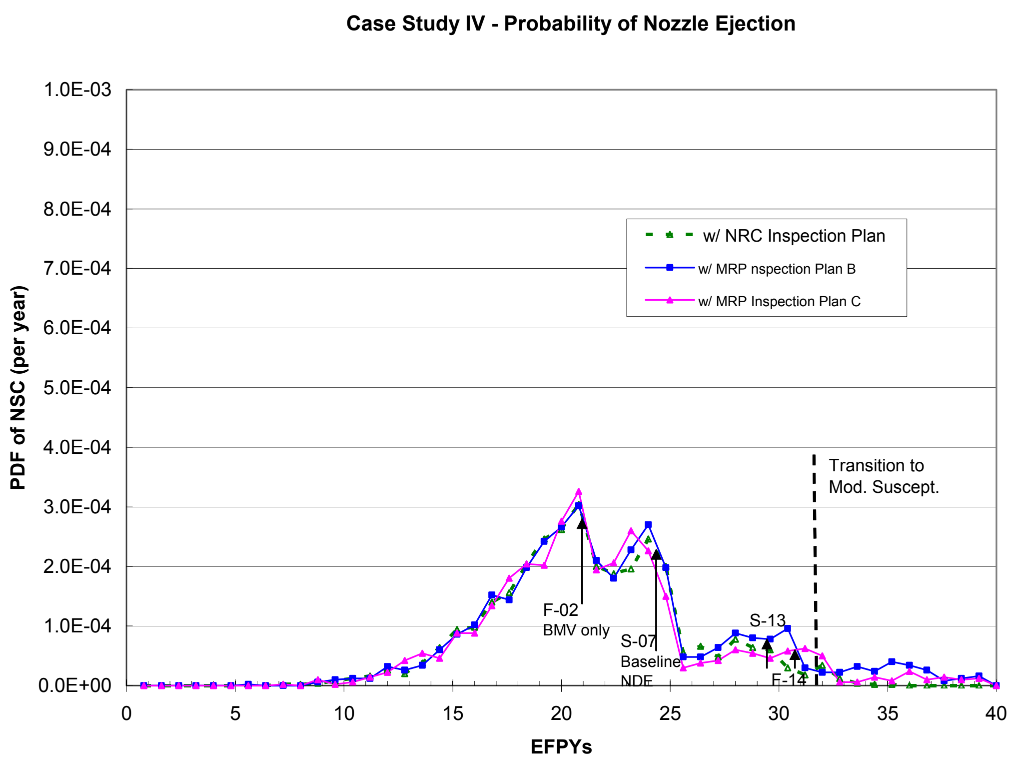

Figure 8-17
PFM Results for Case Study IV (Westinghouse Group 4 Plant, Head Temperature = 567ºF)

In summary, the proposed MRP inspection plan, which offers an incentive in terms of longer inspection intervals if at least 50% of J-groove welds are inspected, is shown to yield essentially identical results as the NRC Order, in terms of probabilities of leakage and nozzle ejection. Table 8-13 summarizes these results.

Plant	Prob. of:	NRC	MRP Plan B	MRP Plan C
Case Study I	NSC	4.8×10^{-4}	4.8×10^{-4}	6.9×10^{-4}
	Leak	1.6%	1.6%	4.9%
Case Study II	NSC	4.1×10^{-4}	3.9×10^{-4}	3.1×10^{-4}
	Leak	4.6%	4.4%	4.6%
Case Study III	NSC	3.7×10^{-4}	2.4×10^{-4}	2.3×10^{-4}
	Leak	1.7%	1.8%	1.79%
Case Study IV	NSC	7.8×10^{-5}	9.6×10^{-5}	6.0×10^{-5}
	Leak	0.47%	0.48%	0.41%

Table 8-14
Summary of PFM Results for Case Studies

The above results are considered generically applicable to plants in Groups 2, 3 and 4 described above, from the standpoint of maintaining the probabilities of leakage and nozzle ejection at acceptably low levels. They illustrate that, for plants that are currently in the NRC high, moderate and low susceptibility categories, the future probabilities of leakage and nozzle ejection are essentially the same for inspections in accordance with the NRC Order as well as with two proposed MRP alternatives. The probabilities are also below generally accepted limits (POL < 5% and POF < 1×10^{-3}) after the initial baseline examinations are performed.

9 DISCUSSION AND CONCLUSIONS

Generic Probabilistic Fracture Mechanics (PFM) analyses have been performed to determine the probabilities of nozzle leakage and failure in PWR top head nozzles due to PWSCC of the Alloy 600 nickel alloy nozzles as well as associated weldments. A PFM software tool, *MRPERCRD* was developed for this purpose. The major computational elements of the software tool include:

- computation of applied stress intensity factors for circumferential cracks in various nozzle geometries as a function of crack length,
- determination of critical circumferential flaw sizes for nozzle failure,
- an empirical (Weibull) analysis of U.S. PWR top head inspection data to determine the probability of nozzle cracking or leakage as a function of operating time and RPV head temperature,
- statistical characterization of PWSCC crack growth rates in the PWR primary water environment as a function of applied stress intensity factor and service temperature, and
- determination of the effects of inspections (inspection type, frequency and effectiveness).

These elements of the analysis are described in detail in this report.

The PFM tool was then benchmarked and calibrated with respect to the observance of leakage and/or circumferential cracking in inspections of a significant data base of U.S. PWRs (30 plants performed NDE of which 14 observed leakage or cracking, and a total of 11 nozzles were found to have circumferential cracking of various lengths). The calibrated tool was used to perform an extensive series of analyses of PWR top heads to achieve an understanding of the significant parameters affecting probabilities of leakage and failure from top head nozzles and welds. Four characteristic RPV head designs were addressed, which are demonstrated to envelope the entire fleet of U.S. PWRs. Conservative stress intensity factors were computed for several nozzles in each of these heads. A series of PFM analyses were then performed covering a wide variety of conditions and assumptions for the four characteristic plants. These include base cases, with and without inspections, and sensitivity studies to evaluate the effects of various statistical and deterministic assumptions in the analysis. The base and sensitivity cases were used to select a set of "benchmarked" analytical parameters that characterize the probabilities of leakage and of large circumferential cracks in a reasonably conservative manner compared with field experience. Finally, the benchmarked parameters were used to analyze four case studies of actual plants, to evaluate three assumed inspection programs with respect to future probabilities of nozzle leakage and failure (after the inspection programs are initiated). The three programs evaluated are inspections in accordance with the NRC Order, and two inspection alternatives proposed by the MRP. In all three cases, baseline inspections and future Bare Metal Visual inspections (BMVs) were assumed in accordance with the NRC Order.

The proposed MRP inspection alternatives are described in detail in a separate report [21]. They were derived on the basis of maintaining the probabilities of leakage and failure in an acceptable range, and essentially identical to those predicted for inspections in accordance with the NRC Order, for a variety of plant types and operating conditions. MRP Plan B consists of performing NDE on an interval of 2 EDYs. MRP Plan C consists of performing NDE, including inspections of at least 50% of J-groove welds, on an interval of 3 EDYs. These alternatives are shown to yield essentially the same probabilities of leakage and failure as are achieved by inspections in accordance with the NRC Order, and they offer an incentive, in term of reduced inspection frequencies, for plants that perform inspections of their J-groove welds.

Although the predicted probabilities of leakage and failure are a function of the many input variables assumed in the analysis, the specific set of variables used to compare inspection programs have been benchmarked and calibrated with respect to field experience. Also, changes to these variables would affect the analyses of the NRC Order as well as of the two MRP inspection plans in approximately the same manner. Thus the comparison and conclusions of this study are expected to remain the same for realistic ranges of these input variables.

10
REFERENCES

1. *MRPERCRD* "Evaluation of Reliability for Control Rod Drive Nozzles in Vessel Top Heads" Version 1.0, Software Users Manual, January 2002.

2. T. L. Anderson, "Fracture Mechanics Fundamentals and Applications", CRC Press, 1991

3. Dominion Engineering, Inc. Calculation No. C-4142-00-2, Rev. 0, "Plant A CRDM Stress Analysis," 8/29/01, (Proprietary)

4. Dominion Engineering, Inc. Calculation No. C-7612-00-1, Rev. 0, "Plant B CRDM Stress Analysis," October 31, 2001, (Proprietary)

5. Dominion Engineering, Inc. Calculation No. R-7613-00-1, Rev. 0, "Plant C Fall 2002 CRDM Repair Analysis", January 2003, (Proprietary)

6. Dominion Engineering, Inc. Calculation No. C-7736-00-8, Rev. 0, "Plant D CEDM and ICI Stress Analysis – Alternate Element Mesh", 03/08/02, (Proprietary)

7. Structural Integrity Associates, Inc. Calculation No. W-EPRI-182-303, "Deterministic Fracture Mechanics Evaluation of Top Head CRDM Nozzle with Through-Wall Flaw – B&W Type Plant A," 3/26/03 (Contains Vendor Proprietary Information)

8. Structural Integrity Associates, Inc. Calculation No. W-EPRI-182-309 "Deterministic Fracture Mechanics Evaluation of Westinghouse 2-Loop Top Head CRDM Nozzle with Through-Wall Flaw, Plant B,"7/22/03 (Contains Vendor Proprietary Information)

9. Structural Integrity Associates, Inc. Calculation No. W-EPRI-182-304, "Deterministic Fracture Mechanics Evaluation of Top Head CRDM Nozzle with Through-Wall Flaw - Westinghouse Type Plant C, 5/09/03, (Contains Vendor Proprietary Information)

10. Structural Integrity Associates Calculation EPRI-182Q-305, "Deterministic Fracture Mechanics Evaluation of Top Head CRDM Nozzle with Through-Wall Flaw - CE Type Plant D", June 2003, (Contains Vendor Proprietary Information)

11. Materials Reliability Program, "Crack Growth Rates for Evaluating Primary Water Stress Corrosion Cracking (PWSCC) of Thick-Wall Alloy 600 Material," MRP-55, Revision 1, November 2002. EPRI Proprietary

12. Materials Reliability Program, "Interim Alloy 600 Safety Assessments for US PWR Plants, Part 2: Reactor Vessel Top Head penetrations," MRP-44, EPRI Report No. TP-1001491, Part 2, May 2001.

13. P. Scott, "Prediction of Alloy 600 Component Failures in RWP System," Research Topical Symposia Part 1 – Life Prediction of Structures Subject to Environmental Degradation, NACE, Houston (1997)

14. R. B. Abernathy, "The New Weibull Handbook, Reliability and Statistical Analysis for Predicting Life, Safety, Survivability, Risk, Cost and Warranty Claims," Fourth Edition, Sept. 2000.

15. "PWSCC Prediction Guidelines," EPRI Report No. TR-104030, 1994.

16. Structural Integrity Associates, pc-CRACK for Windows, version 3.1-98348

17. Structural Integrity Associates Calculation EPRI-182Q-307, "Deterministic Fracture Mechanics Crack Growth Calculations – Circumferential Flaws Above Weld", 9/05/03

18. Structural Integrity Associates Calculation EPRI-182Q-308, "Probability of CRDM Nozzle Ejection due to Through Wall Circumferential Crack Propagation", 9/12/03

19. U.S. NRC Order EA-03-009, "Interim Inspection Requirements for Reactor Pressure Vessel Heads at Pressurized Water Reactors", issued on February 11, 2003

20. Dimitrijevic, V. and Ammirato, F., "Use of Nondestructive Evaluation Data to Improve Analysis of Reactor Pressure Vessel Integrity, " EPRI Report TR-102074, Yankee Atomic Electric Co. March 1993

21. Materials Reliability Program, "Revised PWR Reactor Pressure Vessel (RPV) Upper Head Penetration Inspection Plan," MRP (to be published).